UNIVERSITY OF CALIFORNIA
RIVERSIDE

Coupling Field Data With Modeling Tools to Evaluate Resource Use Efficiency and Environmental Impacts in California Agriculture

A Dissertation submitted in partial satisfaction
of the requirements for the degree of

Doctor of Philosophy

in

Plant Biology

by

Cara N. Fertitta

December 2017

Dissertation Committee:

Dr. G. Darrel Jenerette, Chairperson
Dr. David A. Grantz
Dr. Milt McGiffen
Dr. Samantha Ying

The Dissertation of Cara N. Fertitta is approved:

_____

_____

_____

_____

Committee Chairperson

University of California, Riverside

ACKNOWLEDGEMENTS

I would first like to thank the University of California Riverside and my adviser, Dr. G Darrel Jenerette for providing me the opportunity to pursue my PhD in Plant Biology. I am grateful to those funding sources that have supported me throughout my academic career: the University of California Riverside, the USDA-NIFA (Award No. 2011-67009-30045), the Graduate Research Mentoring Program, and the Graduate Assistance in Areas of National Need Fellowship. I extend my deepest gratitude to all of my committee members, past and present: Dr. G. Darrel Jenerette, Dr. David A. Grantz, Dr. Edith Allen, Dr. Louis Santiago, Dr. Jeffery Diez, and Dr. David Crowley. I am also grateful to Dr. Linda Walling for her continued support and guidance throughout my post-graduate studies. I would also like to thank my collaborators and co-authors: Dr. G. Darrel Jenerette, Dr. David A. Grantz, and Dr. Louis Santiago of the University of California Riverside as well as Dr. Sabrina Spatari of Drexel University, Dr. Patricia Y. Oikawa of California State University, and Dr. Liyin Liang of University of Waikato.

I extend my gratitude to Jeff Dahlberg, Chris Summerville, and Sean Cutler for allowing us to sample sorghum from their experimental plots in order to measure hydraulic properties. I am also grateful to Tim Brodribb, Chris Lucani, Manika Choudhary, and Eleinis A. Avila Lovera for their instrumental assistance in acquiring leaf vulnerability curve and conductance data. I thank Ray Anderson for his assistance in partitioning canopy-level water flux and John Sperry for his expertise in helping us

parameterize and troubleshoot our adapted Profit Maximization model. I thank Fernando Miramontes and Francisco Maciel at the DREC for their assistance and guidance in field operations, and Lindy Allsman for maintaining field records. I am also grateful to Alex Stadel, Meghan Hums, and Long Nguyen for their assistance in LCA model development. I thank Dr. Milt McGiffen at the University of California Riverside for his help in developing and editing this work, as well as the UC Cooperative Extension Rice Specialists, who continue to publish robust datasets on CA rice varietals, which were instrumental in parameterizing our rice model. I am further grateful to Meagan Simmonds of UC Berkeley, who shared her aggregation of chamber methane measurements for CA rice with us, allowing us to parameterize PEPRMT to Butte County rice.

The text of this dissertation, in part, is a reprint of the material as it appears in Global Change Biology Bioenergy 9(12), 1764 – 1779 (2017). The co-author Cara Fertitta-Roberts listed in that publication directed and supervised the research which forms the basis for this dissertation.

DEDICATION

This work is dedicated to:

My loving and supportive husband, Dr. Christopher Roberts, who has encouraged and inspired me every step of the way.

My family who have tirelessly rooted for me my whole life and have supported all of my pursuits – no matter how big, or small, or distant.

The many friends who have celebrated in my joys and successes and, more importantly, who have been a source of comfort and sanity over the past five years.

ABSTRACT OF THE DISSERTATION

Coupling Field Data With Modeling Tools to Evaluate Resource Use Efficiency and Environmental Impacts in California Agriculture

by

Cara N. Fertitta

Doctor of Philosophy, Graduate Program in Plant Biology
University of California, Riverside, December 2017
Dr. G. Darrel Jenerette, Chairperson

The sustainability of California agriculture depends on its ability to adapt to climate change and to mitigate it. Though field and laboratory experiments provide important data to this end, they require time and resources that limit the pace of progress. Coupling these data with modeling tools can accelerate agroecological research and highlight important directions for more comprehensive *in vivo* studies. Here, we use a combination of field data and modeling tools to better understand resource use, stress tolerance, and environmental impacts associated with various products of California agriculture. Chapter one evaluates water use dynamics in *Sorghum bicolor* cv. (Photoperiod LS) grown in California's Imperial Valley (IV) and their implications for stress tolerance. Coupling field data with an optimization model, we found sorghum to exhibit high heat tolerance at the expense of water use efficiency (WUE). However, the extent to which WUE was compromised varied in response to soil water status, suggesting sorghum adjusts its water use patterns depending on the type and severity of stress present. In chapter two, we assess the environmental impacts associated with

biofuel production using IV sorghum as a feedstock. We used field data to parameterize a crop model, allowing us to evaluate a wide range of nitrogen (N) management scenarios for feedstock production. Crop model output was coupled with life cycle assessment models to quantify the well-to-wheel environmental impacts of each production scenario. Overall, biofuels from IV sorghum had about 1/3 the global warming potential (GWP) of gasoline, but had much greater impacts to local air and water pollution. Efficient use of N was an important pathway for mitigating adverse impacts. Using a similar experimental framework, chapter three evaluates the GWP of California rice under a range of irrigation schedules varying in the severity and frequency of drainage events during the growing season. Severe and frequent dry-downs provided the greatest greenhouse gas mitigation potential, but showed potential to reduce grain yields, compromising the advantages of this practice from a global perspective. Our work highlights the diverse and valuable contributions of data-model fusion in preparing California for the conditions and demands of twenty-first century agriculture.

TABLE OF CONTENTS

LIST OF PRIMARY FIGURES

LIST OF PRIMARY TABLES

LIST OF SUPPLEMENTAL FIGURES

LIST OF SUPPLEMENTAL TABLES

Introduction

To maintain food, feed, and fuel production in the twenty-first century, agriculture must adapt to changing climate patterns including increased global temperatures and higher incidence of drought (Godfray et al., 2010; Lobell et al., 2008a & b). At the same time, the agricultural sector is a major contributor to climate change, constituting roughly 13% of anthropogenic greenhouse gas emissions (GHG) and acting as a major source of air and water pollution (IPCC 2014; Bauer et al. 2016). Thus, agricultural production is tasked with becoming more sustainable in terms of both tolerating and mitigating climate change. The former requires rapid advancements in our understanding of stress tolerance and resource use efficiency in major cropping systems while the latter requires quantitative assessments of environmental impacts in agriculture. Coupling field data with modeling tools better equips us to meet these goals by reducing the temporal and financial costs associated with tackling such a large and complex task. The following body of work couples field data with modeling tools to assess resource use efficiency and environmental impacts in agriculture.

Models are instrumental in developing and testing scientific theory and, increasingly, are used to assess large-scale processes and predict future outcomes (Gershenfeld 2011; Frigg & Hartmann 2017). In agriculture, the development of advanced modeling systems has enhanced our understanding of yield stability, resource use efficiency, and stress tolerance (Hammer et al. 2006; Thorp et al. 2008; Wu et al. 2013; Buckley & Mott 2013; Msongaleli et al. 2014), as well as the ecological impacts

associated with agricultural production (Cherubini & Strømman 2011; Guinée et al. 2011). Field trials traditionally used as a means to this end are expensive and cumbersome, requiring a great deal of time and resources to evaluate the impact of even a limited number of variables. While robust field data are essential to the parameterization and validation of models, these models allow rapid exploration of a large number of scenarios *in silico* that would be impractical or cost-prohibitive to explore *in vivo* (Fertitta-Roberts et al. 2017; Lamboni et al. 2009). Knowledge gained from models can, in turn, highlight directed avenues for future field research (Trouwborst et al. 2010). Understanding model limitations and uncertainty is paramount in interpreting modeled outcomes as models are inherently based on assumptions that simplify complex biological systems (Sinclair & Seligman 1996; Lobell & Burke 2008; Biernath et al. 2011). Yet, models can also mitigate uncertainty around field results through sensitivity analyses and allowance of spatial and temporal variation in modeled inputs ranging from environmental conditions to management choices. Further, models allow us to approximate data that is challenging or cost-prohibitive to measure, such as air and water pollution associated with agricultural production. Models can also serve as heuristic tools when used in combination with field data, allowing us to test a model's underlying assumptions and, therefore, enhance our understanding of the biological principles those assumptions reflect (Frigg & Hartmann 2017). Accordingly, coupling field data with modeling tools can be an effective and efficient pathway for improving agricultural sustainability.

We use a variety of models and, often, a combination of models to address specific aspects of agricultural sustainability in two study systems: Imperial Valley sorghum and northern California rice production. California is an opportune environment for assessing agricultural sustainability. Its Mediterranean climate provides high light availability and long growing seasons, making California one of the most productive agricultural regions in the world (CDFA 2017). However, California is also highly susceptible to drought and extreme heat events that threaten its sustained agricultural production (Hayhoe et al. 2004; Snyder et al. 2002). Extreme temperatures and limited precipitation have been shown to be the primary determinants of reduced yields under climate change (Lobell & Field 2007; Lobell, Bonfils, et al. 2008; Schlenker et al. 2010; Lesk et al. 2016). Thus, the future of California agriculture relies heavily on improving stress tolerance and conserving water resources.

Chapter one evaluates stress tolerance and water use dynamics in *Sorghum bicolor* grown in California's Imperial Valley. Sorghum is a C_4 grass grown for food, feed, and fuel around the globe. It is considered to be one of the five most important crops in the world and only stands to increase in popularity under climate change (FAO & NRI 1999; Belton & Taylor 2004; Msongaleli et al. 2014). A native of sub-Saharan Africa, sorghum is well-adapted to high temperatures and drought (de Wet 1978; Belton & Taylor 2004). Its C_4 photosynthetic pathway contributes to its high light and water use efficiencies (Sage 2004; Ghannoum 2009). C_4 photosynthesis increases the efficiency of carbon fixation and reduces photorespiratory losses by effectively shuttling CO_2 to the bundle sheath, where it is fixed in the absence of high oxygen concentrations typical of

the mesophyll (Collatz et al. 1992). This mechanism is particularly advantageous at high temperatures, which tend to increase the rate of photorespiration. Sufficiently high temperatures can also damage photosynthetic machinery within the leaves, leading to irreversible and sometimes lethal losses in assimilation potential (Leuning 2002; Medlyn et al. 2002). Yet some sorghum cultivars have shown remarkable tolerance to extreme temperatures, maintaining high rates of assimilation at temperatures in excess of 45 °C (Prasad et al. 2006; Prasad et al. 2008; Djanaguiraman et al. 2014). Other cultivars have been shown to favor milder temperatures but, in turn, are particularly tolerant to drought.

Drought tolerance in sorghum is both behavioral and physiological. Behaviorally, sorghum displays isohydric tendencies, meaning plants close their stomata in response to declining leaf water potential in order to avoid excessive water loss and adverse physiological impacts (Jones 1998). Physiologically, its vascular structure reduces the risk of these adverse impacts. It is hypothesized that hydraulic architecture in plants reflects a tradeoff between hydraulic safety and efficiency (Tyree & Zimmermann 2002; Meinzer et al. 2010), where efficiency refers to the capacity to rapidly transport water through the xylem and safety refers to the vulnerability of xylem vessels to cavitation. Cavitation occurs when air is pulled into to the xylem, disrupting the water column and causing the vessel to fill with air (Sack & Holbrook 2006). The xylem pressure at which cavitation is induced varies across species but is generally related to vessel length and diameter (Meinzer et al. 2010; Ocheltree et al. 2016). Large xylem vessels, which permit efficient transport of water, tend to be more susceptible to cavitation, leaving species with large vessels vulnerable to drought stress. However, greater efficiency of water transport

generally allows higher rates of assimilation as carbon uptake and water loss are inextricably linked (Cowan 1978; Farquhar & Sharkey 1982; Sade et al. 2012). Conversely, species with smaller xylem vessel display greater resistance to cavitation. This increases drought tolerance but reduces hydraulic conductance and, presumably, assimilation potential. However, recent work suggests that C_4 grasses are less susceptible to safety-efficiency tradeoffs than C_3 plants (Ocheltree et al. 2016; Kocacinar & Sage 2003). While greater resistance to cavitation does appear to constrain hydraulic conductance, high light use efficiency and CO_2 uptake efficiency in C_4 grasses can de-couple hydraulic capacity from assimilation potential, allowing C_4 grasses to exhibit hydraulic safety while retaining high assimilation potential (Ocheltree et al. 2016).

Although the unique capabilities of C_4 plants can reduce carbon-water tradeoffs, all plants must balance demands for CO_2 uptake with inevitable water loss. Regardless of hydraulic structure, stomatal aperture is ultimate what determines this balance (Cowan 1978; Farquhar & Sharkey 1982). Accordingly, many models of stomatal regulation have been posed to describe water use dynamics in plants. As the mechanisms driving stomatal regulation are poorly understood, many of these models have been empirically derived or based on theoretical optimization (Buckley & Mott 2013). Perhaps the most widely used empirical model is the Ball-Berry-Leuning model, in which stomatal conductance is driven by the plant's demand for CO_2 and the atmosphere's demand for water and is constrained by the concentration of CO_2 available at the leaf's surface (Ball et al. 1987; Leuning 1995). Traditionally, this model is paired with the classic Farquhar photosynthesis model (Farquhar et al. 1980; Farquhar et al. 2001). The simplicity of these

models and their accuracy over a wide range of environmental conditions have led to their extensive use across ecosystems and scales. However, the Ball-Berry-Leuning model fails to account for soil water status, which determines the supply of water available for transpiration. Other popular models take an optimization approach to describing stomatal regulation, whereby "profits" are maximized by maximizing photosynthetic gain and minimizing water loss (Cowan & Farquhar 1977). These models tend to include sensitivity to soil water status, but vary in their sensitivity to vapor pressure deficit (VPD). However, the greater limitation of optimization models lies in their inherent assumption that the "cost" of losing water is quantitative. Recent research suggests that the cost of losing water is better assessed in terms of the potential physiological consequences associated with water loss, which varies across species and environments (Wolf et al. 2016).

In response to this shift in perspective, new optimization models have been developed which better incorporate differences in plant physiology and their consequences for water use dynamics. The recently published Profit Maximization model (PMAX) uses integration of vulnerability curves across plant components to assess hydraulic cost in terms of the plant's proximity to hydraulic failure as opposed to quantitative water loss (Sperry, Venturas, et al. 2016). Vulnerability curves describe the loss in hydraulic conductance associated with the spread of cavitation throughout the xylem as water potential declines (Tyree & Sperry 1988). These curves vary substantially across species and generally reflect the degree of isohydry or anisohydry a plant exhibits. Isohydric species, which tend to be more susceptible to cavitation, will more readily

regulate their stomata to avoid adverse physiological consequences, whereas anisohydric species, which are more cavitation resistant, allow their stomata to remain open over a larger range of leaf water potentials (Jones 1998; Tardieu & Simonneau 1998; Sade et al. 2012; Sperry, Wang, et al. 2016). Thus, PMAX can capture much more dynamic stomatal behavior than its predecessors. Water supply in PMAX is constrained by soil water status and resistance to flow across plant components (i.e. roots, stems, leaves). Resistance to flow is determined through inversion of vulnerability curves. As with the Ball-Berry-Leuning model, PMAX incorporates a Farquhar photosynthesis model sensitive to light availability, intercellular concentration of CO_2 (c_i), and enzyme kinetics, to represent the potential for photosynthetic gain (Farquhar et al. 2001). Optimal stomatal conductance in PMAX is determined by maximizing the difference between photosynthetic gain and hydraulic cost (Wolf et al. 2016; Sperry, Venturas, et al. 2016).

Although the Profit Maximization model was designed for woody C_3 species, the underlying assumptions of the model are equally applicable to C_4 grasses, given the C_3 photosynthesis model is replaced with a C_4 photosynthesis model (Collatz et al. 1992; Jenerette et al. 2009). Using an optimization model in conjunction with field data can be particularly advantageous in assessing water use dynamics, as measured behavior that deviates from the predicted optima suggests alternative controls over water use not accounted for by the model. In sorghum, we hypothesized two alternative drivers of stomatal regulation not accounted for by PMAX: VPD and air temperature. VPD has been shown to generate a feed-forward response to stomatal regulation, whereby high vapor pressure deficit, which accelerates water loss, can induce stomatal closure to

conserve water resources (Leuning 1995; Buckley 2005; Buckley & Mott 2013; Sperry, Wang, et al. 2016). This response has been observed in some sorghum cultivars, touted for their robust drought tolerance (Gholipoor et al. 2010; Choudhary et al. 2013; Shekoofa et al. 2014; Riar et al. 2015). However, growing environments with high daytime temperatures tend to select against this conservative behavior in response to VPD, presumably to facilitate transpirational cooling (Machado & Paulsen 2001; Riar et al. 2015). Evaporation and water flow through the leaf reduces leaf temperature, effectively de-coupling leaf temperature from air temperature (Farquhar & Sharkey 1982; Singh et al. 1985; Singh & Singh 1988; Grantz & Meizner 1990). Accordingly, declining stomatal conductance reduces this buffer between leaf and air temperature. When temperatures are mild, tight coupling between air and leaf temperatures is not problematic, however, lack of transpirational cooling in the face of extreme temperatures could threaten irreversible damage to photosynthetic machinery (Farquhar & Sharkey 1982; Riar et al. 2015). Thus, transpirational cooling may be essential for the survival of sorghum cultivars adapted to particularly hot environments.

Our sorghum crop, grown in California's Imperial Valley, was regularly exposed to temperatures in excess of 40 °C and experienced varying levels of drought stress between irrigation events. Despite this extreme environment, we achieved high biomass yields competitive with other highly productive grasses grown in milder climates (Oikawa et al. 2015; Fertitta-Roberts et al. 2017). While stress tolerance is universally valued in agriculture, it may particularly important for biofuel feedstocks, which are increasingly grown on marginal lands to avoid land use competition with food crops

(Monti et al. 2009; Schmer et al. 2014; Searchinger & Heimlich 2015). Plant-based biofuels are a growing part of our fuel economy, currently constituting the largest source of renewable energy worldwide (Hood 2016). However, several concerns have been raised regarding the sustainability of plant-based biofuels. In addition to their demands on land area, biofuels contribute to local air and water pollution and vary widely in their GHG intensity, with some biofuels showing little or no advantage over conventional fuels when emissions over the entire life cycle are considered (Brentrup et al. 2004; Luo et al. 2009; Borrion et al. 2012; Oikawa et al. 2015; Robertson et al. 2008; Ruan et al. 2016). The life cycle of a product encompasses all material, energy, and waste flows associated with the generation, use, and disposal of that product. When evaluating the global warming potential (GWP) of fuel products, it is critically important to consider sources of GHGs throughout the life cycle as less comprehensive evaluations can be misleading (Adler et al., 2012; Adler et al., 2007; Borrion et al., 2012; Fu et al., 2003).

In chapter two, we evaluate life cycle environmental impacts associated with sorghum bioenergy production in the Imperial Valley using coupled crop and life cycle assessment models. Life cycle assessment (LCA) provides a comprehensive, quantitative framework for assessing the environmental impacts of a product. This methodology entails three primary steps: (1) goal and scope definition, (2) compilation of a life cycle inventory, (3) and characterization of environmental impacts (ISO 2006a; ISO 2006b). Defining a clear goal for an LCA is helpful in determining the most relevant scope of analysis. For instance, when evaluating the environmental impacts associated with food crop production, it is both irrelevant and impractical to consider material energy, and

waste flows associated with the "use" and "disposal" phases of the lifecycle (e.g. preparation, consumption, degradation). Conversely, when evaluating the environmental impacts of a fuel product, it is important to consider these phases, as fuels are generally distributed and combusted in a predictable manner which has important consequences for life cycle GWP. The scope of analysis also refers to the system boundaries employed. First order system boundaries include only material and energy flows related to production and transportation and are rarely employed in LCA because of their limited scope. Second order system boundaries are the most common and include all material, energy, and waste flows in the life cycle except those associated with infrastructure and capital goods (e.g. facilities and machinery) (Borrion et al. 2012; B. A. Linquist et al. 2012). Third order system boundaries include material, energy, and waste flows associated with infrastructure and capital goods, but are challenging to implement as determining the fractional contributions of facilities and machinery to the life cycle can be difficult.

Once the goal and scope of an LCA have been defined, a life cycle inventory is complied, which details all of the chemical compounds consumed and produced throughout the life cycle. Characterization models are then employed to quantify the environmental impacts associated with this chemical inventory. These characterization models quantify the contributions of various compounds to each impact category, relative to a reference compound. For example, in the case of global warming potential (GWP), methane (CH_4) is known to be 25 times more potent than CO_2 (Paustian et al. 2006), so we can express the GWP of 1 kg CH_4 and 1 kg CO_2 as 26 CO_2 equivalents

(CO_2e). The number of impact categories considered, their scope, and the assumptions upon which impacts are based varies widely across characterization models (Borrion et al. 2012). We use the EPA's Tool for the Reduction and Characterization of environmental Impacts (TRACI), which characterizes mid-point impacts to nine categories pertaining to human health and the environment (Bare et al. 2003). Mid-point models characterize impacts along the cause-and-effect chain (e.g. global warming potential) but prior to the end point of the chain (e.g. average global temperature increasing by 1 °C), making them easier to quantify than end-point impacts (Bare et al. 2000; Brilhuis-Meijer 2014).

When the goal of an LCA is to provide a general evaluation of the environmental impact of a production system, it is useful to assess these impacts under a variety of plausible scenarios. In the case of land-grown biofuels, emissions associated with the generation and use of nitrogen (N) fertilizers can be a particularly important determinant of life cycle GHGs and other environmental impacts (Borrion et al., 2012; Fazio & Monti, 2011; Ruan et al., 2016; von Blottnitz & Curran, 2007). Both the production and use of N fertilizers are GHG-intensive, however, efficient use of N can improve crop yields. From a global perspective, it is useful to express GWP in terms of yielded product (i.e. $CO_2e\ kg^{-1}$), therefore, if the yield benefits of N fertilizer outweigh the emissions associated with its production and use, N fertilizers may reduce the GWP of feedstock production. Accordingly, assumptions regarding N management during feedstock production in the biofuels life cycle can significantly impact GWP (Lamb et al. 2003; Boehmel et al. 2008; Schmer et al. 2008; Schmer et al. 2014; Mbonimpa et al. 2016).

Assessing the impacts of N management on feedstock production typically requires extensive field trials, which can be costly and time consuming. Instead, we coupled a smaller field trial with a crop modeling system to simulate the effects of varying N management strategies on Imperial Valley sorghum yields across thirty years of historical weather scenarios (Fertitta-Roberts et al. 2017).

We used the Decision Support System for Agrotechnology Transfer (DSSAT) to model sorghum production under varying environmental and management conditions (Jones et al. 2003). DSSAT hosts a variety of crop simulation models that can be coupled with user-defined inputs of soil conditions, meteorological data, and management choices. Inputs to the soil module include physical, chemical, and biological attributes. The weather module requires daily inputs of minimum and maximum air temperature, precipitation, solar radiation, dew point, humidity, and wind. Initial field conditions and preparations (e.g. tillage, residue incorporation), planting date and arrangement (e.g. planting density, row spacing), agrochemical applications, irrigation scheduling, and harvesting processes are defined in the management module. Simulations of crop growth and associated changes in soil water, organic matter, and nutrient balances are process-based and are conducted at hourly to daily time-steps assuming a homogenous land area and crop growth. Growth and development is based on general soil-plant-atmosphere dynamics and specific genetic information regarding crop physiology, allometry, phenological development, and stress tolerance (Jones et al. 2003; White et al. 2013). DSSAT has been widely used to rapidly explore the effects of management practices and environmental conditions on crop yields (Timsina & Humphreys 2006; Thorp et al. 2008;

Wu et al. 2013; Msongaleli et al. 2014; Rosenzweig et al. 2014; Ruan et al. 2016). Coupling DSSAT output with life cycle assessment is a promising tool for exploring the environmental impacts associated with distinct management regimes (Ruan et al. 2016; Fertitta-Roberts et al. 2017). This coupled modeling system can help highlight pathways for more sustainable agricultural production.

As in our sorghum feedstock production system, nitrogen management plays an important role in determining the life cycle GWP of most cropping systems (Smith et al. 2007). Conversely, in rice production, irrigation management tends to dictate life cycle GWP. This divergence arises from a shift in soil biogeochemical fluxes driven by the flooded conditions in which rice is conventionally grown. Most cereal crops experience fluctuations in soil water status, but generally maintain an aerobic soil environment. Denitrification of inorganic nitrogen fertilizers during soil drying and rewetting cycles can produce large fluxes of nitrous oxide (N_2O) (Bouwman 1998; Liang et al. 2015). However, N_2O production is inhibited by anaerobic conditions induced by continuous flooding. This results in N_2O fluxes in flooded rice systems that are generally an order of magnitude lower than those typical of non-flooded cropping systems (De Klein et al. 2006). Conversely, anaerobic decomposition of organic matter under flooded conditions promotes CH_4 production. CH_4 can then be oxidized and released to the atmosphere through ebullition and plant-mediated transport (Conrad 2002; Lasco et al. 2006; Shao et al. 2017). Although CH_4 is a less potent GHG than N_2O, CH_4 fluxes in flooded rice systems tend to be several orders of magnitude greater than N_2O fluxes in other cereal cropping systems. As a result, total GHG emissions produced during rice cultivation are

estimated to be approximately four times those of other major cereal cropping systems (B. Linquist et al. 2012). Efforts to reduce the GWP of rice production have largely been centered around the practice of alternate wetting and drying (AWD), which entails periodic drainage of the field throughout the growing season (Bouman & Tuong 2001; Yao et al. 2012; Linquist et al. 2015; LaHue et al. 2016).

Chapter three explores the GHG mitigation potential of alternate wetting and drying in northern California rice from a life cycle perspective using coupled crop and LCA models. Periodic drainage during AWD inhibits CH_4 emissions by inducing aerobic soil conditions. Accordingly, more frequent and severe dry-downs, which increase the duration of aerobic soil conditions, should result in greater mitigation of CH_4 fluxes (Hou et al. 2000). This phenomena is generally supported in the literature, however, a great deal of variation persists in both field and modeled measures of the CH_4 mitigation potential associated with AWD (Hokazono & Hayashi 2012; Linquist et al. 2015; LaHue et al. 2016). Further, as with the dichotomous role of nitrogen in determining the life cycle GWP of non-flooded cropping systems, water management can have both advantageous and adverse impacts on the GWP of rice systems. While AWD can mitigate CH_4 production, a growing body of evidence suggests yields may be adversely impacted by AWD (Carrijo et al. 2017). Although variation persists across studies, these adverse yield impacts tend increase with increasing frequency, and particularly, with increasing severity of dry-downs during AWD. Thus, it appears that irrigation scenarios with the highest potential for CH_4 mitigation also have the highest potential for reducing grain yields. From a global perspective, where GWP is best normalized by yield, understanding

the magnitude of this tradeoff between CH_4 mitigation and yield reduction is critically important to gauging the effectiveness of AWD as a GHG-mitigation strategy. LCA is a powerful tool for contextualizing these tradeoffs.

We used field data collected throughout Butte County to parameterize a rice model in DSSAT in order to simulate the yield impacts of a range of AWD scenarios varying in the severity and frequency of midseason dry-downs. CH_4 emissions associated with these production management scenarios were modeled with the Peatland Ecosystem Photosynthesis, Respiration, and Methane Transport model (PEPRMT). PEPRMT is a processed-based model of wetland carbon exchange parameterized with high resolution carbon flux data obtained in northern California wetlands (Oikawa et al. 2014; Oikawa et al. 2017). Carbon flux dynamics in PEPRMT are sensitive to water table height, substrate availability, leaf area, temperature, and light. Associated changes in carbon pools are simulated at half hour intervals, providing higher temporal resolution of CH_4 flux than most field studies can achieve. Acquiring high resolution data in the field requires instrumentation and resources that are cost-prohibitive and time-intensive, especially when multiple treatments are being evaluated. An alternative field approach up-scales measurements taken at daily to weekly intervals. This approach relies on linear interpolation between data points to estimate seasonal CH_4 flux (Pittelkow et al. 2014; Adviento-Borbe et al. 2015; Linquist et al. 2015; LaHue et al. 2016). Previous research has shown up-scaling from periodic chamber measurements can fail to capture important pulses and lags in response to changing soil water status, leading to large uncertainties in seasonal methane flux (Sturtevant et al. 2016; Knox et al. 2016). Robust prediction of

carbon flux dynamics at high temporal resolution makes PEPRMT a more suitable and practical tool for predicting changes in cumulative CH_4 flux under AWD (Oikawa et al. 2017). Outputs from DSSAT and PEPRMT were inputs to LCAs used to evaluated life cycle GWP or continuously flooded and AWD rice production in northern California.

Modeling tools provide important pathways for evaluating sustainability in agriculture across multiple dimensions. As a major agricultural region, California must adapt to a changing climate and play its part in helping to mitigate contributions to climate change associated with agricultural production. Field data pertaining to these goals is vital and invaluable, but must be supplemented and expanded upon with modeling tools in order to advance agricultural and ecological science at the rate demanded by global change. Here, we couple field data with a variety of modeling systems to evaluate stress tolerance and environmental impacts in California sorghum and rice.

References

Adler, P.R. et al., 2012. Mitigation Opportunities for Life-Cycle Greenhouse Gas Emissions during Feedstock Production across Heterogeneous Landscapes. In *Managing Agricultural Greenhouse Gases*. Elsevier, pp. 203–219.

Adler, P.R., Grosso, S.J. Del & Parton, W.J., 2007. Life-cycle assessment of net greenhouse-gas flux for bioenergy cropping systems. *Ecological Applications*, 17(3), pp.675–691.

Adviento-Borbe, M.A. et al., 2015. Methane and Nitrous Oxide Emissions from Flooded Rice Systems following the End-of-Season Drain. *Journal of environmental quality*, 44(4), pp.1071–9.

Ball, J.T., Woodrow, I.E. & Berry, J.A., 1987. A Model Predicting Stomatal Conductance and its Contribution to the Control of Photosynthesis under Different Environmental Conditions. In *Progress in Photosynthesis Research*. Dordrecht: Springer Netherlands, pp. 221–224.

Bare, J.C. et al., 2000. Midpoints versus endpoints: The sacrifices and benefits. *The International Journal of Life Cycle Assessment*, 5(6), pp.319–326.

Bare, J.C. et al., 2003. The Tool for the Reduction and Assessment of Chemical and Other Environmental Impacts. *Journal of Industrial Ecology*, 6(3–4), pp.48–78.

Bauer, S.E., Tsigaridis, K. & Miller, R., 2016. Significant atmospheric aerosol pollution caused by world food cultivation. *Geophysical Research Letters*, 43(10), pp.5394–5400.

Belton, P.S. & Taylor, J.R.., 2004. Sorghum and millets: protein sources for Africa. *Trends in Food Science & Technology*, 15(2), pp.94–98.

Biernath, C. et al., 2011. Evaluating the ability of four crop models to predict different environmental impacts on spring wheat grown in open-top chambers. *European Journal of Agronomy*, 35(2), pp.71–82.

von Blottnitz, H. & Curran, M.A., 2007. A review of assessments conducted on bio-ethanol as a transportation fuel from a net energy, greenhouse gas, and environmental life cycle perspective. *Journal of Cleaner Production*, 15(7), pp.607–619.

Boehmel, C., Lewandowski, I. & Claupein, W., 2008. Comparing annual and perennial energy cropping systems with different management intensities. *Agricultural Systems*, 96(1), pp.224–236.

Borrion, A.L., McManus, M.C. & Hammond, G.P., 2012. Environmental life cycle assessment of lignocellulosic conversion to ethanol: A review. *Renewable and Sustainable Energy Reviews*, 16(7), pp.4638–4650.

Bouman, B.A.. & Tuong, T.., 2001. Field water management to save water and increase its productivity in irrigated lowland rice. *Agricultural Water Management*, 49(1), pp.11–30.

Bouwman, A.F., 1998. Environmental science: Nitrogen oxides and tropical agriculture. *Nature*, 392(6679), pp.866–867.

Brentrup, F. et al., 2004. Environmental impact assessment of agricultural production systems using the life cycle assessment methodology. *European Journal of Agronomy*, 20(3), pp.247–264.

Brilhuis-Meijer, E., 2014. Consider Your Audience When Doing Impact Assessment. *PRé Sustainability*.

Buckley, T.N., 2005. The control of stomata by water balance. *New Phytologist*, 168(2), pp.275–292.

Buckley, T.N. & Mott, K.A., 2013. Modelling stomatal conductance in response to environmental factors. *Plant, Cell & Environment*, 36(9), pp.1691–1699.

Carrijo, D.R., Lundy, M.E. & Linquist, B.A., 2017. Rice yields and water use under alternate wetting and drying irrigation: A meta-analysis. *Field Crops Research*, 203, pp.173–180.

CDFA, 2017. *2016 Crop Year Report*, Sacramento, CA. Available at: https://www.cdfa.ca.gov/statistics/.

Cherubini, F. & Strømman, A.H., 2011. Life cycle assessment of bioenergy systems: State of the art and future challenges. *Bioresource Technology*, 102(2), pp.437–451.

Choudhary, S., Sinclair, T.R. & Prasad, P.V.V., 2013. Hydraulic conductance of intact plants of two contrasting sorghum lines, SC15 and SC1205. *Functional Plant Biology*, 40(7), p.730.

Collatz, G., Ribas-Carbo, M. & Berry, J., 1992. Coupled Photosynthesis-Stomatal Conductance Model for Leaves of C4 Plants. *Australian Journal of Plant Physiology*, 19(5), p.519.

Conrad, R., 2002. Control of microbial methane production in wetland rice fields. *Nutrient Cycling in Agroecosystems*, 64(1/2), pp.59–69.

Cowan, I.R., 1978. Stomatal Behaviour and Environment. *Advances in Botanical Research*, 4, pp.117–228.

Cowan, I.R. & Farquhar, G.D., 1977. Stomatal function in relation to leaf metabolism and environment. *Symposia of the Society for Experimental Biology*, 31, pp.471–505. Available at: http://www.ncbi.nlm.nih.gov/pubmed/756635 [Accessed November 21, 2017].

Djanaguiraman, M. et al., 2014. Physiological differences among sorghum (Sorghum bicolor L. Moench) genotypes under high temperature stress. *Environmental and Experimental Botany*, 100, pp.43–54.

FAO & NRI, 1999. *Sorghum: Post-harvest Operations*, Rome, Italy.

Farquhar, G.D., Von Caemmerer, S. & Berry, J.A., 1980. A Biochemical Model of Photosynthetic CO 2 Assimilation in Leaves of C 3 Species. *Planta*, 149, pp.78–90.

Farquhar, G.D., von Caemmerer S, S. von & Berry, J.A., 2001. Models of photosynthesis. *Plant physiology*, 125(1), pp.42–5.

Farquhar, G.D. & Sharkey, T.D., 1982. Stomatal Conductance and Photosynthesis. *Annual review of plant physiology*, 33, pp.317–345.

Fazio, S. & Monti, A., 2011. Life cycle assessment of different bioenergy production systems including perennial and annual crops. *Biomass and Bioenergy*, 35(12), pp.4868–4878.

Fertitta-Roberts, C. et al., 2017. Trade-offs across productivity, GHG intensity, and pollutant loads from second-generation sorghum bioenergy. *GCB Bioenergy*, 9(12), pp.1764–1779.

Frigg, R. & Hartmann, S., 2017. Models in Science. In E. N. Zalta, ed. *Stanford encyclopedia of philosophy.* Stanford, CA: Stanford University.

Fu, G.Z., Chan, A.W. & Minns, D.E., 2003. Life Cycle assessment of bio-ethanol derived from cellulose. *The International Journal of Life Cycle Assessment*, 8(3), pp.137–141.

Gershenfeld, N., 2011. 2011: What Scientific Concept would Improve Everybody's Cognitive Toolkit? *Edge*.

Ghannoum, O., 2009. C4 photosynthesis and water stress. *Annals of botany*, 103(4), pp.635–44.

Gholipoor, M. et al., 2010. Genetic variability of transpiration response to vapor pressure deficit among sorghum genotypes. *Field Crops Research*, 119(1), pp.85–90.

Godfray, H.C.J. et al., 2010. Food Security: The Challenge of Feeding 9 Billion People. *Science*, 327(5967).

Grantz D.A. & Meinzer, F.C., 1990. Stomatal response to humidity in a sugarcane field:

simultaneous porometric and micrometeorological measurements*. *Plant, Cell and Environment*, 13(1), pp.27–37.

Guinée, J.B. et al., 2011. Life Cycle Assessment: Past, Present, and Future. *Environmental Science & Technology*, 45(1), pp.90–96.

Hammer, G. et al., 2006. Models for navigating biological complexity in breeding improved crop plants. *Trends in Plant Science*, 11(12), pp.587–593.

Hayhoe, K. et al., 2004. Emissions pathways, climate change, and impacts on California. *Proceedings of the National Academy of Sciences of the United States of America*, 101(34), pp.12422–7.

Hokazono, S. & Hayashi, K., 2012. Variability in environmental impacts during conversion from conventional to organic farming: a comparison among three rice production systems in Japan. *Journal of Cleaner Production*, 28, pp.101–112.

Hood, E.E., 2016. Plant-based biofuels. *F1000Research*, 5.

Hou, A.X. et al., 2000. Methane and Nitrous Oxide Emissions from a Rice Field in Relation to Soil Redox and Microbiological Processes. *Soil Science Society of America Journal*, 64(6), p.2180.

IPCC, 2014. Agriculture, Forestry, and Other Land Use (AFOLU). In T. Krug & G.-J. Nabuurs, eds. *Climate Change 2014: Mitigation of Climate Change*. Geneva Switzerland: IPCC, pp. 811–922.

ISO, 2006a. *14040: Environmental management–life cycle assessment–principles and framework*, Geneva, Swtizerland.

ISO, 2006b. *14044: Environmental management–life cycle assessment–requirements and guidelines*, Geneva, Swtizerland.

Jenerette, G.D. et al., 2009. Gross primary production variability associated with meteorology, physiology, leaf area, and water supply in contrasting woodland and grassland semiarid riparian ecosystems. *Journal of Geophysical Research*, 114(G4), p.G04010.

Jones, H.G., 1998. Stomatal control of photosynthesis and transpiration. *Journal of Experimental Botany*, 49, pp.387–398.

Jones, J.. et al., 2003. The DSSAT cropping system model. *European Journal of Agronomy*, 18(3–4), pp.235–265.

De Klein, C. et al., 2006. N2O Emissions from Managed Soils and CO2 Emissions from Lime and Urea Application. In *2006 IPCC Guidelines for National Greenhouse Gas Inventories*. Geneva, Swtizerland.

Knox, S.H. et al., 2016. Biophysical controls on interannual variability in ecosystem-scale CO2 and CH4 exchange in a California rice paddy. *Journal of Geophysical Research: Biogeosciences*, 121(3), pp.978–1001.

KOCACINAR, F. & SAGE, R.F., 2003. Photosynthetic pathway alters xylem structure and hydraulic function in herbaceous plants. *Plant, Cell and Environment*, 26(12), pp.2015–2026.

LaHue, G.T. et al., 2016. Alternate wetting and drying in high yielding direct-seeded rice systems accomplishes multiple environmental and agronomic objectives. *Agriculture, Ecosystems & Environment*, 229, pp.30–39.

Lamb, J.F.S., Sheaffer, C.C. & Samac, D.A., 2003. Population Density and Harvest Maturity Effects on Leaf and Stem Yield in Alfalfa. *Agronomy Journal*, 95(3), pp.635–641.

Lamboni, M. et al., 2009. Multivariate global sensitivity analysis for dynamic crop models. *Field Crops Research*, 113(3), pp.312–320.

Lasco, R.D. et al., 2006. Cropland. In *2006 IPCC Guidelines for National Greenhouse Gas Inventories*. Geneva, Swtizerland.

Lesk, C., Rowhani, P. & Ramankutty, N., 2016. Influence of extreme weather disasters on global crop production. *Nature*, 529(7584), pp.84–87.

Leuning, R., 1995. A critical appraisal of a combined stomatal-photosynthesis model for C3 plants. *Plant, Cell and Environment*, 18(4), pp.339–355.

Leuning, R., 2002. Temperature dependence of two parameters in a photosynthesis model. *Plant, Cell and Environment*, 25(9), pp.1205–1210.

Liang, L.L. et al., 2015. Regulation of CO2 and N2O fluxes by coupled carbon and nitrogen availability. *Environmental Research Letters*, 10(3), p.34008.

Linquist, B. et al., 2012. An agronomic assessment of greenhouse gas emissions from major cereal crops. *Global Change Biology*, 18(1), pp.194–209.

Linquist, B.A. et al., 2012. Fertilizer management practices and greenhouse gas emissions from rice systems: A quantitative review and analysis. *Field Crops Research*, 135, pp.10–21.

Linquist, B.A. et al., 2015. Reducing greenhouse gas emissions, water use, and grain arsenic levels in rice systems. *Global Change Biology*, 21(1), pp.407–417.

Lobell, D.B., Bonfils, C.J., et al., 2008. Irrigation cooling effect on temperature and heat index extremes. *Geophys. Res. Lett*, 35.

Lobell, D.B., Burke, M.B., et al., 2008. Prioritizing climate change adaptation needs for food security in 2030. *Science (New York, N.Y.)*, 319(5863), pp.607–10.

Lobell, D.B. & Burke, M.B., 2008. Why are agricultural impacts of climate change so uncertain? The importance of temperature relative to precipitation. *Environ. Res. Lett*, 3.

Lobell, D.B. & Field, C.B., 2007. Global scale climate–crop yield relationships and the impacts of recent warming. *Environmental Research Letters*, 2(1), p.14002.

Luo, L., van der Voet, E. & Huppes, G., 2009. Life cycle assessment and life cycle costing of bioethanol from sugarcane in Brazil. *Renewable and Sustainable Energy Reviews*, 13(6), pp.1613–1619.

Machado, S. & Paulsen, G.M., 2001. Combined effects of drought and high temperature on water relations of wheat and sorghum. *Plant and Soil*, 233(2), pp.179–187.

Mbonimpa, E.G. et al., 2016. Nitrogen rate and landscape impacts on life cycle energy use and emissions from switchgrass-derived ethanol. *GCB Bioenergy*, 8(4), pp.750–763.

Medlyn, B.E. et al., 2002. Temperature response of parameters of a biochemically based model of photosynthesis. II. A review of experimental data. *Plant, Cell and Environment*, 25(9), pp.1167–1179.

Meinzer, F.C. et al., 2010. The blind men and the elephant: the impact of context and scale in evaluating conflicts between plant hydraulic safety and efficiency. *Oecologia*, 164(2), pp.287–296.

Monti, A., Fazio, S. & Venturi, G., 2009. Cradle-to-farm gate life cycle assessment in perennial energy crops. *European Journal of Agronomy*, 31(2), pp.77–84.

Msongaleli, B. et al., 2014. Sorghum Yield Response to Changing Climatic Conditions in Semi-Arid Central Tanzania: Evaluating Crop Simulation Model Applicability. *Agricultural Sciences*, 5(10), pp.822–833.

Ocheltree, T.W., Nippert, J.B. & Prasad, P.V.V., 2016. A safety vs efficiency trade-off identified in the hydraulic pathway of grass leaves is decoupled from photosynthesis, stomatal conductance and precipitation. *New Phytologist*, 210(1), pp.97–107.

Oikawa, P.Y. et al., 2017. Evaluation of a hierarchy of models reveals importance of substrate limitation for predicting carbon dioxide and methane exchange in restored wetlands. *Journal of Geophysical Research: Biogeosciences*, 122(1), pp.145–167.

Oikawa, P.Y. et al., 2014. Unifying soil respiration pulses, inhibition, and temperature hysteresis through dynamics of labile soil carbon and O2. *Journal of Geophysical Research: Biogeosciences*, 119(4), pp.521–536.

Oikawa, P.Y., Ge, C., et al., 2015. Unusually high soil nitrogen oxide emissions influence air quality in a high-temperature agricultural region. *Nature Communications*, 6, p.8753.

Oikawa, P.Y., Jenerette, G.D. & Grantz, D.A., 2015. Offsetting high water demands with high productivity: Sorghum as a biofuel crop in a high irradiance arid ecosystem. *GCB Bioenergy*, 7(5), pp.974–983.

Paustian, K., Ravindranath, N.. & van Amstel, A., 2006. *2006 IPCC Guidelines for National Greenhouse Gas Inventories: Agriculture, Forestry and Other Land Uses*, Geneva, Swtizerland.

Pittelkow, C.M. et al., 2014. Nitrogen Management and Methane Emissions in Direct-Seeded Rice Systems. *Agronomy Journal*, 106(3), p.968.

Prasad, P.V.., Boote, K.J. & Allen, L.H., 2006. Adverse high temperature effects on pollen viability, seed-set, seed yield and harvest index of grain-sorghum [Sorghum bicolor (L.) Moench] are more severe at elevated carbon dioxide due to higher tissue temperatures. *Agricultural and Forest Meteorology*, 139(3), pp.237–251.

Prasad, P.V.V. et al., 2008. Sensitivity of Grain Sorghum to High Temperature Stress during Reproductive Development. *Crop Science*, 48(5), p.1911.

Riar, M.K., Sinclair, T.R. & Prasad, P.V.V., 2015. Persistence of limited-transpiration-rate trait in sorghum at high temperature. *Environmental and Experimental Botany*, 115, pp.58–62.

Robertson, G.P. et al., 2008. Agriculture: Sustainable biofuels redux. *Science*, 322(5898), pp.49–50. Available at: http://www.ncbi.nlm.nih.gov/pubmed/18832631.

Rosenzweig, C. et al., 2014. Assessing agricultural risks of climate change in the 21st century in a global gridded crop model intercomparison. *Proceedings of the National Academy of Sciences of the United States of America*, 111(9), pp.3268–73.

Ruan, L. et al., 2016. Nitrogen fertilization challenges the climate benefit of cellulosic biofuels. *Environmental Research Letters*, 11.

Sack, L. & Holbrook, N.M., 2006. Leaf Hydraulics. *Annual Review of Plant Biology*, 57(1), pp.361–381.

Sade, N., Gebremedhin, A. & Moshelion, M., 2012. Risk-taking plants. *Plant Signaling & Behavior*, 7(7), pp.767–770.

Sage, R.F., 2004. The evolution of C $_4$ photosynthesis. *New Phytologist*, 161(2), pp.341–370.

Schlenker, W. et al., 2010. Robust negative impacts of climate change on African agriculture. *Environmental Research Letters*, 5(1), p.14010..

Schmer, M. et al., 2014. Energy Potential and Greenhouse Gas Emissions from Bioenergy Cropping Systems on Marginally Productive Cropland S. Hu, ed. *PLoS ONE*, 9(3), pp.489–501.

Schmer, M.R. et al., 2008. Net energy of cellulosic ethanol from switchgrass. *Proceedings of the National Academy of Sciences*, 105(2), pp.464–469.

Searchinger, T. & Heimlich, R., 2015. *Avoiding bioenergy competition for food crops and land*, Washington DC, US.

Shao, X. et al., 2017. Methane production potential and emission at different water levels in the restored reed wetland of Hangzhou Bay J. Liu, ed. *PLOS ONE*, 12(10), p.e0185709.

Shekoofa, A., Balota, M. & Sinclar, T.R., 2014. Limited-transpiration trait evaluated in growth chamber and field for sorghum genotypes. *Environmental and Experimental Botany*, 99, pp.175–179.

Sinclair, T.R. & Seligman, N.G., 1996. Crop Modeling: From Infancy to Maturity. *Agronomy Journal*, 88(5), p.698.

Singh, B.R. & Singh, D.P., 1988. Sensing of moisture stress effects by infra-red thermometry in sorghum, maize and pearl millet. *Journal of the Indian Society of Remote Sensing*, 16(2), pp.53–57.

Singh, D.P. et al., 1985. Transpirational Cooling as a Screening Technique for Drought Tolerance in Oil Seed Transpirational Cooling as a Screen for Drought Tolerance in Oil Seed Brassicas. *Source: Annals of Botany*, 56(6), pp.815–820.

Smith, P. et al., 2007. Agriculture. In *Climate Change 2007: Mitigation. Contribution of Working Group III to the Fourth Assessment Report of the Intergovernmental Panel on Climate Change*. Cambirdge, United Kingdom and New York, NY. USA: Cambridge University Press.

Snyder, M.A. et al., 2002. Climate responses to a doubling of atmospheric carbon dioxide for a climatically vulnerable region. *Geophysical Research Letters*, 29(11), p.1514.

Sperry, J.S., Wang, Y., et al., 2016. Pragmatic hydraulic theory predicts stomatal responses to climatic water deficits. *New Phytologist*, 212(3), pp.577–589.

Sperry, J.S., Venturas, M.D., et al., 2016. Predicting stomatal responses to the environment from the optimization of photosynthetic gain and hydraulic cost. *Plant, Cell & Environment*.

Sturtevant, C. et al., 2016. Identifying scale-emergent, nonlinear, asynchronous processes of wetland methane exchange. *Journal of Geophysical Research: Biogeosciences*, 121(1), pp.188–204.

Tardieu, F. & Simonneau, T., 1998. Variability among species of stomatal control under fluctuating soil water status and evaporative demand: modelling isohydric and anisohydric behaviours. *Journal of Experimental Botany*, 49, pp.419–432.

Thorp, K.R. et al., 2008. Methodology for the use of DSSAT models for precision agriculture decision support. *Computers and Electronics in Agriculture*, 64(2), pp.276–285.

Timsina, J. & Humphreys, E., 2006. Performance of CERES-Rice and CERES-Wheat models in rice–wheat systems: A review. *Agricultural Systems*, 90(1), pp.5–31.

Trouwborst, G. et al., 2010. The responses of light interception, photosynthesis and fruit yield of cucumber to LED-lighting within the canopy. *Physiologia Plantarum*, 138(3), pp.289–300.

Tyree, M.T. & Sperry, J.S., 1988. Do woody plants operate near the point of catastrophic xylem dysfunction caused by dynamic water stress? : answers from a model. *Plant physiology*, 88(3), pp.574–80.

Tyree, M.T. & Zimmermann, M.H., 2002. *Xylem Structure and the Ascent of Sap*, Berlin, Heidelberg: Springer .

de Wet, J.M.J., 1978. Systematics and Evolution of Sorghum Sect. Sorghum (Gramineae). *American Journal of Botany*, 65(4), p.477.

White, J.W. et al., 2013. Integrated description of agricultural field experiments and production: The ICASA Version 2.0 data standards. *Computers and Electronics in Agriculture*, 96, pp.1–12.

Wolf, A., Anderegg, W.R.L. & Pacala, S.W., 2016. Optimal stomatal behavior with competition for water and risk of hydraulic impairment. *Proceedings of the National Academy of Sciences of the United States of America*, 113(46), pp.E7222–E7230.

Wu, C., Anlauf, R. & Ma, Y., 2013. Application of the DSSAT Model to Simulate Wheat Growth in Eastern China. *Journal of Agricultural Science*, 5(5), p.198.

Yao, F. et al., 2012. Agronomic performance of high-yielding rice variety grown under alternate wetting and drying irrigation. *Field Crops Research*, 126, pp.16–22.

Chapter 1

A tale of two stressors: How stomatal regulation balances heat and drought tolerance in sorghum

Cara Fertitta-Roberts, David A. Grantz, Louis S. Santiago, Patricia Y. Oikawa, Liyin Liang, G. Darrel Jenerette

---

1.1 Abstract

Sorghum is a globally important source of food, feed, and fuel that has gained increasing attention for its tolerance to extreme environments. Uncovering the mechanisms behind stress tolerance requires an understanding of how sorghum regulates water use. Here, we combine field data collected in a high temperature, arid environment with an optimized model of stomatal regulation to evaluate controls over water use in *Sorghum bicolor* (cv. Photoperiod LS). Water use dynamics were adequately predicted by the model when soil water was limiting and temperatures were relatively mild (r^2 = 0.71 – 0.78). However, the model predicted only half of transpirative water loss measured when daytime temperatures were extreme but soils were well-watered. In measured data, higher rates of transpiration were associated with greater leaf cooling (r^2 = 0.50). Analysis of seasonal patterns in water use dynamics using partitioned eddy covariance data suggested the model overestimated the effect of soil water potential on transpiration (slope = -1.42 and -1.04 for modeled and measured data, respectively) and

underestimated the effect of air temperature (slope = 0.33 and 0.67, respectively). Our results suggest two pathways govern stress responses in heat-tolerant sorghum: (1) avoiding damage to photosynthetic machinery through stomatal opening to allow greater transpirational cooling and (2) avoiding xylem cavitation, induced by water stress, through stomatal closure. These two opposing controls appear to be balanced by stomatal sensitivity to leaf water potential (P_{leaf}), where transpirational cooling is constrained as P_{leaf} declines and threat of xylem cavitation increases. This dynamic water use strategy allows sorghum to achieve a delicate balance between heat and drought tolerance while maintaining high rates of productivity. Our results suggest application of PMAX to annual crops has great potential, but inclusion of transpirational cooling may be necessary to properly account for stomatal regulation in heat-tolerant species.

1.2 Introduction

Sorghum is one of the most important global crops, occupying > 40 million ha of land area and serving as source of food, feed, and fuel around the world (FAO & NRI 1999). This versatile grass has garnered increasing attention for its ability to withstand extreme temperatures and prolonged drought. These traits make sorghum an ideal candidate for increased production under climate change (Bita & Gerats 2013; Singh et al. 2014). However, while much emphasis has been placed on identifying varietals with the highest drought tolerance (Wright et al. 1983; Triggs et al. 2004; Gholipoor et al. 2010; Choudhary et al. 2013; Shekoofa et al. 2014), recent work suggests drought tolerance in sorghum may come at the expense of heat tolerance (Riar et al. 2015).

Enhancing our understanding of water use dynamics and their relation to stress response in sorghum is therefore an important pathway for identifying varietals best suited to withstand the wide ranging effects of climate change. Stomatal optimization models can be useful tools for discerning controls over water use dynamics. We used the Profit Maximization model (PMAX) to simulate optimal stomatal behavior based on tradeoffs between potential photosynthetic gains and hydraulic costs under variable environmental conditions to better understand controls over water use dynamics in sorghum and their implications for stress tolerance (Sperry et al. 2016).

Plant water use dynamics are largely determined by stomatal regulation. As stomata open to allow CO_2 uptake required for photosynthesis, water is lost through transpiration (Cowan 1978; Farquhar & Sharkey 1982). As light availability increases, there is greater incentive for the stomata to open to maximize photosynthetic gain. Conversely, factors such as declining soil water potential (soil drought) and increasing vapor pressure deficit (VPD; atmospheric drought) incentivize down-regulation of stomatal conductance in order to reduce transpirational water loss, particularly when soil water is limiting (Leuning 1995; Sperry & Love 2015; Sperry et al. 2016b). This mechanism has been observed in "stay green" sorghum varietals that show particularly high drought tolerance (Gholipoor et al. 2010; Choudhary et al. 2013; Shekoofa et al. 2014; Riar et al. 2015). Air temperature has received less attention in stomatal control models, but there is some evidence to support high temperatures can increase stomatal conductance in order to facilitate transpirational cooling (Farquhar & Sharkey 1982; Singh et al. 1985; Singh & Singh 1988; Grantz & Meizner 1990).

Classic models of stomatal regulation assume plants respond to changes in their environment by regulating their stomata to maintain a constant ratio of carbon gain to water loss (Cowan & Farquhar 1977; Katul et al. 2010; Medlyn et al. 2011; Prentice et al. 2014). However, the evolution of a wide spectrum of hydraulic strategies challenges this simplistic view stomatal regulation (Wolf et al. 2016). Isohydric species tightly regulate stomatal conductance in response to declining leaf water potential (P_{leaf}), sacrificing carbon uptake by reducing stomatal aperture in order to maintain a favorable P_{leaf} throughout the day. Conversely, anisohydric species keep their stomata open in spite of declining P_{leaf} in order to maintain high rates of assimilation throughout the day (Jones 1998; Tardieu & Simonneau 1998). Each strategy can be advantageous depending on the conditions that typify the plant's environment. Anisohydric species tend to be fairly resistant to drought-induced xylem cavitation, which allows them to take greater risks and reap greater rewards when conditions are favorable or mildly stressful. However, isohydric species, which are often more vulnerable to xylem cavitation, tend to fair better under prolonged exposure to stress due to their conservative water use strategy (Sade et al. 2012).

The Profit Maximization model (PMAX) incorporates dynamic stomatal responses, associated with the spectrum of isohydric to anisohydric behavior, into the framework of a classic stomatal optimization model (Sperry et al. 2016a). Transpirative water loss in PMAX is constrained by soil matric potential and cumulative resistance across plant components. Resistance to water flow is determined by each component's vulnerability to xylem cavitation in response to declining xylem pressure (Sperry et al.

2016a & b). As vessels cavitate, hydraulic conductance is lost and resistance to water flow through the plant increases. Thus, for a given set of environmental conditions, hydraulic cost can be assessed as the plant's proximity to hydraulic failure along a gradient of increasing stomatal conductance. Photosynthetic carbon gain can be assessed by the plant's proximity to the instantaneous maximum rate of assimilation (instantaneous A_{max}) possible under these environmental conditions along this same gradient of increasing stomatal conductance. The optimal rate of stomatal conductance maximizes the difference between the photosynthetic gain function and hydraulic cost function (Wolf et al. 2016; Sperry et al. 2016). Although PMAX was is designed to simulate water use dynamics in woody C_3 angiosperms, its basic hydraulic principles can be extended to C_4 grasses like sorghum. The high efficiency of C_4 photosynthesis may reduce tradeoffs between assimilation potential and water loss (Ocheltree et al. 2016), however, the same fundamental tradeoffs between photosynthetic gain and hydraulic costs persist. Accordingly, the primary assumptions of PMAX should hold for sorghum and deviations from theoretically optimal behavior may highlight alternative controls over water use. Our work also provides a valuable test of PMAX, which has yet to be evaluated using field data.

We coupled diurnal and seasonal measurements of gas exchange, energy balance, soil water status, and micrometeorological data with the Profit Maximization model to explore the environmental factors that dictate water use patterns in sorghum grown in a high temperature, arid environment. We tested the model's inherent hypothesis that stomatal conductance is primarily sensitive to light availability, soil water status, and

vulnerability to xylem cavitation. We alternatively hypothesized that VPD and temperature may play a role in determining stomatal regulation, with the former down-regulating stomatal conductance to avoid excessive water loss and associated hydraulic costs, and the latter up-regulating stomatal conductance to increase transpirational cooling and avoid damage to photosynthetic machinery. Our objectives were (1) to identify controls over water use in sorghum in response to different environmental stressors and (2) to evaluate the ability of our modified PMAX model to simulate water use dynamics in annual C_4 species.

1.3 Materials and Methods

We evaluated environmental controls over water use dynamics in *Sorghum bicolor* (cv. Photoperiod LS) using extensive field data coupled with an optimized model of stomatal regulation (Figure 1.1). Leaf-level data were used to parameterize and validate the Profit Maximization model as well as to transform eddy covariance and micrometeorological data taken at the canopy-level to better reflect conditions *in* the canopy rather than above the canopy. Diurnal measurement campaigns allowed us to assess stomatal regulation under two distinct stressors – heat stress and drought stress – while seasonal measurements were used to evaluate controls over midday transpiration rates under a wide variety of environmental conditions.

Site description

Field data were collected during the 2012 growing season on a 5.3 ha plot at the Desert Research Extension Center in Holtsville, Imperial Valley, CA (32°N 48′42.6″, 115°W 26′ 37.5″). This site was characterized by high daytime temperatures, aridity, and light intensity (41 °C, 4.6 kPa, 874 W m^{-2} seasonal averages at midday, respectively) and infrequent precipitation (20 mm $season^{-1}$) (Oikawa et al. 2015). Soil was classified as mildly alkaline deep silty clay (pH 8.1; 42% clay, 41% silt, 16% sand) with 2.34% organic matter. Prior to planting, the field was tilled, laser-leveled, and fertilized with 110 kg N ha^{-1} and 90 kg P_2O_5 ha^{-1}. *Sorghum bicolor* (cv. Photoperiod LS, Scott Seed, Inc., Hereford, TX, US) was planted at a density of 9 individuals m^{-2} on 28 February 2012. Early planting afforded by the Imperial Valley's mild winters permitted three harvests throughout the growing season. Nitrogen fertilizer was supplemented at the beginning of each growth cycle at a rate of ~ 90 kg N ha^{-1} (Fertitta-Roberts et al. 2017). Each of these three growth cycles were characterized by varying environmental conditions, with average daily VPD and T_{air} being lowest during the first growth cycle (February 28 – June 4), highest during the second growth cycle (5 June – 14 August), and intermediate during the final growth cycle (15 August – 12 November) (Oikawa et al. 2015). Irrigation was supplied by furrow flooding based on apparent plant need or when soil VWC < 0.10 cm^3 cm^{-3}.

Canopy gas exchange, micrometeorological data, and soil data

Extensive methods for collection and processing of canopy gas exchange, micrometeorological, and soil water data can be found in Oikawa et al. (2015). We used eddy-covariance and micrometeorological systems mounted on a tower in the center of the field to measure net ecosystem exchange (NEE) and evapotranspiration (ET) at thirty minute intervals throughout the growing season (Baldocchi et al. 1988; Oikawa et al. 2015). An open path IRGA was used to measure net CO_2 and H_2O flux (LI-7500 LI-CIR Biosciences, Lincoln, NE, USA). The height of these instruments was adjusted throughout the season in accordance with canopy height. The up-welling and down-welling of solar radiation were measured using a four-component net radiation sensor (NR01, Hukseflux Thermal Sensors). A Platinum Resistance Temperature and capacitive sensor probe (HMP45c, Vaisala, Helsinki, Finland) was used to measure T_{air} and relative humidity, and wind speed was measured with a 3D sonic anemometer (CSAT3, Campbell Scientific). We coupled these atmospheric data with measurements of soil VWC at corresponding thirty minute intervals using soil moisture probes buried at 2, 8, and 16 cm depths adjacent to the tower (CS616, Campbell Scientific). Filtering limits, statistical testing, corrections, and gap-filling procedures for these canopy-scale data are detailed in Oikawa et al (2015).

Diurnal campaigns: leaf water potential, gas exchange, energy balance, and micromet

We conducted two diurnal campaigns throughout the growing season to assess water stress, gas exchange, and energy balance at the leaf-level. Our diurnal campaigns took place in mature canopies on 19 July 2012 and 13 October 2012 during our second and third growth cycles, respectively. July and October campaigns took place under varying environmental conditions (Table 1.2). Our July campaign was executed during an extreme heat event, with midday temperatures in the canopy reaching 45 °C and VPD exceeding 3.18 kPa. However, the field was recently irrigated, resulting in a relatively high soil water potential. In October, soil water potential was low, resulting in moderate water stress, but daytime temperatures were nearly 10 °C lower than in July. During each campaign, we measured leaf water potential at 1 – 1.5 hour intervals from pre-dawn until dusk and leaf gas exchange, energy balance, and micrometeorological conditions at similar intervals from roughly 9 am until dusk.

Table 1.1. Average environmental conditions during our July and October measurement campaigns

Variable (unit)		**July**	**October**
Avg P_{soil}	(MPa)	-0.40	-1.02
Avg PAR	(μmol m^{-2} s^{-1})	639	634
Min T_{air}	(°C)	34	26
Max T_{air}	(°C)	45	37
Avg VPD	(kPa)	3.18	2.20
Avg wind	(m s^{-1})	4.65	3.78

We measured leaf water potential using a Scholander Pressure Chamber (PMS Instrument Company, Albany, OR). At each interval, we measured 6 upper leaves and 6 lower leaves from the northwest and southeast quadrants of our plot (n = 24 leaves total). Only intact, undamaged leaves were selected. Leaves were cut approximately 20 cm from the leaf tip and immediately bagged, placed in a cooler, and transported to the lab for pressure measurements. Once leaves were acclimated to morning light (~ 9 AM), we began coordinated measurements of leaf gas exchange, energy balance, and micrometeorological conditions using a Licor-6400 Portable Photosynthesis System (LI-COR). We selected 6 plants in the middle of the northwest and southeast quadrants of the field to make continuous observations. One upper leaf and one lower leaf from each plant were tagged for gas exchange measurements. In the event a leaf was damaged during the measurement campaign, we selected the nearest neighboring leaf to replace it. Measurements were made under 400 ppm CO_2 and ambient PAR (photosynthetically active radiation) conditions, and logged three times over the course of one minute following stabilization.

Light and AC_i photosynthesis response curves for sorghum were collected in August 2012, September 2012, and again in August during the 2013 growing season. Curves were obtained with a minimum of three replicates collected in both the northwest and southeast quadrants of our plot ($n \geq 6$ for each campaign). We used the Li-6400 auto-program for light and AC_i response curves (Figure S1.1). We used Photosynthesis Assistant (ver. 1.1; Dundee Scientific, Dundee, UK) to estimate maximum photosynthetic rate (V_{max}), Michaelis-Menten constants for carboxylation (k_c) and

oxygenation (k_o), and CO_2 compensation point ($\acute{I}$) from our light and AC_i response data (Table 1.2). Due to instrumental constraints on temperature control, we were unable to execute curves at the standard 25 °C. Instead, block temperature was maintained at 35 °C. We corrected for this using a modified Arrhenius equation for temperature sensitivity of photosynthesis (Figure S1.2) (Leuning 2002; Medlyn et al. 2002).

Leaf to canopy scaling

Measurements of leaf area index (LAI) were collected prior to each diurnal campaign. Ten meters of row were destructively sampled from each quadrant of the field. Leaf area was then measured using an Li3100C area meter (LI-COR), validated with a subset of manual measurements. We used LAI (m^2 leaf m^{-2} ground) to scale leaf level data (m^{-2} leaf s^{-1}) to the canopy level (m^{-2} ground area s^{-1}) for data collected during or July and October diurnal campaigns.

Modeling soil water potential

PMAX accounts for soil water status in terms of soil water potential (Sperry, Venturas, et al. 2016). We used an inverse van Genuchten function to attain estimates of soil water potential from VWC measurements collected continuously at our field site (Equation 1; Figure S1.3) (van Genuchten 1980). Residual and saturated soil VWC were identified from these soil sensor measurements, based on the lowest VWC observed prior to field irrigation and the highest VWC observed following an irrigation, respectively. Additional van Genuchten parameters were modeled based on plasticity index (Majdeddin et al. 2011). Plasticity index was derived from published values reported for

El Centro clay soils (Capuzzi & Capuzzi 2016). Using equations from Majdeddin *et al.* (2011), we determined values of 272 cm^{-1} and 1.41for α and *n,* respectively. These values are in good agreement with the average values reported for silty clay loam soils (Tuller & Or 2003).

Equation 1: $$P_{si} = \frac{\left[\left(\frac{\theta_s - \theta_r}{\theta_i - \theta_r}\right)^{1/m} - 1\right]^{1/n}}{\alpha}$$

Where P_{si} is soil water potential (MPa) at instance i, θ_s is saturated soil VWC ($cm^3\ cm^{-3}$), θ_r is residual soil VWC ($cm^3\ cm^{-3}$), θ_i is soil VWC ($cm3\ cm^{-3}$), and m, n, and α are parameters based on soil texture and structure.

Sorghum leaf vulnerability curves & conductance

We used a leaf vulnerability curve to describe sorghum's vulnerability to cavitation (Figure S1.4). Leaf vulnerability curves were conducted on *Sorghum bicolor* (cv. Delta) grown at the University of California Riverside during the summer of 2017. Samples were collected approximately three months after planting, prior to heading but following canopy closure. We retrieved samples at dusk, the day prior to initiation of measurements. Individual shoots were cut at the base of the stem and immediately submerged in water, where they were recut with a sharp blade. Cut stems were kept in water overnight in a dark room with a plastic bag placed over the leaves to allow rehydration.

Vulnerability curves were obtained using the optical method (Brodribb et al. 2016; Skelton et al. 2017). This method uses continuous, high resolution imagery of leaves coupled with continuous measures of leaf water potential to track cavitation and, subsequently, loss in hydraulic conductance, as the plant dries. As vessels cavitate and fill with air, the color changes. Processing high resolution images using an image difference filter and particle analysis allows measurement of these cavitation events. Assuming a fully desiccated specimen exhibits 100% cavitation of vessels, we can then calculate the percent loss in conductance associated with each cavitation event. Pairing this data with associated water potential measurements produces a leaf vulnerability curve. We selected the youngest fully expanded leaf for imaging and the nearest neighboring mature leaf to measure leaf water potential. A high resolution film scanner (Epson 800) was used to take images of the leaf at 2 minute intervals. Leaves were secured to the scanner with cloth tape and a pane of glass to minimize movement and maximize image clarity. Images were processed in ImageJ Fiji (Schindelin et al. 2012) with the OSOV toolbox, using methods provided by Brodribb et al. (2016). Leaf water potential was measured at 30 minute intervals with a leaf thermocouple psychrometer (L-51A; Wescor Inc., Logan, UT, USA) connected to a water potential datalogger (PSYPRO, Wescor Inc.).

Maximum leaf conductance (k_{max}; Table 1.2) was determined using an evaporative flux method (Sack & Scoffoni 2012). Samples were cut at the base of the stem, immediately re-cut under water, and left to rehydrate overnight. On the day of the measurement, individual leaves were cut approximately 20 cm from the leaf tip, under water, with a sharp blade. Only fully expanded, healthy leaves were selected. Using

plumber's putty for support and strips of parafilm as sealant, we rolled the base of the leaf into a cylinder and secured it to the tubing of our evaporative flux system. As long leaf cuttings were acquired, approximately 10 cm of leaf area at the proximal end of the leaf remain fully expanded, allowing us to use the standard evaporative flux methods (Sack & Scoffoni 2012).

Table 1.2. Static parameters and dynamic environmental inputs to the Profit Maximization model

Variable	Value	Units	Description
Static			
C_a	40.00	Pa	atmospheric [CO_2]
O_a	2,100	Pa	atmospheric [O_2]
P_{atm}	101.30	kPa	atmospheric pressure
c'	0.86	(dimensionless)	curvature of the light response curve
d	0.04	m	leaf width, average across manual LAI measurements
k_c	48.00	Pa	Michaelis-Menten constant for carboxylation
k_o	46,199	Pa	Michaelis-Menten constant for oxygenation
k_{max}	36.00	mmol H_2O m^{-2} s^{-1} MPa^{-1}	maximum leaf hydraulic conductance
VC	[2.75, 4.5]	(dimensionless)	Weibull [a, b] for leaf vulnerability curves
vG	[272, 1.41]	(dimensionless)	van Genuchten [α, n] for soil water retention curve
V_{max25}	56.60	µmol CO_2 m^{-2} s^{-1}	maximum rate of carboxylation
$\acute{I}$	0.53	Pa	CO_2 compensation point
e	0.98	(dimensionless)	emissivity, per Lopez et al. (2011)
Dynamic			
D	1.1 – 4.4	kPa	atmospheric vapor pressure defecit
P_s	0.38 – 1.1	MPa	soil water potential
PPFD	0 - 1997	µmol photons m^{-2} s^{-1}	photon flux density
R_{abs}	9 – 563	W m^{-2}	absorbed long and short wave radiation
T_a	29 – 46	°C	air temperature
u	3.6 – 6.2	m s^{-1}	wind speed

Adjustments to the assimilation model in PMAX

Assimilation in PMAX is simulated using the Farquhar C_3 photosynthesis model (Farquhar et al. 2001). As sorghum is a C_4 crop, physiological differences between C_3 and C_4 physiology were resolved by amending the classic C_3 Farquhar model with a commonly used modification described in Equation 3 (Collatz et al. 1992; Jenerette et al. 2009). We fit α_q by inversion using light response curves data (Figure S1.1). Biochemical A_{max} was acquired from the linear portion of light response curves. We assumed the default value of k_{PEP} provided by Collatz et al. (1992).

Equation 3: $$A = min \begin{Bmatrix} J_i \\ J_c \\ J_e \end{Bmatrix}$$

Where A is gross assimilation (µmol CO_2 m^{-2} s^{-1}), J_i is light-limited A, J_c is c_i-limited A, and J_e is Rubisco-limited A, as described by equations 5, 6, and 7, respectively.

Equation 4: $$J_i = \alpha_q PAR$$

Where α_q = effective light use efficiency (mol CO_2 mol photons^{-1})

Equation 5: $$J_c = \frac{k_{PEP}(c_i - \acute{\Gamma})}{P_{atm}}$$

Where k_{PEP} is the rate constant of PEP-carboxylation (mol CO_2 $m^{-2}s^{-1}$), c_i is internal [CO_2] (Pa), $\acute{\Gamma}$ is the CO_2 compensation point (Pa), and P_{atm} is atmospheric pressure (Pa).

Equation 6: $$J_e = A_{max}$$

Where A_{max} is the maximum carboxylation efficiency of Rubisco

PMAX uses a modified Arrhenius equation to describe the temperature sensitivity of several parameters in the photosynthesis model (Figure S1.1 & Equation S1). As described in the supporting information, we initially modified this equation by removing photoinhibition at high temperatures to better describe sorghum's heat-tolerant nature. However, setting photoinhibition to zero generates an exponential increase with increasing temperature. As our site frequently saw temperatures > 40 °C, this resulted in unrealistically high rates of photosynthesis on hot days. As limited temperature control in the field prohibited procurement of the temperature response curves necessary to properly parameterize temperature sensitivity functions, we omitted temperature sensitivity altogether to avoid unrealistically high assimilation values. Removal of temperature sensitivity may over- or underestimate assimilation and results should be interpreted accordingly.

1.4 Results

Diurnal leaf water potential

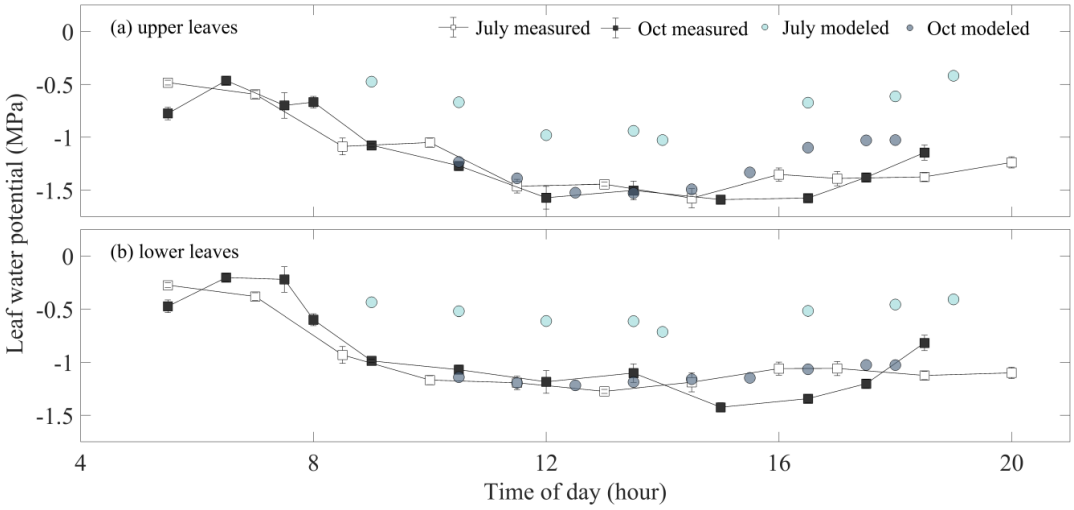

Figure 1.1. Measured and modeled leaf water from July and October measurement campaigns. Diurnal patterns of leaf water potential were similar across campaigns in measured data but diverged strongly in modeled data.

Despite differences in environmental conditions, leaf water potential showed strikingly similar diurnal patterns across campaigns (Figure 1.1). Pre-dawn P_{leaf} was around -0.47 MPa for upper leaves and -0.25 for lower leaves. As plants began photosynthesizing, P_{leaf} dropped to roughly -1.6 and -1.3 MPa for upper and lower leaves, respectively. Leaf water potential was relatively stable from noon until about 4pm. In the evening, as light levels declined, P_{leaf} began to recover. This recovery was more notable in October due to short day length relative to July. Modeled P_{leaf} did not reflect this uniform pattern across campaigns (Figure 1.3). Although modeled P_{leaf} was within the range of measured P_{leaf} for October, it was substantially over-estimated (less negative) for

July. Evening recovery was also more notable in modeled output, likely due to the model's limitations in sensitivity to time of day and continuity across time points.

PMAX validation with diurnal gas exchange measurements

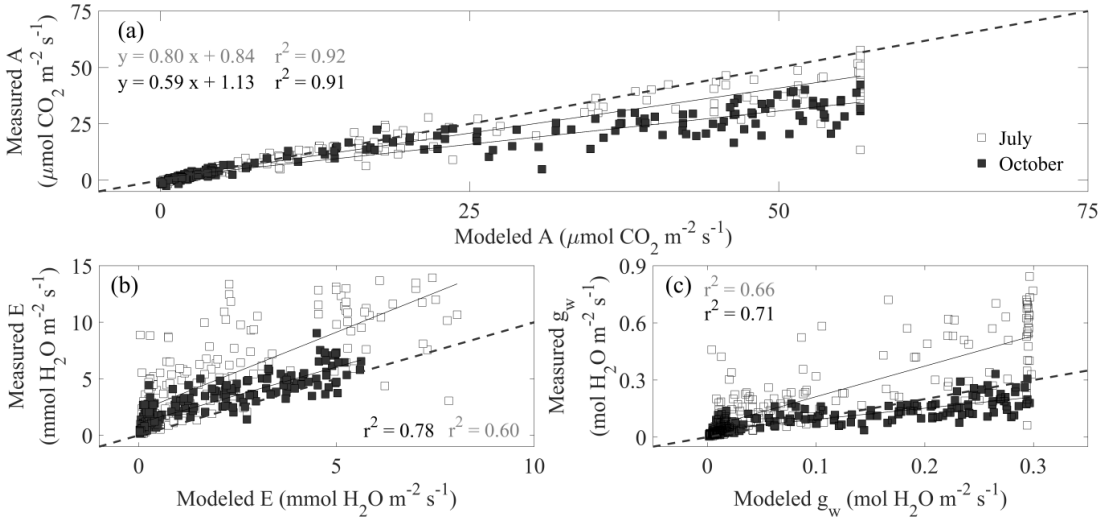

Figure 1.2. Fit of modeled data to measured data during our July and October diurnal campaigns. Assimilation modeled in PMAX was slightly overestimated, but overall showed good fit to measured data. Fit of E and g_w was near 1:1 for October data, but modeled E and g_w were substantially underestimated by the model in July.

PMAX showed varied ability to predict carbon and water flux dynamics across campaigns (Figure 1.2). Overall fit between measured and modeled values for A was good (r^2 = 0.92 in July and 0.91 in October), however, the model tended to over-predict assimilation. In July, the model had a tendency to predict biochemical A_{max}, indicating neither carbon uptake nor light limited modeled assimilation. This maximum assimilation rate appeared to correspond to a maximal rate of stomatal conductance. However, conductance rates predicted by the model in July were roughly 1/3 of measured

conductance rates. Further, measured values of conductance showed no evidence of reaching a maximum value. Transpiration was similarly under-predicted by the model. Both measured and modeled assimilation were lower in October than in July. These reduced rates of assimilation were associated with reduced rates of transpiration and stomatal conductance. Modeled values of conductance and transpiration in October showed good fit to measured values (r^2 = 0.71 and 0.78, respectively) and generally fell along the 1:1 line.

Water use dynamics & temperature

We evaluated the interaction between air temperature and water use dynamics in sorghum using energy balance and micrometeorological data collected at the leaf-level during our diurnal campaigns. Leaf temperature was consistently lower than air temperature and the two were increasingly de-coupled at as air temperature peaked (Figure 1.3a). Differences between leaf and air temperature, indicative of transpirational cooling, were highest during peak heat hours in July and were positively correlated to increasing rates of transpiration (Figure 1.3b). No significant relationship was found between leaf to air temperature differences and transpiration in October.

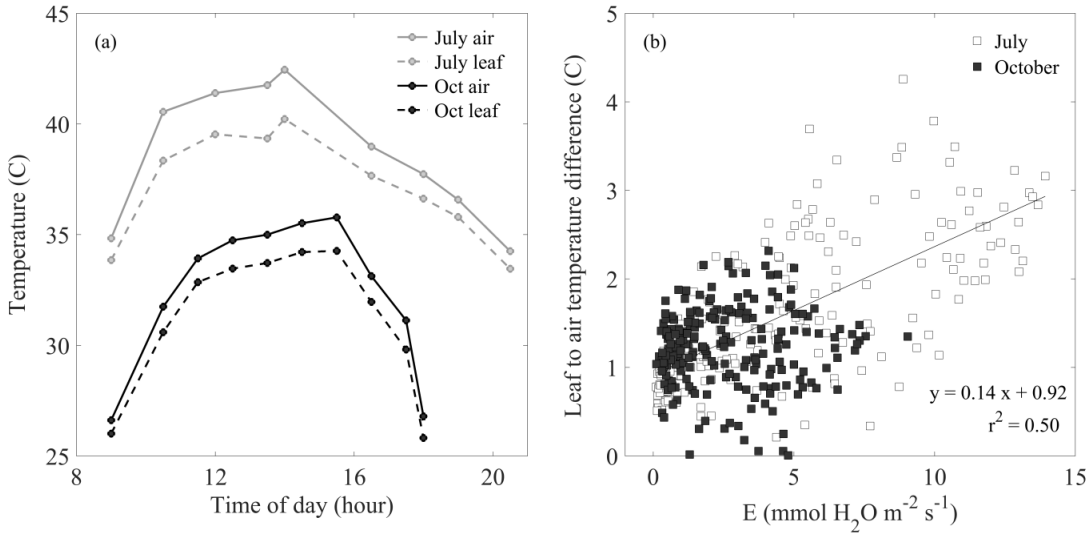

Figure 1.3. Average diurnal patterns of air and leaf temperature and their relation to transpiration. Leaf temperature was cooler than air temperature and the disparity between the two was greatest during midday hours. Increasing differences between leaf and air temperature were correlated with increasing E in July, but not significantly so in October.

Leaf to tower scaling

We found good agreement between up-scaled leaf-level gas flux and micromet measurements and partitioned canopy-level gas flux and micromet data (Figure 1.2a &b). Up-scaled leaf-level assimilation was slightly lower than canopy NEE, which was expected as NEE includes heterotrophic respiration (Figure 1.4a). PAR measured above the canopy was nearly double that of PAR measured within the canopy (Figure 1.4c). Conversely, air temperature was higher in the canopy than above the canopy (Figure 1.4d).

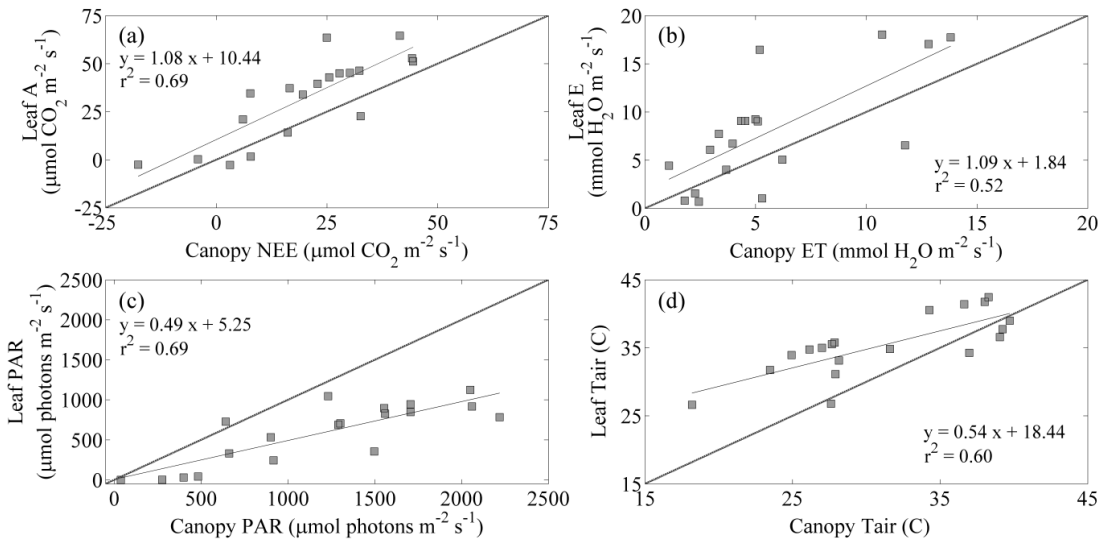

Figure 1.4. Linear regression of A, E, PAR, and T_{air} measured at the leaf level against NEE, ET, PAR, and T_{air} measured at the canopy level. All variables are expressed on a ground area basis. A and E were slightly higher for up-scaled leaf measurements than corresponding canopy measurements. PAR in the canopy was approximately half of PAR measured above the canopy. Conversely, T_{air} in the canopy tended to be higher than T_{air} measured above the canopy, particularly in the mornings and evenings, when ambient T_{air} was relatively cool.

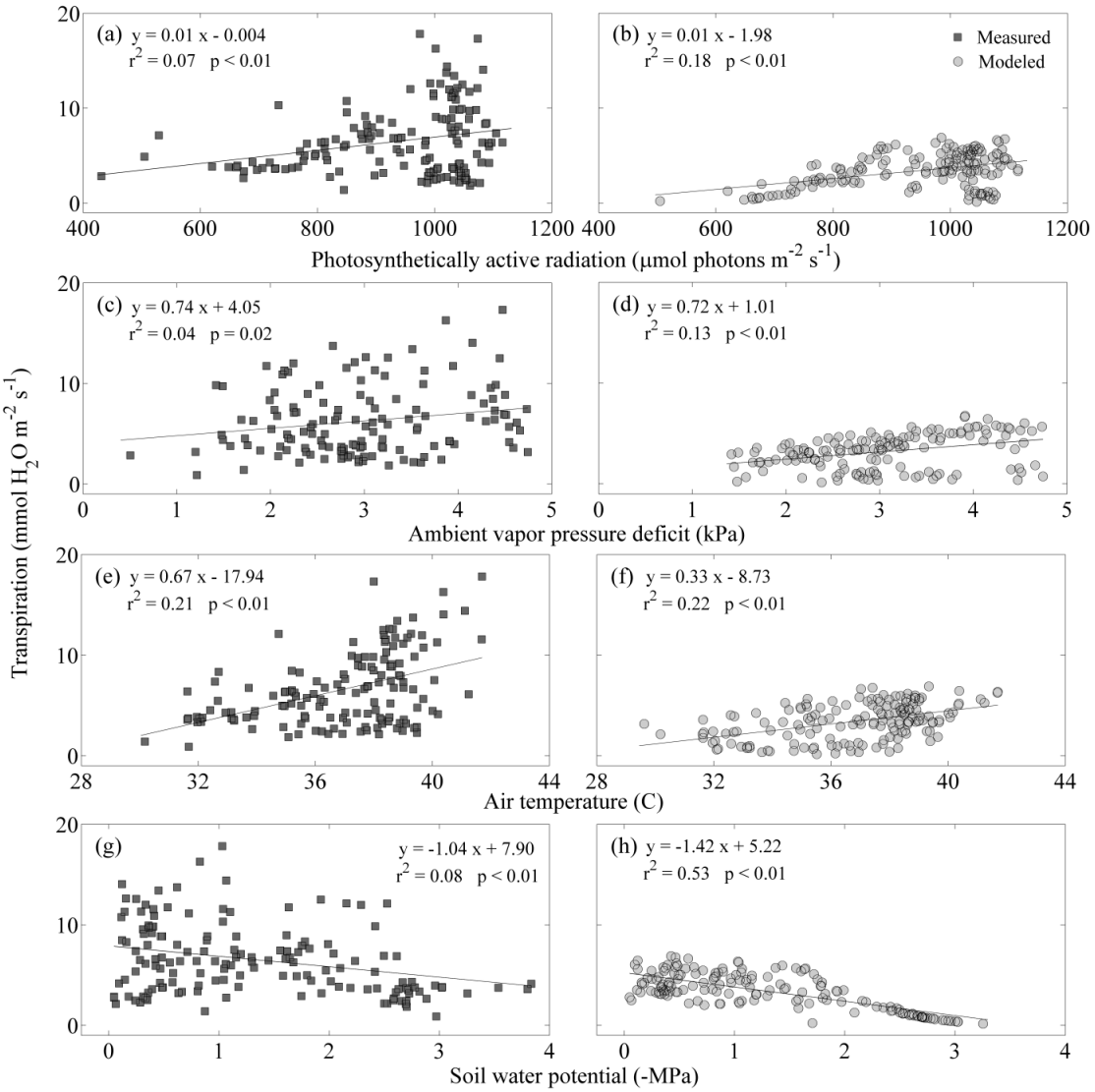

Figure 1.5. Exploring environmental drivers of transpiration (E) at the whole canopy scale in measured and modeled data throughout the 2012 growing season. Modeled E was approximately half of measured E. In measured data, E increased slightly in response to increasing PAR and VPD. Measured E increased more notably with increasing air temperature and declined slightly with declining P_{soil}. Modeled E was more responsive to environmental conditions, increasing with increasing PAR, T_{air}, and, particularly, VPD, and decreasing notably with declining P_{soil}.

Using transformed midday canopy-scale data from the 2012 season, we found significant relationships between all of the environmental drivers explored and transpiration. The strength of these relationships varied for measured and modeled data. In both measured and modeled data, transpiration increased by a similar magnitude in response to PAR (slope = 0.01 for measured and modeled; Figure 1.5 a – b) and VPD (slope = 0.2 and 0.74 for measured and modeled, respectively; Figure 1.c –d). However, measured data showed a stronger positive effect of air temperature on transpiration than modeled data (slope = 0.67 and 0.33, respectively; Figure 1.5 e – f) and a weaker negative relationship between soil water potential and transpiration (-1.04 and-1.44, respectively; Figure 1.5g – h).Overall, modeled E was less than half the rate of measured E and measured E showed the tightest coupling with T_{air} (r^2 = 0.21) while modeled E showed the tightest coupling with soil water potential (r^2 = 0.53).

1.5 Discussion

We sought to determine controls over water use in *Sorghum bicolor* grown in a high temperature, arid agroecosystem. When plants were not under overly stressed, maximizing light use efficiency appeared to dictate stomatal aperture. In the presence of water stress, threat of cavitation increased and stomatal regulation was evident. These mechanisms are more or less in line with the theoretical basis for the Profit Maximization model. However, measured conductance rates exceeded those modeled in PMAX when daytime temperatures were high, even when assimilation was light-limited. This suggests transpirational cooling can play an important role in stomatal regulation under

temperature stress. The act of transpirational cooling reduces instantaneous water use efficiency, but in turn provides a buffer to heat stress that allows high productivity in the face of extreme temperatures. This process appears to be safe-guarded by strong stomatal regulation in response to declining leaf water potential, which helps sorghum avoid excessive water loss and associated adverse physiological impacts. Together, our results suggest controls over water use in heat-tolerant sorghum are dependent on the type and severity of stress the plant is exposed to. This dynamic approach to stomatal regulation makes heat-tolerant sorghum cultivars particularly well-suited to acclimate to high temperatures and more limited water resources anticipated under climate change.

Performance of the modified PMAX model

Our modified Profit Maximization model appeared more than adequate for describing carbon and water use dynamics in C_4 grasses in general. Substituting the Farquhar C_3 assimilation model for a modified Collatz C_4 assimilation model allowed fairly accurate predictions of assimilation, and, in the presence of water stress, associated rates of transpiration. Our modified PMAX model also excluded temperature sensitivity of assimilation and respiration as sorghum has been shown to maintain high photosynthetic rates at temperatures exceeding those observed at our field site. While modeled A showed good fit to measured A under a wide range of temperatures, assimilation was slightly overestimated in the model and this overestimation could be a consequence of omitted temperature response. Our findings regarding transpirational cooling suggest that photosynthesis in heat-tolerant sorghum is not necessarily insensitive

to increasing temperatures, but rather buffered from them through excess transpirative water loss (Riar et al. 2015). This would suggest that a temperature response function based on leaf temperature vs. the conventionally used air temperature may more satisfactorily describe temperature sensitivity in heat-tolerant species. However, further research is needed to determine the role of transpirational cooling in the temperature sensitivity of photosynthetic and respiratory processes.

Coupling field data with modeled PMAX output suggested instantaneous A_{max} could be sustained throughout the day during our July campaign at relatively low rates of conductance compared to measured values. This supports the idea that water use dynamics and gas flux can be, to some extent, de-coupled in carbon-efficient C_4 grasses (Ocheltree et al. 2016). PMAX assumes stomata never open more than is necessary to achieve instantaneous A_{max} (Sperry et al. 2016). This is evident when instantaneous A_{max} was equal to biochemical A_{max}, which effectively set a g_{wmax} within the model. Subsequently, modeled leaf water potential was higher (less negative) than measured leaf water potential in July. Water loss in excess of rates predicted by PMAX appears to be attributable to transpirational cooling. This is supported by the fact that the disparity between leaf and air temperature increased linearly with increasing transpiration in July. In October, no significant relationship was found between transpiration and leaf cooling because water stress induced stomatal closure and limited transpirational cooling.

As sensitivity to soil water status is more line with the assumptions of PMAX, modeled transpiration, conductance, and leaf water potential for October showed much better fit to measured values than July data.

Evidence of isohydry

Despite differences in environmental stressors, leaf water potential followed strikingly similar patterns throughout the day across diurnal measurement campaigns, with midday P_{leaf} holding relatively constant at a rate just above the threshold at which vessels began to cavitate (Figure S1.4). This suggests strong avoidance of cavitation through stomatal regulation regardless of the source of abiotic stress. Tight stomatal regulation indicated strongly isohydric behavior in sorghum, and this was supported by the shape of the Weibull function fitted to our vulnerability curve. Recent work suggests that sorghum cultivars adapted to growing environments characterized by high temperatures tend to show higher conductance rates than cultivars adapted to mild climates because transpirational cooling is favored over water conservation (Riar et al. 2015). While our data support this idea, they also suggest that sorghum's isohydric behavior safeguards against excessive water loss and associated physiological damages as leaf water potential declines throughout the day. Thus heat tolerance via transpirational cooling is balanced with water conservation and cavitation avoidance.

PMAX was unable to replicate similarities in diurnal leaf water potentials across campaigns, largely because it did not account for super-optimal stomatal regulation to facilitate transpirational cooling (Farquhar & Sharkey 1982; Singh et al. 1985; Singh & Singh 1988; Grantz & Meizner 1990).

Trends in midday water use dynamics throughout the growing season

Our data generally supported the inherent hypotheses of the Profit Maximization model but also found strong support for the role of air temperature regulating water use dynamics. When midday carbon and water exchange were modeled in PMAX, transpiration rates were lower than those partitioned from measurements of canopy water flux. The highest rates of measured transpiration appeared to be associated with high light levels and high temperatures. As light availability and high midday temperatures often coincided, this difference in the magnitude of transpiration is likely the result of transpirational cooling not accounted for by the model. Higher sensitivity to temperature and lower sensitivity to soil water status in measured data support the idea that sorghum up-regulates conductance in the face of heat stress and down-regulates conductance in response to water stress. When both stresses are present, a middle of the road approach is likely, which would explain the persistence of some relatively low E rates at high temperatures and some relatively high E rates at low soil water potentials observed in field data.

In both measured and modeled data, transpiration did not decline with increasing VPD, as has been observed in “stay green” sorghum cultivars touted for their high water

use efficiency (Gholipoor et al. 2010; Choudhary et al. 2013; Shekoofa et al. 2014; Riar et al. 2015). High aridity at our field site increased atmospheric VPD to nearly 5 kPa, yet the both measured and modeled E increased linearly with increasing VPD. Recent work suggests stomatal sensitivity to VPD is selected against when the growing environment regularly reaches 37 °C or higher (Choudhary et al. 2013; Riar et al. 2015) in order to facilitate transpirational cooling. Thus "stay green" cultivars likely lack the degree of heat tolerance exhibited in cultivars that do not prioritize soil water conservation in the presence of atmospheric drought. This may represent an important tradeoff between degree of heat tolerance and degree of drought tolerance. However, stomatal regulation in response to declining leaf water potential evident in our diurnal data suggest heat-tolerant cultivars retain a degree of drought tolerance. When heat stress is dominant, transpirational cooling is enhanced to avoid damage to photosynthetic machinery. This response has the added benefit of maximizing light use efficiency, thereby retaining high rates of productivity in an otherwise inhospitable environment.

The extent of transpirational cooling appears to be constrained when leaf water potentials near the threshold at which cavitation becomes likely. When water stress is dominant, leaf water potential drops more rapidly in response to transpiration and stomatal regulation kicks in more readily to avoid cavitation. Water use efficiency in heat-tolerant sorghum cultivars therefore appears to be strongly dependent on the type and severity of abiotic stress the plant faces, with stomatal regulation functioning such that damage to both photosynthetic machinery and xylem conduits are avoided whenever possible.

Synthesis

Stomatal closure is thought to be a mechanism of resource conservation and stress avoidance, however for species adapted to high temperatures, stomatal opening can be an equally important pathway for avoiding stress. Our data suggest some sorghum cultivars balance their tolerance to heat and drought stress by shifting patterns of stomatal regulation based on environmental conditions and leaf water potential. Provided sorghum is moderately well-watered during extreme heat events, it should be well poised to maintain high rates of productivity in the face of rising global temperatures and more erratic precipitation events. While many studies have focused on "stay green" cultivars as climate-change ready crops, prioritization of water conservation in response to soil and atmospheric drought appears to limit heat-tolerance and reduce overall productivity. Our results highlight the importance of transpirational cooling in determining water use patterns for sorghum and, likely, other heat-tolerant crops. Our adaptation of the Profit Maximization model of stomatal control was able to simulate assimilation rates with surprising accuracy. When water stress was dominant, water use dynamics were also well predicted by the model. Inclusion of transpirational cooling as a determining factor of optimal stomatal aperture, while challenging, would improve the accuracy of Profit Maximization to simulate heat-tolerant species. This appears to be the main limitation of extending this model to C_4 grasses. Understanding water use dynamics in sorghum and other major cereal cropping systems is increasingly important as crop production shifts to accommodate climate change.

1.6 References

Baldocchi, D.D., Hincks, B.B. & Meyers, T.P., 1988. Measuring Biosphere-Atmosphere Exchanges of Biologically Related Gases with Micrometeorological Methods. *Ecology*, 69(5), pp.1331–1340.

Bita, C.E. & Gerats, T., 2013. Plant tolerance to high temperature in a changing environment: scientific fundamentals and production of heat stress-tolerant crops. *Frontiers in plant science*, 4, p.273.

Brodribb, T.J. et al., 2016. Visual quantification of embolism reveals leaf vulnerability to hydraulic failure. *New Phytologist*, 209(4), pp.1403–1409.

Capuzzi, M. & Capuzzi, D.M., 2016. *Geotechnical Investigation Report*, El Centro, CA.

Choudhary, S., Sinclair, T.R. & Prasad, P.V.V., 2013. Hydraulic conductance of intact plants of two contrasting sorghum lines, SC15 and SC1205. *Functional Plant Biology*, 40(7), p.730.

Collatz, G., Ribas-Carbo, M. & Berry, J., 1992. Coupled Photosynthesis-Stomatal Conductance Model for Leaves of C4 Plants. *Australian Journal of Plant Physiology*, 19(5), p.519.

Cowan, I.R., 1978. Stomatal Behaviour and Environment. *Advances in Botanical Research*, 4, pp.117–228.

Cowan, I.R. & Farquhar, G.D., 1977. Stomatal function in relation to leaf metabolism and environment. *Symposia of the Society for Experimental Biology*, 31, pp.471–505.

Djanaguiraman, M. et al., 2014. Physiological differences among sorghum (Sorghum bicolor L. Moench) genotypes under high temperature stress. *Environmental and Experimental Botany*, 100, pp.43–54.

FAO & NRI, 1999. *Sorghum: Post-harvest Operations*, Rome, Italy. Available at: http://www.fao.org/3/a-ax443e.pdf [Accessed November 27, 2017].

Farquhar, G.D., von Caemmerer S, S. von & Berry, J.A., 2001. Models of photosynthesis. *Plant physiology*, 125(1), pp.42–5.

Farquhar, G.D. & Sharkey, T.D., 1982. Stomatal Conductance and Photosynthesis. *Annual review of plant physiology*, 33, pp.317–345.

Fertitta-Roberts, C. et al., 2017. Trade-offs across productivity, GHG intensity, and pollutant loads from second-generation sorghum bioenergy. *GCB Bioenergy*, 9(12), pp.1764–1779.

van Genuchten, M., 1980. *A closed-form equation for predicting the hydraulic conductivity of unsaturated soils*, Soil Science Society of America.

Gholipoor, M. et al., 2010. Genetic variability of transpiration response to vapor pressure deficit among sorghum genotypes. *Field Crops Research*, 119(1), pp.85–90.

Grantz, D.A. & Meizner, F.C., 1990. Stomatal response to humidity in a sugarcane field: simultaneous porometric and micrometeorological measurements*. *Plant, Cell and Environment*, 13(1), pp.27–37.

Jenerette, G.D. et al., 2009. Gross primary production variability associated with meteorology, physiology, leaf area, and water supply in contrasting woodland and grassland semiarid riparian ecosystems. *Journal of Geophysical Research*, 114(G4), p.G04010.

Jones, H.G., 1998. Stomatal control of photosynthesis and transpiration. *Journal of Experimental Botany*, 49, pp.387–398.

Katul, G. et al., 2010. A stomatal optimization theory to describe the effects of atmospheric CO2 on leaf photosynthesis and transpiration. *Annals of Botany*, 105(3), pp.431–442.

Leuning, R., 1995. A critical appraisal of a combined stomatal-photosynthesis model for C3 plants. *Plant, Cell and Environment*, 18(4), pp.339–355.

Leuning, R., 2002. Temperature dependence of two parameters in a photosynthesis model. *Plant, Cell and Environment*, 25(9), pp.1205–1210.

Majdeddin, S. et al., 2011. Estimation of the water retention curve for unsaturated clay. *Canadian Journal of Soil Science*, (91), pp.543–549.

Medlyn, B.E. et al., 2002. Temperature response of parameters of a biochemically based model of photosynthesis. II. A review of experimental data. *Plant, Cell and Environment*, 25(9), pp.1167–1179.

Medlyn, B.E. et al., 2011. Reconciling the optimal and empirical approaches to modelling stomatal conductance. *Global Change Biology*, 17(6), pp.2134–2144.

Ocheltree, T.W., Nippert, J.B. & Prasad, P.V.V., 2016. A safety vs efficiency trade-off identified in the hydraulic pathway of grass leaves is decoupled from photosynthesis, stomatal conductance and precipitation. *New Phytologist*, 210(1), pp.97–107.

Oikawa, P.Y., Jenerette, G.D. & Grantz, D.A., 2015. Offsetting high water demands with high productivity: Sorghum as a biofuel crop in a high irradiance arid ecosystem. *GCB Bioenergy*, 7(5), pp.974–983.

Prasad, P.V., Boote, K.J. & Allen, L.H., 2006. Adverse high temperature effects on pollen viability, seed-set, seed yield and harvest index of grain-sorghum [Sorghum bicolor (L.) Moench] are more severe at elevated carbon dioxide due to higher tissue temperatures. *Agricultural and Forest Meteorology*, 139(3), pp.237–251.

Prasad, P.V.V. et al., 2008. Sensitivity of Grain Sorghum to High Temperature Stress during Reproductive Development. *Crop Science*, 48(5), p.1911.

Prentice, I.C. et al., 2014. Balancing the costs of carbon gain and water transport: testing a new theoretical framework for plant functional ecology J. Penuelas, ed. *Ecology Letters*, 17(1), pp.82–91.

Riar, M.K., Sinclair, T.R. & Prasad, P.V.V., 2015. Persistence of limited-transpiration-rate trait in sorghum at high temperature. *Environmental and Experimental Botany*, 115, pp.58–62.

Sack, L. & Scoffoni, C., 2012. Measurement of Leaf Hydraulic Conductance and Stomatal Conductance and Their Responses to Irradiance and Dehydration Using the Evaporative Flux Method (EFM). *Journal of Visualized Experiments*, (70).

Sade, N., Gebremedhin, A. & Moshelion, M., 2012. Risk-taking plants. *Plant Signaling & Behavior*, 7(7), pp.767–770.

Schindelin, J. et al., 2012. Fiji: an open-source platform for biological-image analysis. *Nature Methods*, 9(7), pp.676–682.

Shekoofa, A., Balota, M. & Sinclar, T.R., 2014. Limited-transpiration trait evaluated in growth chamber and field for sorghum genotypes. *Environmental and Experimental Botany*, 99, pp.175–179.

Singh, B.R. & Singh, D.P., 1988. Sensing of moisture stress effects by infra-red thermometry in sorghum, maize and pearl millet. *Journal of the Indian Society of Remote Sensing*, 16(2), pp.53–57.

Singh, D.P. et al., 1985. Transpirational Cooling as a Screening Technique for Drought Tolerance in Oil Seed Transpirational Cooling as a Screen for Drought Tolerance in Oil Seed Brassicas. *Source: Annals of Botany*, 56(6), pp.815–820.

Singh, P. et al., 2014. Quantifying potential benefits of drought and heat tolerance in rainy season sorghum for adapting to climate change. *Agricultural and Forest Meteorology*, 185, pp.37–48.

Skelton, R.P., Brodribb, T.J. & Choat, B., 2017. Casting light on xylem vulnerability in an herbaceous species reveals a lack of segmentation. *New Phytologist*, 214(2), pp.561–569.

Sperry, J.S., Wang, Y., et al., 2016. Pragmatic hydraulic theory predicts stomatal responses to climatic water deficits. *New Phytologist*, 212(3), pp.577–589.

Sperry, J.S., Venturas, M.D., et al., 2016. Predicting stomatal responses to the environment from the optimization of photosynthetic gain and hydraulic cost. *Plant, Cell & Environment*.

Sperry, J.S. & Love, D.M., 2015. What plant hydraulics can tell us about responses to climate-change droughts. *New Phytologist*, 207(1), pp.14–27.

Tardieu, F. & Simonneau, T., 1998. Variability among species of stomatal control under fluctuating soil water status and evaporative demand: modelling isohydric and anisohydric behaviours. *Journal of Experimental Botany*, 49, pp.419–432.

Triggs, J.. et al., 2004. Free-air CO2 enrichment effects on the energy balance and evapotranspiration of sorghum. *Agricultural and Forest Meteorology*, 124(1–2), pp.63–79.

Tuller, M. & Or, D., 2003. *Retention of Water in Soil and the Soil Water Characteristic Curve*, Storrs, CT.

Wolf, A., Anderegg, W.R.L. & Pacala, S.W., 2016. Optimal stomatal behavior with competition for water and risk of hydraulic impairment. *Proceedings of the National Academy of Sciences of the United States of America*, 113(46), pp.E7222–E7230.

Wright, G., Smith, R. & Morgan, J., 1983. Differences between two grain sorghum genotypes in adaptation to drought stress. III. Physiological responses. *Australian Journal of Agricultural Research*, 34(6), p.637.

1.7 Supporting Information

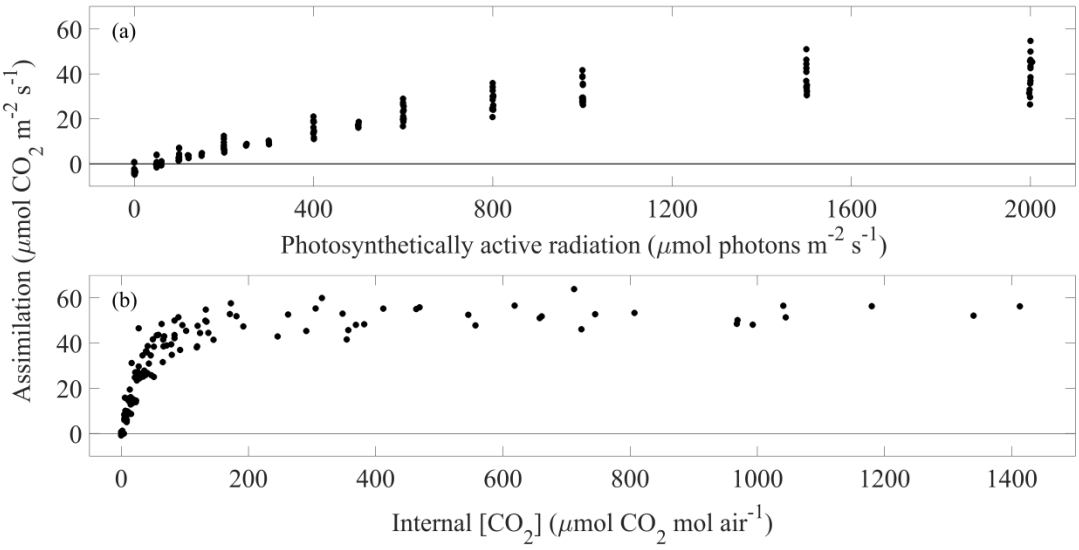

Figure S1.1 Light and Ac_i curves obtained throughout the 2012 and 2013 growing season. The light response curve shows data for upper leaves only (panel a) while the Ac_i curve (panel b) reflect data collected for both upper and lower leaves.

Temperature Sensitivity

Leunig (2002) provides parameters describing average temperature sensitivity dynamics across a wide range of species (Equation S1). However, these average parameters are inadequate for describing temperature response dynamics in sorghum, which shows no evidence of photosynthetic inhibition at temperatures as high as 46 °C (Prasad et al. 2006; Prasad et al. 2008; Djanaguiraman et al. 2014). In lieu of adequate temperature response data for sorghum, we modified these temperature sensitivity parameters to eliminate photoinhibition at high temperatures. This was accomplished by setting H_d and S_v equal to zero, as has been observed in tobacco, another heat-tolerant annual (Leuning 2002).

Equation S1:

$$\frac{V_{maxi}}{V_{max0}} = \frac{C \exp[(H_a/RT_0)(1 - T_0/T_i]}{1+\exp[(S_v T_i - H_d)/(RT_i)]}$$

Where V_{maxi} is max photosynthetic rate (µmol CO_2 m^{-2} s^{-1}) at instance i, V_{max0} is max photosynthetic rate (µmol CO_2 m^{-2} s^{-1}) at instance 0, H_a is activation energy, H_d is deactivation energy, S_v is an entropy term, R is an ideal gas constant, T_0 = 298.2 °K, T_i is temperature at instance i (°K), and C is defined by Equation 2.

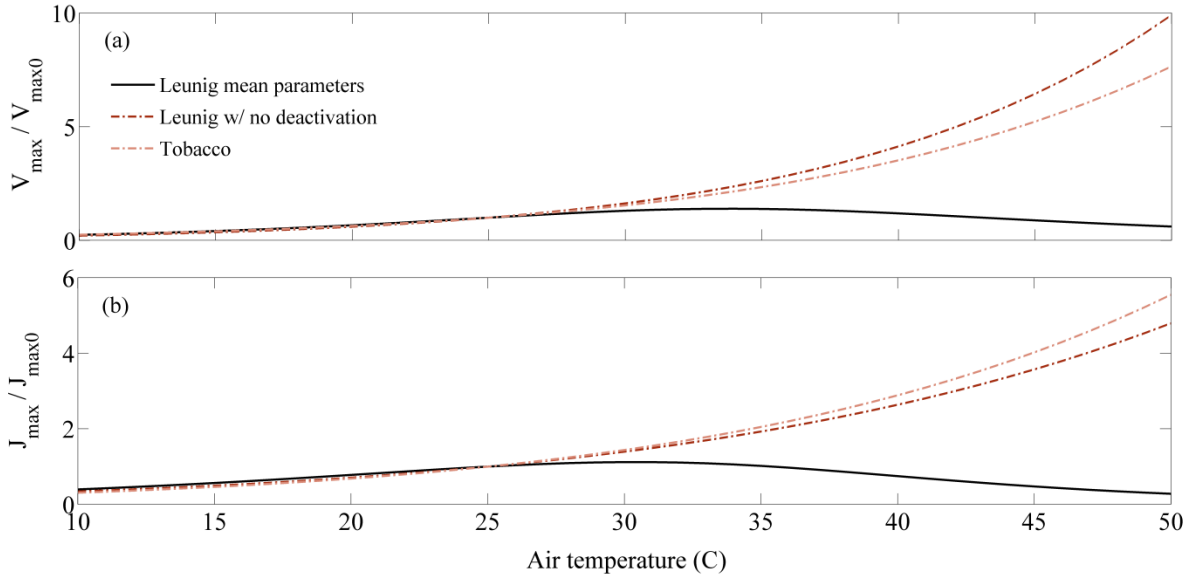

Figure S1.2. Adjustments to temperature sensitivity of V_{max} and J_{max}. Leunig et al. (2002) determined mean parameters of activation energy, deactivation energy, and entropy, in order to broadly describe temperature sensitivity across species (black line). Tobacco (light red dotted line) was found to have an exponentially increasing rate of V_{max} and J_{max} in response to increasing temperatures. We modified the mean parameters described by Leunig et al. (2002) to remove deactivation in order to estimate temperature sensitivity in sorghum (dark red dotted line).

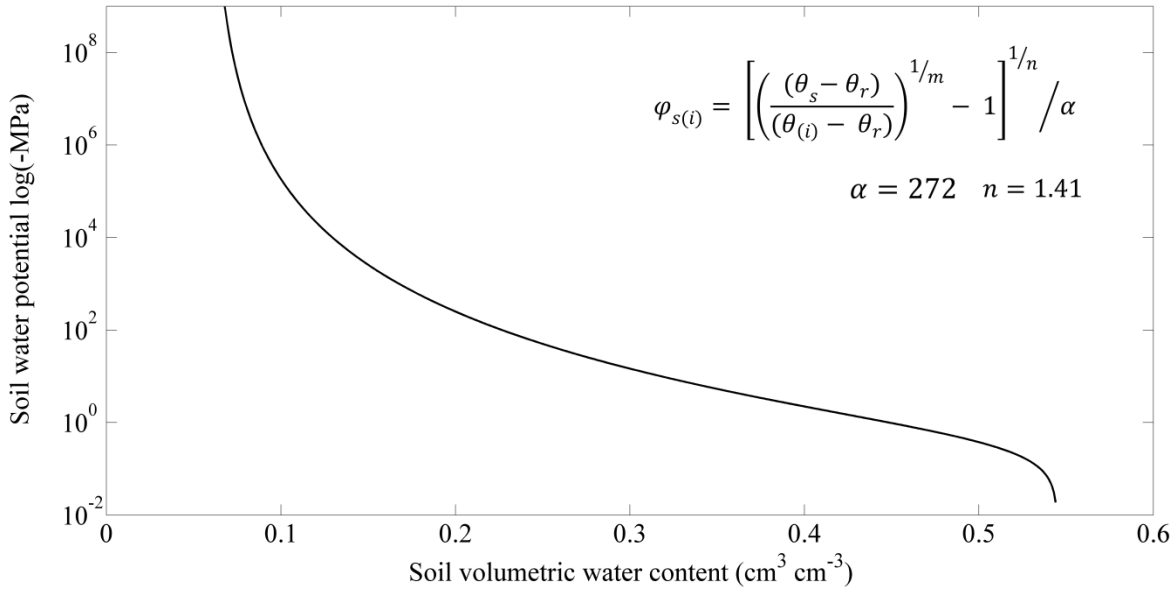

Figure S1.3. Soil water retention was described by a van Genuchten function. Parameters α and n were fitted using the plasticity index of silty clay soil and in good agreement with previously published values for this soil type. We inverted the van Genuchten function to model soil water potential for soil VWC. van Genuchten parameters also served as direct inputs to the PMAX model.

Leaf vulnerability curve

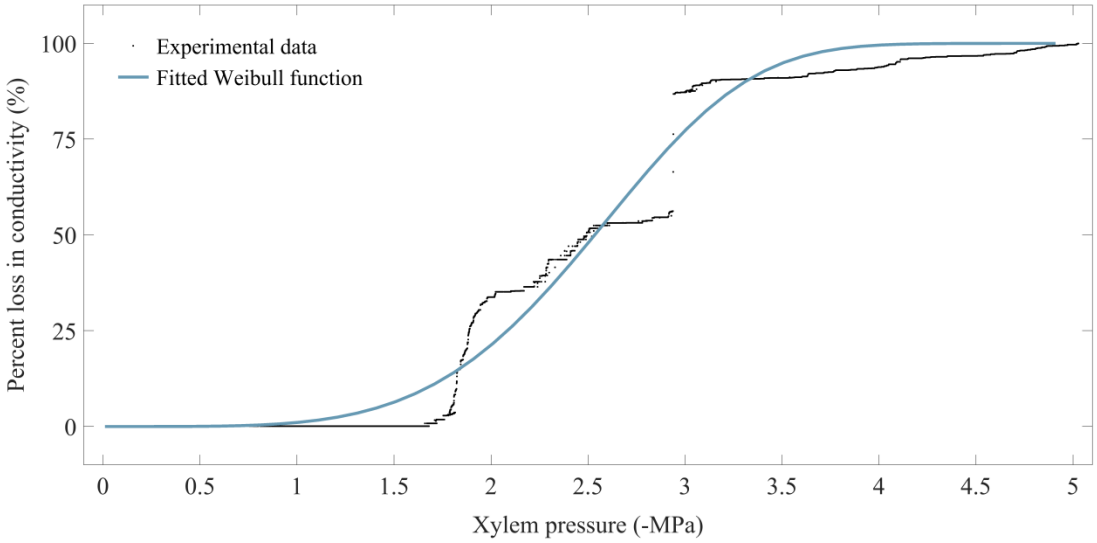

Figure S1.4. Sorghum leaf vulnerability curves. Experimental data (black dots) were obtained using the Optical Method. A Weibull function (solid blue line) was fitted to our experimental data using least sun of squares.

Using the optical method, we found no evidence of cavitation until leaf water potential surpassed -1.6 MPa. Fifty percent of hydraulic conductance was lost at -2.5 MPa and 98% was lost at -4.7 MPa. The shape of the fitted Weibull function was sigmoidal (c = 4.5) but not particularly severe (b = 2.75) suggesting isohydry. Although Weibull functions model smooth transitions in the response of conductivity to leaf water potential (P_{leaf}), measured data showed a more dynamic response. Once leaf water potential dropped below -1.7 MPa, cavitation occurred rapidly, inducing a 35% loss in conductivity before roughly stabilizing at -2 MPa. At -2.3 MPa, cavitation increased slowly but steadily before again stabilizing around -2.6 MPa at 53% loss in conductivity.

Full cavitation of the midvein occurred at approximately -2.9 MPa, resulting in a sudden jump from 53 to 87% loss in conductivity.

1.8 References for Supporting Information

Leuning, R., 2002. Temperature dependence of two parameters in a photosynthesis model. *Plant, Cell and Environment*, 25(9), pp.1205–1210.

Medlyn, B.E. et al., 2002. Temperature response of parameters of a biochemically based model of photosynthesis. II. A review of experimental data. *Plant, Cell and Environment*, 25(9), pp.1167–1179.

Chapter 2

Tradeoffs across productivity, GHG intensity, and pollutant loads from second generation sorghum bioenergy

Cara Fertitta-Roberts, Sabrina Spatari, David A. Grantz, G. Darrel Jenerette

---

2.1 Abstract

Greenhouse gas (GHG) intensity is frequently used to assess the mitigation potential of biofuels, however, failure to quantify other environmental impacts may result in unintended consequences, effectively shifting the environmental burden of fuel production rather than reducing it. We modeled production of E_{85}, a gasoline/ethanol blend, from forage sorghum (*Sorghum bicolor* cv. Photoperiod LS) grown, processed, and consumed in California's Imperial Valley in order to evaluate the influence of nitrogen (N) management on well-to-wheel (WTW) environmental impacts from cellulosic ethanol. We simulated 25 N management scenarios varying application rate, application method, and N source. Life cycle environmental impacts were characterized using the EPA's criteria for emissions affecting the environment and human health. Our results suggest efficient use of N is an important pathway for minimizing WTW emissions on an energy yield basis. Simulations in which N was injected had the highest nitrogen use efficiency. Even at rates as high as 450 kg N ha^{-1}, injected N simulations generated a yield response sufficient to outweigh accompanying increases in most N-

induced emissions on an energy yield basis. Thus, within the biofuel life cycle, tradeoffs across productivity, GHG intensity, and pollutant loads may be possible to avoid at regional to global scales. However, tradeoffs were seemingly unavoidable when impacts from E_{85} were compared to those of conventional gasoline. The GHG intensity of sorghum-derived E_{85} ranged from 29 – 44 g CO_2 eq MJ^{-1}, roughly 1/3 to 1/2 that of gasoline. Conversely, emissions contributing to local air and water pollution tended to be substantially higher in the E_{85} life cycle. These adverse impacts were strongly influenced by N management and could be partially mitigated by efficient application of N fertilizers. Together, our results emphasize the importance of minimizing on-farm emissions in maximizing both the environmental benefits and profitability of biofuels.

2.2 Introduction

Biofuels from cellulosic ethanol have been widely reported to have GHG intensities less than half those of conventional fuels (Schmer et al., 2008; CARB, 2009; Wang et al., 2011; Adler et al., 2012; van der Weijde et al., 2013; Murphy & Kendall, 2015; LeDuc et al., 2016). GHG intensity is determined through life cycle assessment (LCA) modeling of emissions associated with generation and use of the fuel product. Feedstock production is among the most GHG-intensive components of the biofuel life cycle (Adler et al., 2012; Adler et al., 2007; Borrion et al., 2012; Fu et al., 2003) and can also contribute substantially to non-GHG environmental impacts such as acidification and eutrophication of local waterways (Robertson et al. 2008; Wagner & Lewandowski 2016). Nitrogen fertilizers are strongly linked to both increased crop yield and increased

environmental impacts (Borrion et al., 2012; Fazio & Monti, 2011; Ruan et al., 2016; von Blottnitz & Curran, 2007). Thus, pursuit of high biomass yields for fuel production may occur at the expense of GHG mitigation potential and local air and water pollution. Recently, increasing attention has been drawn to non-GHG impacts, as evidence accumulates that some air and water pollutant loads from cellulosic fuels can exceed those of conventional fuels (da Silva et al., 2014; Diaz-Chavez et al., 2013; Jeswani et al., 2015; Mbonimpa et al., 2016; Robledo-Abad et al., 2016; Weldu & Assefa, 2016). Exploring these tradeoffs is increasingly important as cellulosic ethanol is mandated to take on a growing role in meeting the renewable energy demands of the United States (EIA, 2016; EPA, 2010).

LCA is a comprehensive, quantitative method used to evaluate sustainability metrics and frequently implemented in the assessment of alternative fuels (Cherubini et al. 2009; Guinée et al. 2011). Methodological variations in LCA are considerable, thus the International Organization for Standardization (ISO) guidelines are frequently referenced to offer a certain degree of continuity across methods (ISO 2006a; ISO 2006b; Cherubini & Strømman 2011). Most biofuel life cycles use a well-to-wheel (WTW) scope (Singh et al. 2010; Borrion et al. 2012), which includes processes inherent to generation of the fuel product, intermediary processes (e.g. transportation), and fuel combustion. System boundaries define the limits of the analysis. Second order system boundaries are commonly employed in fuel LCAs (Borrion et al. 2012) and include upstream and downstream emissions (i.e. those occurring pre- and post-use of a product, respectively) but exclude embodied energy sources such as facilities and machinery.

Under a clearly defined scope and system boundary, a life cycle inventory (LCI) is complied, which accounts for all of the chemical compounds consumed and emitted throughout the life cycle. The resulting chemical inventory is then used to characterize environmental impacts based on each compound's projected influence on human health and the environment. This is accomplished by expressing each compound in equivalent units (eq) of a reference compound. Emissions are then summed and used to describe their projected contribution to a specific impact category. For instance, GHG emissions are expressed in terms of CO_2 eq based on the global warming potential of each individual GHG relative to that of CO_2. Although biofuel life cycles frequently consider only GHG emissions and energy consumption (Hsu et al., 2010; McKechnie et al., 2010; Searcy & Flynn, 2008; Spatari et al., 2005; Stephenson et al., 2010; Stichnothe & Azapagic, 2009; Zamboni et al., 2011), LCA can be used to explore a diverse range of environmental impacts (Bare et al., 2003; Brentrup et al., 2004; Hauschild et al., 2013; Jeswani et al., 2015; Mbonimpa et al., 2016; Monti et al. 2009; Sanz Requena et al., 2011; Sabrina Spatari & MacLean, 2010; Wagner & Lewandowski, 2016).

The large proportion of WTW emissions attributed to feedstock production suggests management choices can play an important role in determining pollutant loads from cellulosic fuels. In the case of annual crops, management is likely to play an especially important role as they generally sequester less carbon and have higher fertilizer demands than perennials (Fazio & Monti, 2011; LeDuc et al., 2016; Monti et al., 2009; Somerville et al., 2010; Wang et al., 2012). Increasing nitrogen (N) fertilizer rates have been shown to reduce the climate benefits associated with cellulosic fuels by increasing

nitrous oxide (N_2O) emissions and can adversely impact air and water quality (Brentrup et al., 2004; Luo, et al., 2009; Oikawa, 2015a; Robertson et al., 2008; Ruan et al., 2016). Despite the impacts of N fertilizers on the environment and the significant variability in management practices observed across growers (Baumgart-Getz et al., 2012), biofuel LCAs often assume a single scenario for agronomic feedstock production (Spatari et al. 2005; Sanderson et al. 2006; Adler et al. 2007; Fargione et al. 2010; Spatari et al. 2010; Davis et al. 2012; Pourhashem et al. 2013; Jeswani et al. 2015; LeDuc et al. 2016). Some field studies have attempted to address this variability by examining alternate management scenarios (Lamb et al. 2003; Boehmel et al. 2008; Schmer et al. 2008; Schmer et al. 2014; Mbonimpa et al. 2016), however, the lengthy and expensive nature of these experiments limits exploration at the field level. Coupling field data with crop models allows exploration of a large breadth of management practices *in-silico* before further testing in a field or commercial setting.

We use a field data-driven crop model coupled with LCA modeling to explore the potential impacts of N management choices on biomass yields, GHG intensity, and local air and water pollutant loads from sorghum-derived cellulosic ethanol produced in California's Imperial Valley. Sorghum is a heat- and drought-tolerant C_4 grass (Tonitto & Ricker-Gilbert 2016) that thrives in the high-irradiance environment and long seasons afforded by the Imperial Valley's mild winters (Oikawa et al. 2015b). These conditions can lead to N demands exceeding those of most biofuel crops (Fazio & Monti 2011; Schmer et al. 2014; Ruan et al. 2016) or of sorghum grown in other parts of the United States (Hao et al. 2014; Haankuku et al. 2014; Bonin et al. 2016). We simulated

contrasting N management scenarios for Imperial Valley sorghum as inputs to LCA models for sorghum-derived E_{85} fuel (85% ethanol-15% gasoline, by volume) to determine the potential range of WTW emissions associated with different feedstock production strategies. We hypothesized that increasing N application rate would mitigate environmental impacts on an energy yield basis at low to moderate application rates, where yield gains per kg N would be highest, but would amplify impacts at higher application rates as yield gains per kg N decline (Tilman et al., 2002). Alternatively, we hypothesized that increasing yields may be sufficient to compensate for increased emissions from N even at high N application rates if WTW emissions are largely derived from non-N sources. Emissions from non-N sources will decline with increasing biomass yields as these emissions are fixed and impacts are assessed on the basis of energy yield, which increases with biomass yield. As N uptake, and subsequently, yield-response, differ based on N source and application method, we simulated variations in both of these parameters to gain a more comprehensive understanding of nitrogen use efficiency (NUE) dynamics and associated WTW emissions.

We then investigated how substitution of conventional gasoline with sorghum-derived E_{85} may influence environmental impacts from the fuel sector across all nine impact categories evaluated by the U.S. Environmental Protection Agency (Bare et al. 2003). Previous work suggests that GHG intensity will be reduced for cellulosic fuels, but emissions contributing to air and water pollution may be higher (von Blottnitz & Curran 2007; Borrion et al. 2012; Diaz-Chavez et al. 2013; da Silva et al. 2014; Weldu & Assefa 2016; Mbonimpa et al. 2016; Robledo-Abad et al. 2016). Quantifying WTW

impacts across N management scenarios and across fuel sources will identify opportunities for mitigation of adverse impacts and highlight environmental tradeoffs associated with the increased use of biofuels.

2.3 Materials and Methods

Three major phases of data collection and analysis were undertaken to address our objectives (Figure 2.1). We used a field trial to provide data for parameterization of a crop model, which was used to simulate biomass outputs under a range of N management scenarios. Crop model outputs were used as LCA inputs for E_{85} fuel life cycles. A separate LCA of conventional gasoline was constructed as a reference scenario.

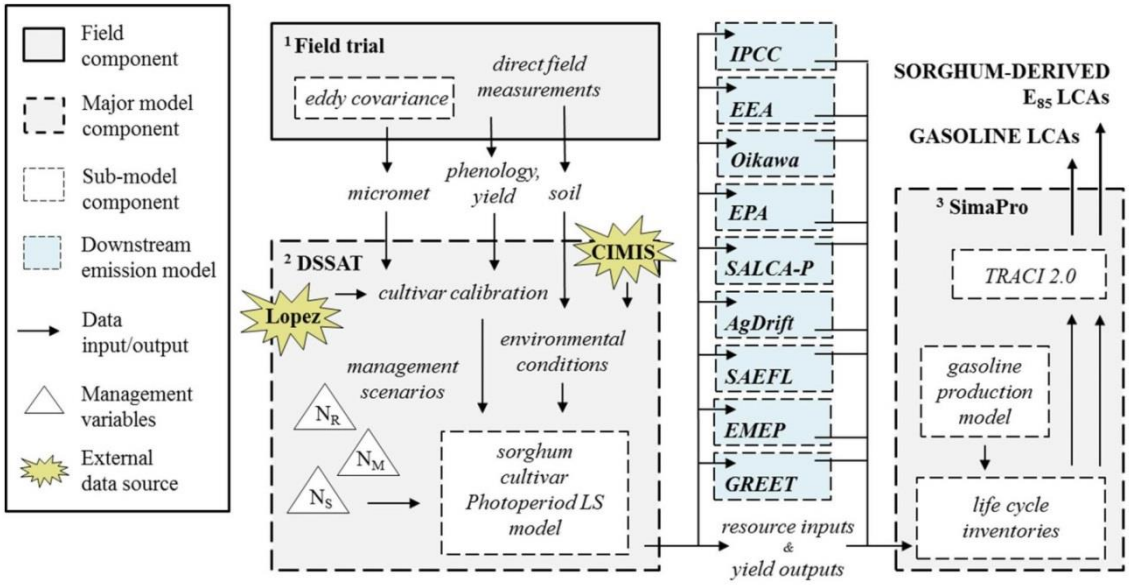

Figure 2.1. Major phases of data collection and analysis and their respective inputs and outputs. Outputs from the field trial were inputs to the crop model (DSSAT) and outputs from the crop model were inputs to the life cycle inventories (SimaPro). Lopez et. al (2017) provided crop coefficients and historical weather data was obtained from CIMIS. Management scenarios varied N application rate (N_R), N application method (N_M), and N source (N_S). Downstream emissions were determined using IPCC, EEA, Oikawa, EPA, SALCA-P, AgDrift, SAEFL, EMEP, and GREET emission models.

Field trial

Field data from in 2012 and 2014 were obtained from a 5.3 ha plot at the University of California's Desert Research Extension Center in Holtville, Imperial Valley, CA (32°N 48′42.6″, 115°W 26′ 37.5″). The 2013 season was sacrificed to eliminate an infestation of barnyard grass (*Echinochloa colona*). The Imperial Valley is characterized as a high-irradiance, arid environment with hot summers, mild winters, and infrequent rainfall (Oikawa et al. 2015b). Irrigation has allowed the Imperial Valley to become a major food and feed producing region in the United States (CDFA 2015). This region is also poised to become hub for bioenergy production, with plans to build the state's first cellulosic ethanol facility there to help meet the competitive renewable energy goals set by the state of California (CEC & CARB 2007).

Our Imperial Valley field site had deep alluvial soil, characterized as mildly alkaline, deep silty clay (pH 8.1; 42% clay, 41% silt, 16% sand). Field operations were logged by field managers and confirmed during frequent site visits. Following an eight month fallow period, the soil was tilled and laser leveled on 14 January 2012. Soil nutrient analysis from spatially replicated soil samples taken 30 January 2012 showed high initial soil N levels, 186 kg N ha^{-1}. A pre-plant fertilizer regime of 90 kg P_2O_5 ha^{-1} and 110 kg N ha^{-1} as urea was implemented on 10 February 2012. On 28 February *Sorghum bicolor* (cv. Photoperiod LS, Scott Seed, Inc., Hereford, TX, US) was planted at a density of 9 individuals m^{-2} on 76 cm beds. We applied supplemental N at the beginning of each growth cycle (80 kg N ha^{-1} on 2 March, 90 kg N ha^{-1} on 18 June, and 105 kg N

ha^{-1} on 16 August 2012) as either urea or urea ammonium nitrate (UAN). Irrigation was gravity fed via furrow flooding with scheduling based on plant need as assessed by field managers or when soil volumetric water content fell below 0.10 cm^3 cm^{-3}. Pesticide applications of chlorpyrifos and bromoxynil were applied on 27 March and 30 April 2012, respectively. Above-ground crop biomass was harvested 3 times throughout the 2012 growing season (4 June, 14 August, and 12 November) resulting in a total annual yield of 54.6 Mg dry weight (DW) ha^{-1} (Table 2.1). Eddy covariance measurements were used to assess net ecosystem exchange (NEE) throughout the growing season (Oikawa et. al 2015b).

Table 2.1. Agreement between modeled dry weight yields and actual dry weight yields expressed as percent difference (PD) for 2012 and 2014.

Period	**Field** *(Mg DW ha^{-1})*	**Modeled**	**Agreement** *(PD)*
	2012		
Harvest 1	18.363	18.369	0.03 %
Harvest 2	19.562	19.833	1.38 %
Harvest 3	16.437	15.874	-3.48 %
Annual	54.635	54.076	-1.03 %
	2014		
Harvest 1	11.584	11.638	0.47 %
Harvest 2	14.107	12.429	-12.65 %
Annual	25.691	24.067	-6.53 %

In 2014 a pre-plant herbicide regime of glyphosate, s-metolachlor, and atrazine was applied shortly after the field was cultivated and leveled. These efforts to reduce weed pressures delayed planting in 2014 to 4 April, allowing only 2 growth cycles in that year (Table 2.1). Four applications of urea at 90 kg N ha^{-1} were applied throughout the 2014 growing season, including one pre-plant application on 25 March, two supplemental applications during the first growth cycle (14 May and 4 June), and a third supplemental application following re-sprouting on 18 July. Eddy co-variance measurements were again recorded throughout the growing season, however instrument failure resulted in large gaps in our 2014 NEE flux data. Thus, 2012 field data was the primary dataset used to parameterize our crop model and served as the basis for our sorghum management scenarios.

Crop modeling: parameters and adjustments

We used 2012 field data to parameterize the Crop Environment Resource Synthesis (CERES) model for grain sorghum in DSSAT (Decision Support System for Agrotechnology Transfer v.4.5, Georgia USA; Figure 2.1). DSSAT is a process-based crop modeling system that simulates soil processes, weather, and crop growth, allowing investigation of a multitude of growing conditions and management choices (Jones et al., 2003). We first constructed an *in silico* soil profile representative of our field conditions, gap-filled where necessary with DSSAT's default soil profile for deep silty clay (Table S2.2). Historic (30 year) weather data for the site were compiled from nearby meteorological stations accessed through the California Irrigation Management

Information System (CIMIS; Table S2.2 and accompanying text). Management activities simulated logged field practices in 2012.

Parameterization of the grain sorghum model to simulate our forage sorghum crop entailed several steps. We adjusted allocation to vegetative growth based on published parameter adjustments for sweet sorghum (Lopez et al. 2017). Sensitivity analyses were then used to adjust phenological parameters. We used cumulative net primary productivity (NPP) curves from eddy co-variance data and field observations of phenological transitions in our parameterization (Figures S1 & S2 with details in accompanying text). Lastly, we increased the radiation use efficiency to better simulate yield outputs observed in the field (Table 2.1 & Figure S2.2.1). We then modeled the 2014 growing season according to reported management practices for that year. Although eddy covariance data from 2014 was insufficient for cultivar calibration purposes, our production model for 2014 also showed reasonably good fit in terms of phenology and yield (Table 2.1, Figure S2.2b).

Although a multi-year dataset is favorable for cultivar calibration, we used multiple growth cycles (3 in 2012 and 2 in 2014) to compensate for the limited duration of our field experiments. Importantly, as DSSAT does not simulate re-sprouting post-harvest, each growth cycle was modeled as a distinct planting event. We eliminated the first 14 days post-planting for secondary and tertiary growth cycles to better simulate aboveground growth following re-sprouting, but the model may inadequately simulate root dynamics and consequently underestimate N and water uptake. The extensive

parameter adjustments required to simulate a forage sorghum would benefit from future field trials to validate the model. Our model relies on several assumptions that were not thoroughly validated results should be interpreted accordingly. However, the model remains a useful tool for exploring the impacts of N management on WTW environmental impacts.

Crop modeling: scenario analyses

We simulated 25 management scenarios varying N fertilizer application rate, application method, and source to investigate productivity and NUE dynamics (Figure 2.2). In all scenarios, irrigation was simulated as furrow flooding, applied such that water was non-limiting. Our simulated values for N application rate were based on optimal rates reported in the literature for forage sorghum (Hallam et al. 2001; Hao et al. 2014; Haankuku et al. 2014; Bonin et al. 2016). As most sorghum-producing regions in the U.S. have a shorter growing season consisting of only one harvest, we normalized recommended N application rates by days in the growing season and extrapolated a rate of ~250 kg N ha^{-1} as optimal for our crop. However, we anticipated higher N demands in our system than those referenced, as each growth cycle would result in a spike in N demands not observed in a single, continuous growing season. Additionally, the high irradiance growing environment coupled with the lack of water limitations in our model suggested N consumption in our system might exceed those of other sorghum-producing regions in the United States. Accordingly, we explored a range of 50 – 450 kg N ha^{-1} simulated in 100 kg N ha^{-1} increments (Figure 2.2). The dates of each fertilizer

application followed our field practices, which were recorded in detailed crop logs from 2012 field trials. We simulated fertilizer applications as broadcast without incorporation or injected at 8 cm depth. Although the latter is recommended, the former is still common practice due to its lower costs (Mahler 2001; Jones 2013).

Management scenarios were simulated over a 30-year period using historical weather data (1983 – 2012) to introduce environmental variation (Table S2.3 and accompanying text). For all simulations, initial soil N was set to 68 kg N ha^{-1} for the first growth cycle, a rate typical of U.S. sorghum fields (Hao et al. 2014). Simulated residual N following the first and second harvests for each fertilizer scenario were used as initial N levels for the secondary and tertiary growth cycles, respectively.

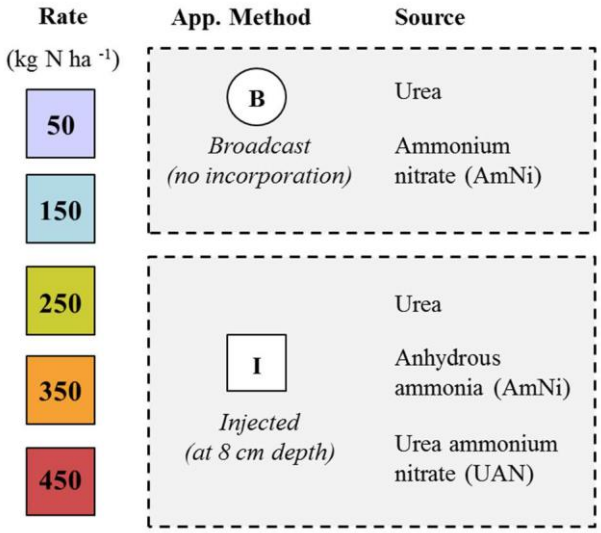

Figure 2.2. Nitrogen management scenarios imposed in the DSSAT model. We varied fertilizer rate from 50 – 450 kg N ha^{-1} in increments of 100 kg N ha^{-1}, and simulated applications are either broadcast without incorporation or injected at 8 cm depth. Two fertilizer types were simulated as broadcast fertilizer treatments (urea and ammonium nitrate) and three were simulated as injected (urea, anhydrous ammonia, and urea ammonium nitrate solution).

Life cycle assessment modeling: scope and system boundaries

Life cycle inventories (LCI) were constructed using SimaPro v.8 (Pré Consultants 2013) in compliance with ISO 14040 and 14044 standards (ISO 2006a; ISO 2006b). We chose a well-to-wheel (WTW) scope and 1 MJ combusted energy from E_{85} as the functional unit. An energy yield basis was selected as it allows direct comparison across energy sources (Borrion et al. 2012). Importantly, expressing emissions on an energy yield basis is most useful for assessing regional to global scale impacts and may obscure some local impacts. With the exception of select data originating from the Ecoinvent database (Wernet et al. 2016) within SimaPro v.8, we used second order system boundaries throughout our analyses, considering all relevant material, energy, and waste flows except those of embodied energy associated with facilities and machinery (Figure 2.3). The life cycle consisted of six sub-process modules: feedstock production, transportation of biomass from the farm to the conversion facility, conversion of biomass to ethanol, transportation of ethanol from the conversion facility to the refinery, blending and pumping of E_{85} fuel, and finally, combustion.

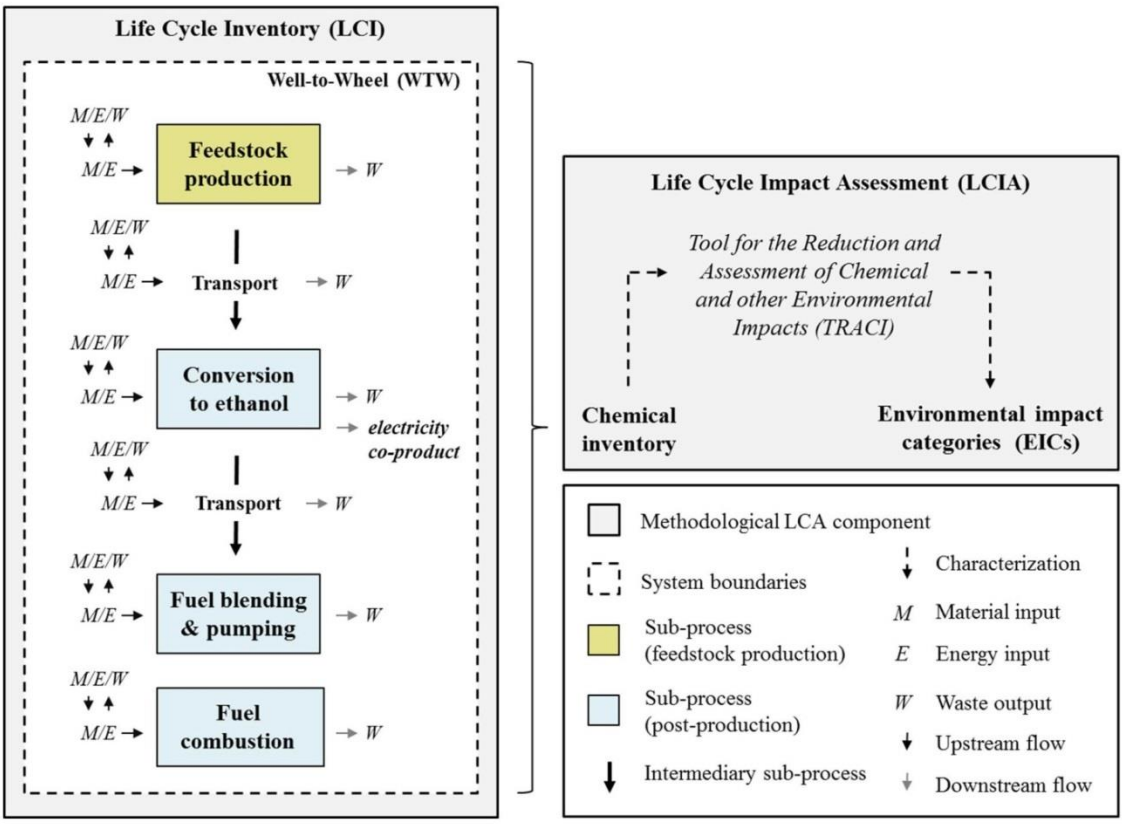

Figure 2.3. System boundary for life cycle inventory and life cycle impact assessment modeling processes for a WTW scope of sorghum-derived E_{85} production and use. System boundaries included relevant material (M), energy (E), and waste (W) flows of all processes and all process inputs (i.e. materials and energy consumed within processes).

E_{85} life cycle inventories: upstream flows

Chemical inventories associated with resource inputs were selected from the Ecoinvent database within SimaPro using U.S. regional unit process data when available and European unit process data otherwise. Feedstock production considered inputs of seed, fertilizers, pesticides, and diesel fuel combusted during field operations. Pesticides were accounted for by their active ingredients. Fuel inputs were estimated for field operations reported in 2012 management logs using average fuel requirement data

(Hanna 2005). Field operations reported for 2012 were fairly consistent with typical on-farm operations, operations reported in the literature, and recommendations of university extension programs (Miller & Stroup 2004; Haankuku et al. 2014; Hao et al. 2014; Bonin et al. 2016). For biomass and ethanol transport processes we assumed a transport distance of 80 km (Grift et al. 2012) by truck. Refinery processes for E_{85} fuel assumed a blend of 81% ethanol and 19% distilled petroleum, by weight, and $0.86e^{-3}$ kWh kg E_{85}^{-1} electricity for pumping (Hsu et al. 2010).

Chemical inputs to the conversion process were based on near-term means of Monte-Carlo simulations (Spatari et al. 2010). We assumed a relatively high conversion efficiency of 340 l ethanol Mg DW^{-1} under dilute acid pre-treatment based on a switchgrass conversion LCI model (Spatari et al. 2010) assuming NREL technology using simultaneous saccharification and co-fermentation conversion processes and organic Rankine cycle energy recovery processes. The organic Rankine cycle uses excess heat from upstream reactions to vaporize organic fluids generated during the conversion process. These high-entropy, vaporized fluids are then passed through a turbine, generating electricity. The organic vapors can then be condensed back to a liquid phase and the cycle can be renewed, minimizing heat waste and maximizing electricity recovery (Laser et al. 2009; Bronicki 2016). This results in co-production of electricity during cellulosic ethanol conversion.

Emissions from feedstock conversion are largely dependent on how co-products, such as electricity, are allocated in the fuel life cycle (Pimentel & Patzek 2005; Kaufman

et al. 2010; Singh et al. 2010; Kendall & Yuan 2013; Murphy & Kendall 2015). We allocated electricity generated during conversion using system expansion (i.e. displacement) as ISO 14044 standards explicitly support this method (ISO 2006b). Electricity co-products were parameterized to the United States Western Grid. Electricity generation corresponding to our biomass to ethanol conversion rate was previously determined to be 0.70 kWh electricity l ethanol^{-1} (Spatari et al. 2010).

Emissions from feedstock conversion are also influenced by the assumed biomass to ethanol conversion efficiency (Borrion et al. 2012; McKone et al. 2011; Kendall & Yuan 2013). As commercial production of cellulosic ethanol is limited, published conversion efficiencies remain uncertain (Fargione et al. 2010). Given that commercial investment would only be possible with a high ethanol yield, we assumed a conversion efficiency of 340 l ethanol Mg DW^{-1}. Assuming a high-efficiency conversion rate also provides a more liberal estimation of conversion-induced GHG emissions. Low-efficiency conversion generates lower ethanol yields but higher electricity yields (Spatari et al. 2010). Under system expansion, displaced GHG emissions from electricity co-production are often greater than emissions induced by cellulosic ethanol conversion processes (Pimentel & Patzek 2005; Spatari et al. 2010). Therefore, favoring more efficient ethanol production lowers the electricity co-product credit and, as a result, increases GHG emissions compared to less efficient conversion rates. Conversely, higher biomass demands under low-efficiency conversion required to generate the same energy outputs as high-efficiency conversion systems may inflate emissions associated with feedstock production. To evaluate the influence of conversion efficiency on overall

WTW emissions and WTW emissions across N management scenarios, we constructed additional LCAs assuming a low conversion efficiency (Figure S2.4 and accompanying text).

E_{85} life cycle inventories: downstream flows

Downstream emissions were modeled for fertilizer, pesticide, and fuel inputs in all applicable life cycle sub-processes (Table 2.2). Importantly, while DSSAT models nitrogen cycling and associated N loss pathways, these outputs reflect the summed emissions of multiple N species and were therefore inadequate for our purposes. Accordingly, no downstream emissions from crop production were adopted from the DSSAT model output. The majority of downstream models selected were tier 1 models, as robust regional emissions factors are lacking in the literature. Tier 1 models have high uncertainty ranges and results should be interpreted accordingly. Nonetheless, these models are designed to be broadly applied and are frequently employed in biofuels life cycle inventories (Adler et al. 2007; Burney et al. 2010; Tilman et al. 2011; Pourhashem et al. 2013; Schmer et al. 2014; Hudiburg et al. 2016; Zhong et al. 2016). In addition to downstream emission models detailed in Table 2.2, we inventoried downstream emissions from feedstock conversion based on published values for the most similar corresponding conversion scenario (scenario T7 in Spatari et al. 2010).

Table 2.2 Downstream emissions modeled for fertilizer, pesticides, and fuel combustion.

Input	Emission	Model	Source
Fertilizer	N_2O [a], CO_2 [b]	IPCC tier 1	(De Klein et al., 2006)
	NO_x	EEA tier 1	(Hutchings et al., 2016)
		Oikawa [c]	(Oikawa et al., 2015a)
	NH_3	EPA tier 2	(Battye et al., 1994)
	PO_4	SALCA-P	(Prasuhn, 2006)
Pesticides	MCPA, broxymil, chlorpyrifos	AgDRIFT tier 1 terrestrial [d]	(Teske et al., 2002)
Diesel & gasoline	CO_2 , CH_4 , N_2O	IPCC tier 1	(Waldron et al., 2006)
	Cd, Cr, Cu, Pb, Ni, Se, Zn, NH_3, SO_2, benzene, benzo(a)pryene, benzo(a)anthracene, benzo(b)flouranthene, chrysene, dibenz(a,h)anthracene, flouranthene, phenanthrene	SAEFL tier 1	(SAEFL, 2000)
	non-methane VOCs, particulates	EMEP tier 1	(Winther et al., 2016)
E_{85} fuel	CO_2, CH_4, N_2O, VOCs, CO, NO_x, SO_x, black carbon, organic carbon, particulates	GREET 2015 [e]	(Burnham, Wang, & Wu, 2006)

[a] includes direct and indirect N_2O emissions

[b] CO_2 emission model only applicable when N source is urea

[c] the Oikawa model was empirically derived based on NO_x flux measurements from our field site and was used as an alternative to the generalized EEA model to calculate NO_x emissions for urea and UAN fertilizer scenarios

[d] AgDRIFT ®; Air Resources Laboratory/NOAA, Research Triangle Park, NC, USA for pesticide deposition assuming fine particle size of applied pesticides, low boom application, and a 15.25 m buffer strip

[e] GREET 2015 ©; Agronne National Laboratory, Agronne, IL USA for a flexible fuel vehicle with AR4 global warming potential values (Forster et al., 2007), which are in alignment with the upstream values used for fuel production

In the case of NO_x emissions from N fertilizer, we introduced an alternative model specifically parameterized to our field site. The Oikawa NO_x models are empirically derived models of seasonal NO_x flux based on the baseline flux observed at our field site and the fluxes induced by application of broadcast urea fertilizer or UAN fertilizer applied through irrigation (Figure S2.3). As NO_x flux at our field site was found

to be substantially greater than predictions from then widely-used MEGAN emission model (Oikawa et al. 2015a) or the EEA model (Figure S2.3), the Oikawa model was preferred. However, its specific orientation to broadcasted urea and irrigation-applied UAN prohibited its use across the majority of our simulated scenarios. Therefore, we assumed the EEA NO_x model throughout, but constructed additional LCAs for broadcast urea scenarios using the Oikawa NO_x model.

Gasoline life cycle inventory

We also conducted an LCA for conventional gasoline in order to compare its emissions to those from E_{85} across consistent emission and characterization criteria (Figure 2.1). As in our E_{85} LCAs, this life cycle considered a WTW scope, a functional unit of 1 MJ combusted energy, and second order system boundaries. We used a U.S. regional unit process inventory of gasoline in the Ecoinvent database in SimaPro for emissions related to fuel extraction, processing, and transportation in our gasoline LCI. Electricity required for pumping was assumed to be the same for gasoline as for E_{85}. Emissions from combustion were modeled using published petroleum emission factors (SAEFL 2000; Waldron et al. 2006) from sources consistent with those used in our E_{85} life cycles (Table 2.2).

Life cycle impact assessment: characterization

Following the construction of life cycle inventories, emissions were characterized using the Tool for the Reduction and Assessment of Chemical and Other Environmental Impacts (TRACI 2 v. 3.03; Environmental Protection Agency, Washington DC, USA).

TRACI characterizes midpoint impacts to the environment and human health (Bare et al. 2003). Midpoint models characterize the impacts of individual chemical compounds along that compound's cause-and-effect chain but prior to the end point of the chain (Bare et al. 2000; Brilhuis-Meijer 2014). For instance if phosphorus is leached into the groundwater, it will eventually enter a body of water and, in doing so, increase the concentration of phosphorus in that water body. This increased concentration of phosphorus is the midpoint of the cause and effect chain of eutrophication. A sufficiently high concentration of phosphorus can cause an algal bloom, which may result in fish die-offs. The loss of fish species would then be an endpoint of the cause and effect chain of eutrophication. While end-point impacts are easier to interpret, they also have higher uncertainties (Bare et al. 2000). Further midpoint impact assessments are favorable when considering tradeoffs across environmental impact categories as endpoint impact categories are considerably more broad and may obscure these relationships (Brilhuis-Meijer 2014).

Nine impact categories are characterized in TRACI based on their relevance for regulatory purposes as appraised by the U.S. Environmental Protection Agency. Environmental impacts considered by TRACI are global warming, ozone depletion, smog, acidification, eutrophication, and ecotoxicity (aquatic and terrestrial). Impacts to human health are assessed in terms of carcinogenics, non carcinogenics, and respiratory effects. Equivalent units and midpoint criteria for these impact categories can be found in the supporting information (Table S2.2.1). TRACI characterizes emissions contributing

to each of these impact categories based on the relative potency of individual chemical compound inventoried in the life cycle in contributing to each impact (Bare et al. 2003).

2.4 Results

Crop model outputs

Yield saturation was not observed across the range of N application rates simulated in our crop model. Though yield response to N was consistently positive, the nature of this response varied considerably across fertilizer application methods, and in some instances, fertilizer sources (Figure 2.4). Modeled yields from injected fertilizer scenarios varied by < 1% across N sources at any given N application rate. However, among broadcast scenarios yields varied by as much as130% across N sources, with simulated yields from broadcast ammonium nitrate (AmNi) consistently exceeding those of broadcast urea. Simulated yields in broadcast ammonium nitrate scenarios were more similar to injected scenarios, with < 18% difference in yields across the N application rates simulated. Both injected and broadcast ammonium nitrate simulations were characterized by a positive sigmoidal yield response to increasing N inputs (Figure 2.4). For instance, simulated yields in injected fertilizer scenarios nearly doubled from 50 to 150 kg N ha^{-1} but increased by only 15% from 350 to 450 kg N ha^{-1}. Broadcast urea simulations resulted in a weak but linear yield response to applied nitrogen that also declined with increasing N inputs (31% increase from 50 to 150 kg N ha^{-1} and 12% increase from 350 to 450 kg N ha^{-1}). This subdued response to nitrogen in broadcast urea scenarios resulted in maximum simulated yields of 21.8 Mg dry weight ha^{-1}. Conversely,

maximum simulated yields for broadcast ammonium nitrate and injected fertilizer scenarios were 50.4 and 59.2 Mg DW ha^{-1}, respectively (Figure 2.4).

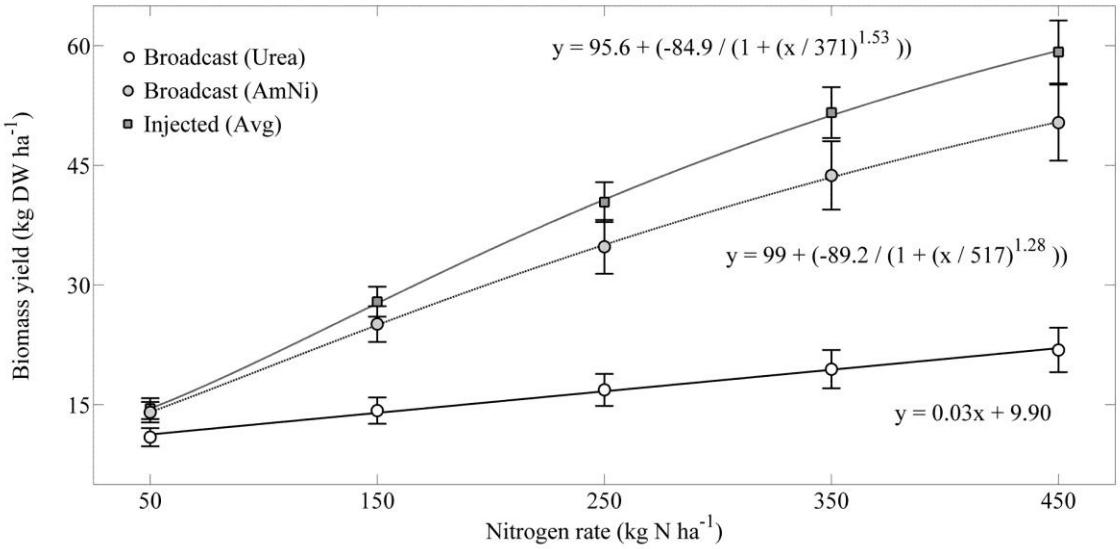

Figure 2.4. Simulated yield response to N for broadcast urea and ammonium nitrate (AmNi) treatments and injected fertilizer treatments, averaged across fertilizer sources. Error bars for broadcast scenarios depict standard deviation across simulated weather years while error bars for injected scenarios depict combined standard deviation across weather years and fertilizer types. Model parameters were fit in Matlab. All relationships had an $r^2 \geq 0.94$ and $p \leq 0.02$.

Life cycle assessment: trends in emissions across N management scenarios

At any given N application rate, WTW emissions were always highest in broadcast urea scenarios (Figure 2.5). Emissions tended to be lowest in injected fertilizer scenarios. Broadcast ammonium nitrate scenarios had lower emissions contributing to acidification, eutrophication, and ecotoxicity than the average emissions from injected fertilizer treatments. However, when injected scenarios were parsed by N source, only

emissions from injected urea scenarios were higher than those from broadcast ammonium nitrate scenarios (Table S2.4).

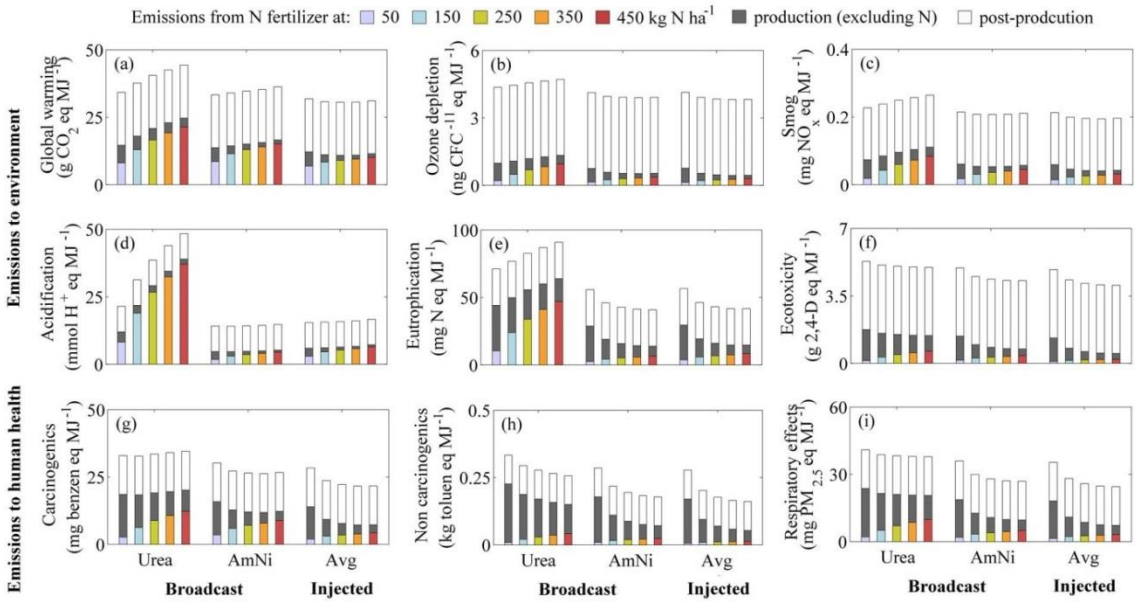

Figure 2.5. Modeled WTW emissions for sorghum-derived E_{85} across N management scenarios. Emissions from production are shown for broadcast scenarios, separated by type, and injected scenarios, averaged across fertilizer types. Emissions from N fertilizers are shown by the colored portion of the bar, with color indicating fertilizer rate. The remaining emissions from production are shown by the dark grey portion of the bar. Emissions from post-production processes (transportation, conversion, blending, pumping, and combustion) are shown in white.

Emissions contributing to human health tended to decline or stabilize with increasing N application rate, regardless of application method or source (Figure 2.5). Emissions contributing to the environment showed a more diverse response to increased N application rate. WTW emissions in broadcast urea scenarios almost always increased with increasing N inputs. Conversely, WTW emissions in broadcast ammonium nitrate and injected scenarios tended to decline or stabilize with increasing N application rate.

On an energy yield basis, the most emission-conservative scenarios were injected application of anhydrous ammonia at 350 or 450 kg N ha^{-1}, with differences in emissions across these scenarios varying by < 3% in all cases (Figure 2.5 & Table S2.5). Injected UAN at 350 and 450 kg N ha^{-1} followed closely behind. Broadcast urea applied at 450 kg N ha^{-1} resulted in the highest WTW emissions per MJ energy in most impact categories (Figure 2.5). Emissions contributing to non carcinogenics, respiratory effects, and ecotoxicity, however, were highest for broadcast urea applied at 50 kg N ha^{-1}.

Life cycle assessment: emissions contributing to the environment

The carbon intensity of sorghum-derived E_{85} fuel ranged from 29 – 44 g CO_2 eq MJ^{-1} across simulated feedstock production scenarios (Table S2.5). WTW GHG emissions in broadcast urea scenarios were 3 – 18% higher than in corresponding broadcast ammonium nitrate scenarios and 7 – 30% higher than in corresponding injected scenarios (Figure 2.5a). GHGs increased by 27% and 8% with increasing N application rate in broadcast urea and ammonium nitrate scenarios, respectively, and varied by < 5% in injected scenarios. WTW emissions contributing to ozone depletion in broadcast urea scenarios were 5 – 19% higher than broadcast ammonium nitrate and injected scenarios (Figure 2.5b). These emissions were not strongly affected by N application rate at the WTW level, increasing or decreasing by $\leq$ 8% across N application rates depending on fertilizer application method and source. Emissions contributing to smog increased by 16% across N application rates in broadcast urea scenarios, varied by < 3% in ammonium

nitrate scenarios, and declined by 9% in injected scenarios before roughly stabilizing at 250 kg N ha^{-1} (Figure 2.5c).

Emissions contributing to acidification tended to increase with increasing N application rate regardless of fertilizer strategy (Figure 2.5d). N source, however, was an important determinant of emissions contributing to acidification. These emissions increased by only 6% across N application rates in broadcast ammonium nitrate scenarios, but increased by 93% across the same range in broadcast urea scenarios. Impacts to acidification also varied across N sources in injected scenarios, with emissions increasing by 28% across N application rates for injected urea, decreasing by 8% for injected anhydrous ammonia, and remaining relatively stable across N application rates for UAN (Table S2.4).WTW emissions contributing to eutrophication were also strongly influenced by fertilizer source and application method (Figure 2.5e). These emissions increased by 25% across N application rates in broadcast urea scenarios and decreased by a similar magnitude in broadcast ammonium nitrate scenarios. Emissions contributing to eutrophication also declined across N application rates in injected scenarios, but the magnitude of this response varied from 17 – 33% across N sources (Table S2.4). Emissions contributing to ecotoxicity consistently declined with increasing N application rate but were not substantially affected by N source or application method at the WTW level (Figure 2.5f).

Life cycle assessment: emissions contributing to the human health

Emissions impacting human health almost always declined with increasing N application rate (Figure 2.5g – i). The only exception was carcinogenic emissions in broadcast urea scenarios, which were relatively unaffected up to 150 kg N ha^{-1} and increased by a modest 5% thereafter (Figure 2.5g). Carcinogenic emissions declined from 50 to 350 kg N ha^{-1} by 13% in broadcast ammonium nitrate scenarios and by 18 – 29% in injected scenarios, but remained relatively stable thereafter. Non carcinogenic emissions declined by 25%, 43%, and 49% across N application rates in broadcast urea, broadcast ammonium nitrate , and injected scenarios, respectively (Figure 2.5h &Table S2.5). Emissions contributing to respiratory effects for these scenarios declined by 8%, 27%, and 34%, respectively.

Life cycle assessment: localized NO_x model

The Oikawa NO_x model for broadcast urea resulted in higher NO_x emissions than the tier 1 EEA model (Figure S2.3). These higher NO_x emissions translated to a 12 – 25% increase in emissions contributing to acidification, a 2 – 15% increase in emissions contributing to eutrophication, and a 7 – 33% increase in emissions contributing to respiratory effects (Table 2.3). Emissions contributing to smog were most strongly affected by the assumed NO_x model, increasing by 17 – 113% across N application rates.

Table 2.3. Percent increase in modeled WTW emissions and emissions from E_{85} relative to gasoline assuming the Oikawa NO_x model for broadcast urea scenarios in place of the EEA tier 1 NO_x model.

Impact Category	N Application rate (kg N ha^{-1})									
	50	*150*	*250*	*350*	*450*	*50*	*150*	*250*	*350*	*450*
	Increased WTW emissions (%)					***Increased emissions relative to gasoline (%)***				
Acidification	12	5	7	14	25	173	274	370	469	585
Resp. effects	7	4	8	17	33	146	128	133	150	183
Eutrophication	4	2	4	8	15	1,133	1,211	1,330	1,464	1,634
Smog	28	17	28	60	113	125	115	146	216	333

Life cycle assessment: E_{85} vs. gasoline

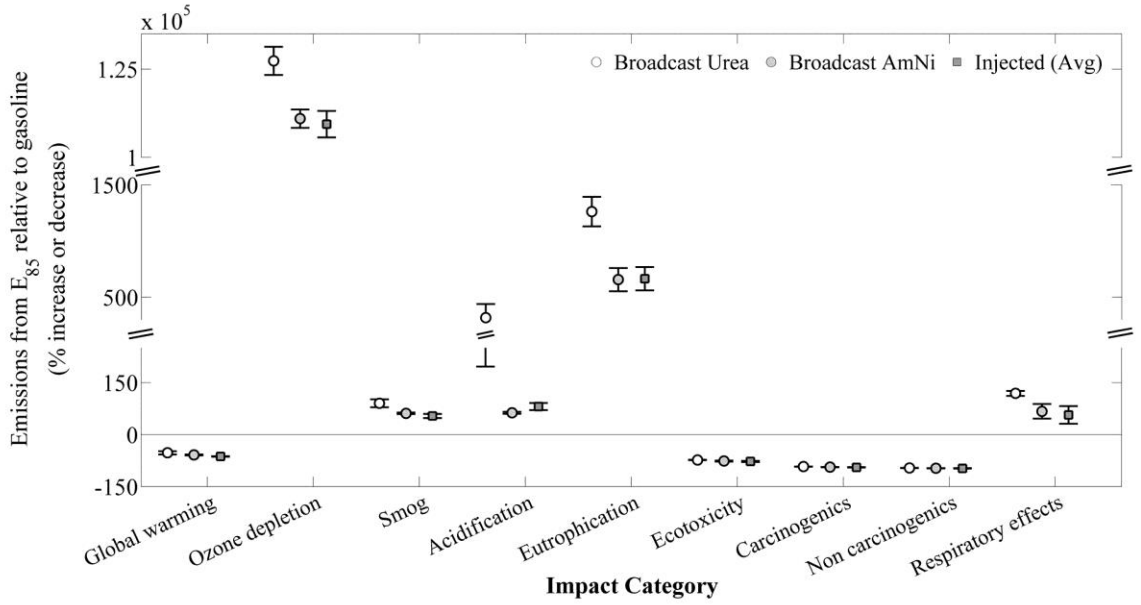

Figure 2.6. Mean percent change in modeled WTW fuel emissions when substituting conventional gasoline for E_{85} fuel from sorghum-derived cellulosic ethanol, determined as [(emissions from E_{85} – emissions from gasoline)/emissions from gasoline] * 100. Error bars represent standard deviations in mean percent change in emission across simulated N application rates for broadcast urea and ammonium nitrate scenarios and across N application rates and N sources for injected scenarios.

Relative to gasoline, sorghum-derived E_{85} reduced emissions contributing to global warming by 47 – 65%, to ecotoxicity by 74 – 79%, to carcinogenics by 92 – 96%, and to non-carcinogenics by 97 – 98% (Figure 2.6). However, substitution of gasoline with E_{85} resulted in increased emissions contributing to ozone depletion by 105,050 – 132,030%, to smog by 49 – 103%, to acidification by 39 – 449%, to eutrophication by 498 – 1,414%, and to respiratory effects by 31 – 114% assuming the EEA NO_x model. Scenarios assuming the Oikawa NO_x model resulted in higher emissions contributing to

smog, acidification, eutrophication, and respiratory effects. These emissions increased by as much as 333%, 585%, 1,634%, and 183%, respectively, for E_{85} compared to gasoline (Table 2.3).

2.5 Discussion:

Fertilizer management during feedstock production affected most pollutant loads from sorghum-derived E_{85}. Increasing N inputs generated higher biomass yields (Figure 2.4) but were also a major source of emissions to the environment (Figure 2.5). Fertilizer application rate, application method, and source all contributed to emission intensities. Broadcast urea simulations resulted in the highest WTW emissions, with increasing N application rate tending to increase emissions. Conversely, anhydrous ammonia applied at 350 – 450 kg N ha^{-1} via injection resulted in the lowest WTW emissions of all scenarios simulated, suggesting the carbon intensity and pollutant loads of cellulosic fuels are not necessarily compromised by high N use at regional to global scales. Sorghum-derived cellulosic ethanol had clear advantages over gasoline in terms of GHG intensity and several other impact categories. Emissions contributing to air and water pollution, however, tended to be substantially higher for E_{85} than for gasoline and were often heavily influenced by feedstock management (Figure 2.6). Together, our results suggest that N management choices strongly influence life cycle tradeoffs between the productivity, GHG intensity, and pollutant loads of cellulosic fuels, particularly in terms of local air and water pollution. Minimizing on-farm emissions through efficient N management should be a priority area for future field research.

WTW emissions from E_{85}: N application rate

Across all impact categories, increasing N contributed to increasing emissions in absolute terms. However, assessed on an energy yield basis (MJ^{-1}) at the WTW scope, higher yields associated with increasing N inputs down-scale these additional emissions from N. Higher yields associated with increasing N inputs also down-scale emissions from non-N sources incurred during feedstock production (e.g. phosphorus, fuel) on an energy yield basis, as lesser quantities of these non-N inputs were required to generate a similar volume of E_{85} when N inputs were increased. Therefore, WTW impacts expressed on an energy yield basis only intensified with increasing N rate when the increase in emissions associated with additional N exceeded the decrease in emissions resulting from the corresponding yield response. Inefficient N uptake in broadcast urea simulations resulted in a modest yield response. As a result, corresponding WTW emissions tended to worsen with increasing N inputs (Figures 4 & 5). Conversely, in broadcast ammonium nitrate and injected fertilizer scenarios, simulated yield increases tended to outweigh modeled emission increases on an energy yield basis at N application rates as high as 350 – 450 kg N ha^{-1}. Our hypothesis that increasing N inputs would reduce emissions at modest fertilizer rates and increase them at higher N rates was, therefore, largely not supported by our simulations even when N constituted a major source of emissions. Emissions to several impact categories roughly stabilized at 250 – 350 kg N ha^{-1}in injected and broadcast ammonium nitrate scenarios, increasing or decreasing by no more than 2% at 450 kg N ha^{-1}. This suggests that higher N application rates, which would elicit an increasingly marginal yield response, would eventually generate higher WTW

emissions. However, limited field validation precludes determination of an optimal N value for Imperial Valley sorghum.

Importantly, while expressing emissions on an energy yield basis is appropriate for assessing regional to global impacts, it can obscure impacts at the local level. In the present study, where emissions are most intensive during feedstock production, local impacts may be better characterized on a land area basis. If higher yields achieved with increasing N are not concurrent with a commensurate reduction in hectares planted, these local impacts will be intensified as N inputs increase, regardless of productivity.

WTW emissions from E_{85}: N application method and source

Our analysis revealed lower emissions and higher yields with injection of N-fertilizers, a win-win for both productivity and sustainability. Low NUE in broadcast urea simulations resulted in higher emissions across the board, though some impact categories were more strongly affected than others. Previous research has shown surface applications of urea results in high volatilization and denitrification losses that curtail nitrogen uptake (Linquist et al. 2012; Millar et al. 2014). Ammonium nitrate is less susceptible than urea to volatile losses during surface application, but still less efficient than injected fertilizer applications, which concentrate nutrients in the root zone (Millar et al. 2014). These differences in N accessibility and loss rates were observed across fertilizer sources and application methods in our crop model and the influence of these factors on simulated N uptake were reflected in WTW life cycles based on their yield implications (Figure 2.4). However, downstream emission models largely did not account

for these factors. Consequently, WTW emissions from broadcast urea scenarios presented here may be underestimated while emissions from injected scenarios may be overestimated. Our results may be similarly skewed by our model's inability to capture the root maturation across growth cycles. In broadcast urea scenarios, where N loss primarily occurs through volatilization and uptake occurs in shallow soil layers, inadequate root development may not strongly inhibit N uptake. Uptake similarly occurs in shallow soil layers when ammonium nitrate is broadcast without incorporation.

However, in injected scenarios, where N loss primarily occurs through leaching and uptake occurs at $\geq$ 8 cm depth, our model may underestimate N uptake and, consequently, NUE. Underestimation of NUE would result in overestimation of WTW emissions. Thus, the advantages of injected N fertilizers discussed here may be understated.

In injected scenarios, N source had virtually no impact on yield in our simulations, but did appear to influence emissions from several impact categories. Differences in emissions contributing to acidification, eutrophication, and carcinogenics were the most prominent (Table S2.4) and were all associated with source-specific emission factors for NH_3 volatilization, which are highest for urea (Battye et al. 1994). However, while these emissions factors consider N source, they do not consider N application method. Accordingly, modeled NH_3 volatilization rates for urea were the same for broadcast and injected scenarios and, as a consequence, almost certainly overestimate NH_3 emissions from injected urea (Mahler 2001; Millar et al. 2014).

Similarly, although volatilization rates for anhydrous ammonia and UAN were relatively low, these emissions may also be overestimated if emission factors assumed an unincorporated application method. Differences in emissions from injected scenarios across fertilizer sources should therefore be interpreted with caution. Along these lines, we stress the need for more refined emission factors to improve the ability to model emission outcomes associated with different fertilizer sources and application methods.

WTW emissions from E_{85}: GHG intensity

The GHG intensity of sorghum-derived E_{85} varied by as much as 33% across N management scenarios (Figure 2.5a, Table S2.5). Greenhouse gas emissions were roughly divided between emissions from feedstock production and post-feedstock production processes, which mitigated the impacts of nitrogen management on overall GHG intensity. Low NUE in broadcast urea simulations resulted in a weak yield response that was not sufficient to compensate for increased N_2O emissions (Figures 4 & 5a). Conversely, increased N_2O emissions from N fertilizer were largely compensated for by increased yields in injected scenarios and, to a lesser extent, in broadcast ammonium nitrate scenarios. These results contrast with recent assertions that increased N application rate compromises the GHG mitigation benefits of cellulosic fuels (Ruan et al. 2016). Although GHGs increased with N in broadcast urea scenarios, they were minimally affected by N application rate in broadcast ammonium nitrate scenarios and tended to decline slightly with increasing N application rate in injected scenarios, at least when expressed on an energy yield basis. Our results instead suggest that the effect of N

on the GHG intensity of cellulosic fuels hinges on both NUE at baseline N application rates and on the degree of change in NUE as N rate increases.

Greenhouse gas emissions from N fertilizer are dominated by N_2O emissions (Adler et al. 2007; Fazio & Monti 2011; Shcherbak et al. 2014; Ruan et al. 2016). We modeled these emissions using a tier 1 IPCC model, which, while useful for benchmarking and comparing with other research, is known to have high uncertainty (De Klein et al. 2006; Singh et al. 2010; Wang et al. 2012). This model is largely based on applied N and does not distinguish between synthetic N sources, fertilizer application method, or soil properties. Given these unresolved limitations, N_2O emissions reported here may be underestimated in broadcast urea scenarios and overestimated in injected fertilizer scenarios. Although a growing body of research suggests an exponential relationship between N application rate and N_2O emissions (Hoben et al., 2011; McSwiney & Robertson, 2005; Ruan et al., 2016; Shcherbak et al., 2014; Liang et al., 2016) as opposed to the IPCC's linear relationship, the assumptions of existing exponential N_2O models do not align with the observed and simulated dynamics in our system. These models assume N application rates exceeding ~100 kg N ha^{-1} are saturating (McSwiney & Robertson 2005; Hoben et al. 2011; Shcherbak et al. 2014), which our field data and crop model suggest is inaccurate for Imperial Valley sorghum production. Therefore, these models may vastly overestimate emissions in our system. Further, differences in NUE across broadcast and injected treatments would likely result in different exponential responses not currently accounted for by existing exponential

models. Increasing refinement of these N_2O models is an important area for future research.

WTW emissions from E_{85}: air and water pollutant loads

Emissions contributing to ozone depletion and ecotoxicity were largely derived from post-feedstock production processes in the E_{85} life cycle and therefore not strongly affected by N management during feedstock production (Figures 5b and 5f). Nonetheless, injected and broadcast ammonium nitrate scenarios retained slight advantages over broadcast urea scenarios. Emissions contributing to smog also tended to be dominated by post-feedstock production emissions and showed a similarly muted response to N management (Figure 2.5c). However, while these emissions were only modestly affected using the EEA tier 1 emission model for NO_x, emissions from broadcast urea scenarios more than doubled from 50 to 450 kg N ha^{-1} when we applied the Oikawa NO_x model (Figures 6). As this model was derived from NO_x fluxes measured at our Imperial Valley field site following broadcast application of urea (Figure S2.3), these amplified NO_x emissions are likely more accurate for our system. Unfortunately, the Oikawa NO_x model was not parameterized for broadcast ammonium nitrate or injected fertilizer applications, which remains a needed research direction.

The remaining impact categories were at least partially dominated by emissions from feedstock production. Emissions contributing to acidification, eutrophication, and carcinogenics were the most variable across N management scenarios as they were highly sensitive to nitrogen, and subsequently, NUE (Figures 5d, 5e, & 5g). In N-inefficient

broadcast urea scenarios, N was an important source of emissions. Conversely, in N-efficient broadcast ammonium nitrate and injected scenarios, emissions were predominantly from non-N sources, allowing a decline in energy yield-scaled emissions across N rates corresponding to higher simulated biomass yields. Emissions contributing to non carcinogenics and respiratory effects were also largely derived from non-N sources and, therefore declined with increasing N across all scenarios (Figures 5h & 5i).

WTW environmental impacts across fuel sources

GHG estimates from our LCA of gasoline were roughly 7% lower than those reported from other sources (Table S2.5) (Sheehan et al. 2000; CARB 2009); likely due to a difference in assumed emissions factors. Even against these conservative estimates, the carbon intensity of sorghum-derived cellulosic ethanol was, on average, less than half that of gasoline on the basis of WTW GHG emissions (34 and 84 – 95 g CO_2 eq MJ^{-1}, respectively) (Table S2.5). However, when evaluated across multiple impact categories, tradeoffs were evident (Figure 2.6). Adverse impacts to local air and water quality tended to be more severe and more variable across management scenarios than beneficial impacts to global warming, human health, and ecotoxicity. These results highlight the importance of feedstock management in determining the environmental impacts of cellulosic fuels. Notably, the potential for adverse impacts to smog were strongly influenced by our choice of NO_x model (Figure 2.6). Other emission potentials may similarly be influenced by model specificity, again highlighting the importance of developing management-specific regional emission factors.

Our results are generally in agreement with those of previous studies considering non-GHG emissions. Emissions contributing to acidification and eutrophication in our model increased by several orders of magnitude for E_{85} relative to gasoline, which is more or less in agreement with previously reported estimates for cellulosic ethanol-based fuels (von Blottnitz & Curran 2007; Bai et al. 2010; Borrion et al. 2012; Jeswani et al. 2015; Mbonimpa et al. 2016; Robledo-Abad et al. 2016; Weldu & Assefa 2016). Importantly, emissions contributing to eutrophication may be overestimated in our model, as the SALCA-P model for phosphorus leaching does not account for low percolation rates typical of heavy clay soils found in the Imperial Valley (Prasuhn 2006). Still, emissions derived from N and post-feedstock production practices comprise $\geq$ 50% of emissions contributing to eutrophication, suggesting eutrophication potential would be substantially higher for sorghum-derived E_{85} than gasoline even in the event that no phosphorus was leached during production.

Emissions contributing to human toxicity have also been previously reported to be higher for cellulosic fuels than gasoline (von Blottnitz & Curran 2007; Jeswani et al. 2015; Mbonimpa et al. 2016; Robledo-Abad et al. 2016; Weldu & Assefa 2016). Although human toxicity is not specifically characterized in TRACI, several impacts to human health are. Our results show higher contributions to respiratory effects for cellulosic ethanol, but lower carcinogenic and non-carcinogenic emissions. Importantly, higher emissions contributing to smog and respiratory effects for E_{85} relative to gasoline may present an important tradeoff for bioenergy production in the Imperial Valley, where air quality is already greatly compromised (ALA 2016). Declining local air quality may

increase incidence of asthma and has been linked to increased mortality in other biofuel-producing regions (Ashworth et al., 2013; Tsao et al., 2011). While our study shows a potential reduction in emissions contributing to air and water pollution with increasing injected N inputs on an energy yield basis, recognizing that emissions will increase with increasing N inputs on a land area basis is important and may exacerbate these adverse local impacts.

Although water use impacts and land use change were not considered in this study, other studies have shown they can pose additional tradeoffs for bioenergy sources (Bonsch et al., 2016). For instance, in California, water use for bioenergy can be 100 – 1000% higher than for gasoline (Fingerman et al. 2010) and land use impacts have been estimated to contribute an additional 10 – 340 g CO_2 MJ^{-1} to bioenergy lifecycles (Plevin et al. 2010). Development and widespread implementation of standardized metrics for water and land use impacts is necessary to further evaluate these tradeoffs across feedstocks and fuel technologies.

Synthesis

Coupled crop-LCA modeling systems are a useful tool for exploring multiple dimensions of the biofuels life cycle and highlighting possible pathways for emission reductions and paving the way for future field studies. When compared to gasoline, sorghum-derived cellulosic ethanol was advantageous in terms of GHG emissions and, generally, impacts to human health, but resulted in substantially higher local air and water pollutant loads. It is important to recognize the environmental tradeoffs associated with alternative fuels so

that adverse impacts can be avoided, or at least mitigated, whenever possible. In agreement with previous work, we found efficient application of N fertilizer to reduce environmental impacts associated with feedstock production on an energy basis (Schmer et al. 2008; Singh et al. 2010). However, we also found that high rates of N can support low GHG intensities and pollutant loads from cellulosic fuels on an energy yield basis, so long as a sufficient yield-response is elicited. Meeting demands of mandates for cellulosic ethanol production (CEC & CARB 2007; EPA 2010) necessitates examination of multi-dimensional life cycle impacts of renewable energy production to more accurately assess their environmental impacts and to avoid solving one pollution problem at the expense of another.

2.6 References:

Adler, P. R., Del Grosso, S. J., Inman, D., Jenkins, R. E., Spatari, S., & Zhang, Y. (2012). Mitigation Opportunities for Life-Cycle Greenhouse Gas Emissions during Feedstock Production across Heterogeneous Landscapes. In *Managing Agricultural Greenhouse Gases* (pp. 203–219). Elsevier.

Adler, P. R., Grosso, S. J. Del, & Parton, W. J. (2007). Life-cycle assessment of net greenhouse-gas flux for bioenergy cropping systems. *Ecological Applications*, *17*(3), 675–691.

ALA. (2016). *State of the Air 2016*. American Lung Association, Chicago, IL.

Ashworth, K., Wild, O., & Hewitt, C. N. (2013). Impacts of biofuel cultivation on mortality and crop yields. *Nature Climate Change*, *3*(5), 492–496.

Bai, Y., Luo, L., & van der Voet, E. (2010). Life cycle assessment of switchgrass-derived ethanol as transport fuel. *The International Journal of Life Cycle Assessment*, *15*(5), 468–477.

Bare, J. C., Hofstetter, P., Pennington, D. W., & de Haes, H. A. U. (2000). Midpoints versus endpoints: The sacrifices and benefits. *The International Journal of Life Cycle Assessment*, *5*(6), 319–326.

Bare, J. C., Norris, G. A., Pennington, D. W., & Mckone, T. (2003). The Tool for the Reduction and Assessment of Chemical and Other Environmental Impacts. *Journal of Industrial Ecology*, *6*(3–4), 48–78.

Battye, R., Battye, W., Overcash, C., & Fudge, S. (1994). *Development and selection of ammonia emission factors: Final report*. Environmental Protection Agency, Research Tirangle Park, NC.

Baumgart-Getz, A., Prokopy, L. S., & Floress, K. (2012). Why farmers adopt best management practice in the United States: A meta-analysis of the adoption literature. *Journal of Environmental Management*, *96*(1), 17–25.

Boehmel, C., Lewandowski, I., & Claupein, W. (2008). Comparing annual and perennial energy cropping systems with different management intensities. *Agricultural Systems*, *96*(1), 224–236.

Bonin, C. L., Heaton, E. A., Cogdill, T. J., & Moore, K. J. (2016). Management of Sweet Sorghum for Biomass Production. *Sugar Tech*, *18*(2), 150–159.

Bonsch, M., Humpenöder, F., Popp, A., Bodirsky, B., Dietrich, J. P., Rolinski, S., … Stevanovic, M. (2016). Trade-offs between land and water requirements for large-scale bioenergy production. *GCB Bioenergy*, *8*(1), 11–24.

Borrion, A. L., McManus, M. C., & Hammond, G. P. (2012). Environmental life cycle assessment of lignocellulosic conversion to ethanol: A review. *Renewable and Sustainable Energy Reviews*, *16*(7), 4638–4650.

Brentrup, F., Küsters, J., Kuhlmann, H., & Lammel, J. (2004). Environmental impact assessment of agricultural production systems using the life cycle assessment methodology. *European Journal of Agronomy*, *20*(3), 247–264.

Brilhuis-Meijer, E. (2014). Consider Your Audience When Doing Impact Assessment. Pre Sustainbility, the Netherlands,.Retrieved February 3, 2016, from https://www.pre-sustainability.com/consider-your-audience-when-doing-lca

Bronicki, L. Y. (2016). *Organic Rankine Cycle Power Plant for Waste Heat Recovery*. ORMAT International, Inc., Reno, NV. Retrieved from http://www.ormat.com/

Burney, J. A., Davis, S. J., & Lobell, D. B. (2010). Greenhouse gas mitigation by agricultural intensification. *Proceedings of the National Academy of Sciences of the United States of America*, *107*(26), 12052–7.

Burnham, A., Wang, M. Q., & Wu, Y. (2006). *Development and applications of GREET 2.7 -- The Transportation Vehicle-CycleModel.* Argonne, IL.

CARB. (2009). *Proposed Regulation for Implementing Low Carbon Fuel Standards (Staff Report: Initial Statement of Reasons)* (Vol. 1). California Air and Resources Board, Sacramento, CA.

CDFA. (2015). *California County Agricultural Commissioners' Reports: Crop Year 2013 - 2014*. California Department of Food and Agriculture, Sacramento, CA.

CEC, & CARB. (2007). *State Alternative Fuels Plan*. Caliornia Energy Comission & California Air and Resources Board, Sacramento, CA.

Cherubini, F., Bird, N. D., Cowie, A., Jungmeier, G., Schlamadinger, B., & Woess-Gallasch, S. (2009). Energy- and greenhouse gas-based LCA of biofuel and bioenergy systems: Key issues, ranges and recommendations. *Resources, Conservation and Recycling*, *53*(8), 434–447.

Cherubini, F., & Strømman, A. H. (2011). Life cycle assessment of bioenergy systems: State of the art and future challenges. *Bioresource Technology*, *102*(2), 437–451.

da Silva, C. R. U., Franco, H. C. J., Junqueira, T. L., van Oers, L., van der Voet, E., & Seabra, J. E. A. (2014). Long-Term Prospects for the Environmental Profile of Advanced Sugar Cane Ethanol. *Environmental Science & Technology*, *48*(20), 12394–12402.

Davis, S. C., Parton, W. J., Grosso, S. J. Del, Keough, C., Marx, E., Adler, P. R., & DeLucia, E. H. (2012). Impact of second-generation biofuel agriculture on greenhouse-gas emissions in the corn-growing regions of the US. *Frontiers in Ecology and the Environment*, *10*(2), 69–74.

De Klein, C., Novoa, R. S. A., Ogle, S., Smith, K. A., Rochette, P., Wirth, T. C., … Williams, S. A. (2006). N2O Emissions from Managed Soils and CO2 Emissions from Lime and Urea Application. In *2006 IPCC Guidelines for National Greenhouse Gas Inventories*. Intergovernmental Panel on Climate Change, Geneva, Swtizerland.

Diaz-Chavez, R., Kunen, E., Walden, D. *et al.* (2013). *Mandatory requirements in relation to air, soil, or water protection: analysis of need and feasibility*. ECOFYS, London, UK.

EIA. (2016). *June 2016 Monthly Energy Review*. Energy Information Administration, Washington DC, US.

EPA. (2010). *Renewable Fuel Standard Program (RFS2) Regulatory Impact Analysis*. Environmental Protection Agency, Washington D.C.

Fargione, J. E., Plevin, R. J., & Hill, J. D. (2010). The Ecological Impact of Biofuels. *Annual Review of Ecology, Evolution, and Systematics*, *41*(1), 351–377.

Fazio, S., & Monti, A. (2011). Life cycle assessment of different bioenergy production systems including perennial and annual crops. *Biomass and Bioenergy*, *35*(12), 4868–4878.

Fingerman, K. R., Torn, M. S., O'Hare, M. H., & Kammen, D. M. (2010). Accounting for the water impacts of ethanol production. *Environmental Research Letters*, *5*(1), 14020.

Forster, P., Ramaswamy, V., Artaxo, P., Berntsen, T., Betts, R., Fahey, D. W., … Van, R. (2007). Changes in Atmospheric Constituents and in Radiative Forcing. In *Climate Change* (pp. 129–234). Cambridge University Press.

Fu, G. Z., Chan, A. W., & Minns, D. E. (2003). Life Cycle assessment of bio-ethanol derived from cellulose. *The International Journal of Life Cycle Assessment*, *8*(3), 137–141.

Grift, T. E., Miao, Z., Shastri, Y., Hansen, A. C., & Ting, K. C. (2012). Lignocellulosic biomass feedstock transportation alternatives, logistics, equipment confi gurations, and modeling. *Biofuels, Bioproducts and Biorefining*, *6*, 351–362.

Guinée, J. B., Heijungs, R., Huppes, G. et *al.* (2011). Life Cycle Assessment: Past, Present, and Future. *Environmental Science & Technology*, *45*(1), 90–96.

Haankuku, C., Epplin, F. M., & Kakani, V. G. (2014). Forage Sorghum Response to Nitrogen Fertilization and Estimation of Production Cost. *Agronomy Journal*, *106*, 1659–1666.

Hallam, A., Anderson, I. C., & Buxton, D. R. (2001). Comparative economic analysis of perennial, annual, and intercrops for biomass production. *Biomass and Bioenergy*, *21*(6).

Hanna, M. (2005). Fuel Required for Field Operations. Iowa State University Extension & Outreach: Ag Decision Maker. Retrieved from https://www.extension.iastate.edu/agdm/crops/html/a3-27.html

Hao, B., Xue, Q., Bean, B. W., Rooney, W. L., & Becker, J. D. (2014). Biomass production, water and nitrogen use efficiency in photoperiod-sensitive sorghum in the Texas High Plains. *Biomass and Bioenergy*, *62*, 108–116.

Hauschild, M. Z., Goedkoop, M., Guinée, J. et *al.* (2013). Identifying best existing practice for characterization modeling in life cycle impact assessment. *The International Journal of Life Cycle Assessment*, *18*(3), 683–697.

Hoben, J. P., Gehl, R. J., Millar, N., Grace, P. R., & Robertson, G. P. (2011). Nonlinear nitrous oxide (N2O) response to nitrogen fertilizer in on-farm corn crops of the US Midwest. *Global Change Biology*, *17*(2), 1140–1152.

Hsu, D. D., Inman, D., Heath, G. A., Wolfrum, E. J., Mann, M. K., & Aden, A. (2010). Life Cycle Environmental Impacts of Selected U.S. Ethanol Production and Use Pathways in 2022. *Environmental Science & Technology*, *44*(13), 5289–5297.

Hudiburg, T. W., Wang, W., Khanna, M., Long, S. P., Dwivedi, P., Parton, W. J., … Onal, H. (2016). Impacts of a 32-billion-gallon bioenergy landscape on land and fossil fuel use in the US. *Nature Energy*, *1*(1), 15005.

Hutchings, N., Webb, J., Amon, B., Dämmgen, U., Hinz, T., Van Der Hoek, K., … Mikkelsen, M. H. (2016). Crop production and agricultural soils. In *EMEP/EEA air pollutant emission inventory guidebook*. European Environmental Protection Agency, Geneva, Swtizerland.

ISO. (2006a). *14040: Environmental management–life cycle assessment–principles and framework. British Standards Institution*. International Organization of Standardization, Geneva, Swtizerland.

ISO. (2006b). *14044: Environmental management–life cycle assessment–requirements and guidelines. British Standards Institution*. International Organization of Standardization, Geneva, Swtizerland.

Jeswani, H. K., Falano, T., & Azapagic, A. (2015). Life cycle environmental sustainability of lignocellulosic ethanol produced in integrated thermo-chemical biorefineries. *Biofuels, Bioproducts and Biorefining*, *9*(6), 661–676.

Jones, C. (2013). *Management to Minimize Nitrogen Fertilizer Volatilization Nitrogen Fertilizer Volatilization Management to Minimize Nitrogen Fertilizer Volatilization*. Montana State University Extension, Bozeman, Montana.

Jones, J. ., Hoogenboom, G., Porter, C. ., Boote, K. ., Batchelor, W. ., Hunt, L. ., … Ritchie, J. . (2003). The DSSAT cropping system model. *European Journal of Agronomy*, *18*(3–4), 235–265.

Kaufman, A. S., Meier, P. J., Sinistore, J. C., & Reinemann, D. J. (2010). Applying life-cycle assessment to low carbon fuel standards—How allocation choices influence carbon intensity for renewable transportation fuels. *Energy Policy*, *38*(9), 5229–5241.

Kendall, A., & Yuan, J. (2013). Comparing life cycle assessments of different biofuel options. *Current Opinion in Chemical Biology*, *17*(3), 439–443.

Lamb, J. F. S., Sheaffer, C. C., & Samac, D. A. (2003). Population Density and Harvest Maturity Effects on Leaf and Stem Yield in Alfalfa. *Agronomy Journal*, *95*(3), 635–641.

Laser, M., Jin, H., Jayawardhana, K., & Lynd, L. R. (2009). Coproduction of ethanol and power from switchgrass. *Biofuels, Bioproducts and Biorefining*, *3*(2), 195–218.

LeDuc, S. D., Zhang, X., Clark, C. M., & Izaurralde, R. C. (2016). Cellulosic feedstock production on Conservation Reserve Program land: potential yields and environmental effects. *GCB Bioenergy* (early view).

Linquist, B. A., Adviento-Borbe, M. A., Pittelkow, C. M., Van Kessel, C., & Van Groenigen, J. (2012). Fertilizer management practices and greenhouse gas emissions from rice systems: A quantitative review and analysis. *Field Crops Research*, *135*, 10–21.

Lopez, J. R., Erickson, J. E., Asseng, S., & Lopez-Bobeda, E. (2017). Modification of the CERES grain sorghum model to simulate optimum sweet sorghum rooting depth for rainfed production on coarse textured soils in a sub-tropical environment. *Agricultural Water Management*, *181*, 47–55.

Luo, L., van der Voet, E., & Huppes, G. (2009). Life cycle assessment and life cycle costing of bioethanol from sugarcane in Brazil. *Renewable and Sustainable Energy Reviews*, *13*(6), 1613–1619.

Mahler, R. L. (2001). Fertilizer Placement. Moscow, Idaho: University of Idaho Cooperative Extension System. Retrieved from http://www.cals.uidaho.edu/edcomm/pdf/cis/cis0757.pdf

Mbonimpa, E. G., Kumar, S., Owens, V. N., Chintala, R., Sieverding, H. L., & Stone, J. J. (2016). Nitrogen rate and landscape impacts on life cycle energy use and emissions from switchgrass-derived ethanol. *GCB Bioenergy*, *8*(4), 750–763.

McKechnie, J., Colombo, S., Chen, J., Mabee, W., & MacLean, H. L. (2010). Forest Bioenergy or Forest Carbon? Assessing Trade-Offs in Greenhouse Gas Mitigation with Wood-Based Fuels. *Environmental Science & Technology*, *45*(2), 789–795.

McKone, T. E., Nazaroff, W. W., Berck, P., Auffhammer, M., Lipman, T., Torn, M. S., … Horvath, A. (2011). Grand Challenges for Life-Cycle Assessment of Biofuels. *Environmental Science & Technology*, *45*(5), 1751–1756.

McSwiney, C. P., & Robertson, G. P. (2005). Nonlinear response of N2O flux to incremental fertilizer addition in a continuous maize (Zea mays L.) cropping system. *Global Change Biology*, *11*(10), 1712–1719.

Millar, N., Doll, J. E., & Robertson, G. P. (2014). Management of nitrogen fertilizer to reduce nitrous oxide (N2O) emissions from field crops. Lansing, Michigan: MSU Extension Bulletin.

Miller, F. R., & Stroup, J. A. (2004). Growth and Management of Sorghums for Forage Production. In *Proceedings of the National Alfalfa Symposium*. San Diego, CA: University of California Cooperative Extension.

Monti, A., Fazio, S., & Venturi, G. (2009). Cradle-to-farm gate life cycle assessment in perennial energy crops. *European Journal of Agronomy*, *31*(2), 77–84.

Murphy, C. W., & Kendall, A. (2015). Life cycle analysis of biochemical cellulosic ethanol under multiple scenarios. *GCB Bioenergy*, *7*(5), 1019–1033.

Oikawa, P. Y., Ge, C., Wang, J., Eberwein, J. R., Liang, L. L., Allsman, L. A., … Jenerette, G. D. (2015a). Unusually high soil nitrogen oxide emissions influence air quality in a high-temperature agricultural region. *Nature Communications*, *6*, 8753.

Oikawa, P. Y., Jenerette, G. D., & Grantz, D. A. (2015b). Offsetting high water demands with high productivity: Sorghum as a biofuel crop in a high irradiance arid ecosystem. *GCB Bioenergy*, *7*(5), 974–983.

Pimentel, D., & Patzek, T. W. (2005). Ethanol Production Using Corn, Switchgrass, and Wood; Biodiesel Production Using Soybean and Sunflower. *Natural Resources Research*, *14*(1), 65–76.

Plevin, R. J., Jones, A. D., Torn, M. S., Gibbs, H. K., & Gibbs, H. K. (2010). Greenhouse Gas Emissions from Biofuels' Indirect Land Use Change Are Uncertain but May Be Much Greater than Previously Estimated. *Environmental Science & Technology*, *44*(21), 8015–8021.

Pourhashem, G., Adler, P. R., McAloon, A. J., Spatari, S., E, G., Fargione, J., … Hawthorne, P. (2013). Cost and greenhouse gas emission tradeoffs of alternative uses of lignin for second generation ethanol. *Environmental Research Letters*, *8*(2), 25021.

Prasuhn, V. (2006). Erfassung der PO4-Austräge für die Ökobilanzierung. *SALCA-Phosphor. Zürich, CH, Agrocope FAL*.

Pré Consultants. (2013). SimaPro 8. The Netherlands.

Robertson, G. P., Dale, V. H., Doering, O. C., Hamburg, S. P., Melillo, J. M., Wander, M. M., … Wilhelm, W. W. (2008). Agriculture: Sustainable biofuels redux. *Science*, *322*(5898), 49–50.

Robledo-Abad, C., Althaus, H.-J., Berndes, G. et *al.* (2016). Bioenergy production and sustainable development: science base for policymaking remains limited. *GCB Bioenergy*.

Ruan, L., Bhardwaj, A. K., Hamilton, S. K., Robertson, G. P., & Kellogg, W. K. (2016). Nitrogen fertilization challenges the climate benefit of cellulosic biofuels. *Environmental Research Letters*, *11*.

SAEFL. (2000). *Handbuch Offroad-Datenbank.* Swiass Agency for Forest, Landscapes, and Environment, Bern, Switzerland.

Sanderson, M. A., Adler, P. R., Boateng, A. A., Casler, M. D., & Sarath, G. (2006). Switchgrass as a biofuels feedstock in the USA. *Canadian Journal of Plant Sciences*, *86*(5), 1315.

Sanz Requena, J. F., Guimaraes, A. C., Quirós Alpera, S. et *al.* (2011). Life Cycle Assessment (LCA) of the biofuel production process from sunflower oil, rapeseed oil and soybean oil. *Fuel Processing Technology*, *92*(2), 190–199.

Schmer, M. R., Vogel, K. P., Mitchell, R. B., & Perrin, R. K. (2008). Net energy of cellulosic ethanol from switchgrass. *Proceedings of the National Academy of Sciences*, *105*(2), 464–469.

Schmer, M., Vogel, K., Varvel, G. et *al.* (2014). Energy Potential and Greenhouse Gas Emissions from Bioenergy Cropping Systems on Marginally Productive Cropland. *PLoS ONE*, *9*(3), 489–501.

Searcy, E., & Flynn, P. C. (2008). Processing of Straw/Corn Stover: Comparison of Life Cycle Emissions. *International Journal of Green Energy*, *5*(6), 423–437.

Shcherbak, I., Millar, N., & Robertson, G. P. (2014). Global metaanalysis of the nonlinear response of soil nitrous oxide (N2O) emissions to fertilizer nitrogen. *Proceedings of the National Academy of Sciences of the United States of America*, *111*(25), 9199–204.

Sheehan, J., Camobreco, V., Duffield, J., Shapouri, H., Graboski, M., & Tyson, K. S. (2000). *An Overview of Biodiesel and Petroleum Diesel Life Cycles*. National Renewable Energy Laboratory, Golden, CO.

Singh, A., Pant, D., Korres, N. E., Nizami, A.-S., Prasad, S., & Murphy, J. D. (2010). Key issues in life cycle assessment of ethanol production from lignocellulosic biomass: Challenges and perspectives. *Bioresource Technology*, *101*(13), 5003–12.

Somerville, C., Youngs, H., Taylor, C. et *al.* (2010). Feedstocks for lignocellulosic biofuels. *Science (New York, N.Y.)*, *329*(5993), 790–2.

Spatari, S., Bagley, D. M., & MacLean, H. L. (2010). Life cycle evaluation of emerging lignocellulosic ethanol conversion technologies. *Bioresource Technology*, *101*(2), 654–667.

Spatari, S., & MacLean, H. L. (2010). Characterizing Model Uncertainties in the Life Cycle of Lignocellulose-Based Ethanol Fuels. *Environmental Science & Technology*, *44*(22), 8773–8780.

Spatari, S., Zhang, Y., & MacLean, H. L. (2005). Life Cycle Assessment of Switchgrass- and Corn Stover-Derived Ethanol-Fueled Automobiles. *Environmental Science & Technology*, *39*(24), 9750–9758.

Stephenson, A. L., Dupree, P., Scott, S. A., & Dennis, J. S. (2010). The environmental and economic sustainability of potential bioethanol from willow in the UK. *Bioresource Technology*, *101*(24), 9612–9623.

Stichnothe, H., & Azapagic, A. (2009). Bioethanol from waste: Life cycle estimation of the greenhouse gas saving potential. *Resources, Conservation and Recycling*, *53*(11), 624–630.

Teske, M. E., Bird, S. L., Esterly, D. M., Curbishley, T. B., Ray, S. L., & Perry#, S. G. (2002). AgDRIFT: A Model for estimating near-field spray drift from aerial applications. *Environmental Toxicology and Chemistry*, *21*(3), 659–671.

Tilman, D., Balzer, C., Hill, J., & Befort, B. L. (2011). Global food demand and the sustainable intensification of agriculture. *Proceedings of the National Academy of Sciences of the United States of America*, *108*(50), 20260–4.

Tilman, D., Cassman, K. G., Matson, P. A., Naylor, R., & Polasky, S. (2002). Agricultural sustainability and intensive production practices. *Nature*, *418*(6898), 671–7.

Tonitto, C., & Ricker-Gilbert, J. E. (2016). Nutrient management in African sorghum cropping systems: applying meta-analysis to assess yield and profitability. *Agronomy for Sustainable Development*, *36*(1), 10.

Tsao, C.-C., Campbell, J. E., Mena-Carrasco, M., Spak, S. N., Carmichael, G. R., & Chen, Y. (2011). Increased estimates of air-pollution emissions from Brazilian sugar-cane ethanol. *Nature Climate Change*, *2*(1), 53–57.

von Blottnitz, H., & Curran, M. A. (2007). A review of assessments conducted on bio-ethanol as a transportation fuel from a net energy, greenhouse gas, and environmental life cycle perspective. *Journal of Cleaner Production*, *15*(7), 607–619.

Wagner, M., & Lewandowski, I. (2016). Relevance of environmental impact categories for perennial biomass production. *GCB Bioenergy*, *9*(1), 215–228.

Waldron, C. D., Harnisch, J., Lucon, O., Mckibbon, R. S., Saile, S. B., Wagner, F., … Pesmajoglou, S. (2006). Mobile Combustion. In *IPCC Guidelines for National Greenhouse Gas Inventories*. Intergovernmental Panel on Climate Change, Geneva, Switzerland.

Wang, M., Han, J., Dunn, J. B., Cai, H., & Elgowainy, A. (2012). Well-to-wheels energy use and greenhouse gas emissions of ethanol from corn, sugarcane and cellulosic biomass for US use. *Environmental Research Letters*, *7*(4), 45905.

Weldu, Y. W., & Assefa, G. (2016). Evaluating the environmental sustainability of biomass-based energy strategy: Using an impact matrix framework. *Environmental Impact Assessment Review*, *60*, 75–82.

Wernet, G., Bauer, C., Steubing, B., Reinhard, J., Moreno-Ruiz, E., & Weidema, B. (2016). The ecoinvent database version 3 (part I): overview and methodology. *The International Journal of Life Cycle Assessment*, *21*(9), 1218–1230.

Winther, M., Dore, C., Lambrecht, U., Norris, J., Samaras, Z., & Zierock, K.-H. (2016). Combustion: Non road mobile machinery. In *EMEP/EEA air pollutant emission inventory guidebook*. European Environmental Agency, Geneva, Swtizerland.

Zamboni, A., Murphy, R. J., Woods, J., Bezzo, F., & Shah, N. (2011). Biofuels carbon footprints: Whole-systems optimisation for GHG emissions reduction. *Bioresource Technology*, *102*(16), 7457–7465.

Zhong, J., Yu, T. E., Larson, J. A., English, B. C., Fu, J. S., & Calcagno, J. (2016). Analysis of environmental and economic tradeoffs in switchgrass supply chains for biofuel production. *Energy*, *107*, 791–803.

2.7 Supporting Information

Table S2.1. Environmental impact categories evaluated in SimaPro using TRACI 2 v. 3.03 midpoint characterization (Bare et al. 2003). Emissions that contribute to a particular impact category are expressed in terms of equivalence units (eq) based on their proportional influence to that impact category relative to that of the referenced unit (e.g. CO_2 eq).

Impact Category [a]	***Unit***	***Midpoint level*** [b]
Emissions to the environment		
Global warming	CO_2 eq	Potential global warming based on chemical's relative forcing and lifetime [c]
Acidification	H^+ eq	Potential to cause wet and dry acid deposition
Eutrophication	N eq	Potential to cause eutrophication
Ozone depletion	CFC^{-11} eq	Potential to destroy ozone based on chemical's reactivity and lifetime
Ecotoxicity	2,4-D eq	Potential of a chemical released into an evaluative environment to cause ecological harm
Smog	NO_x eq	Potential to cause photochemical smog
Emissions to human health		
Carcinogenics	benzen eq	Potential of a chemical released into an evaluative environment to cause human cancer effects
Non carcinogenics	toluen eq	Potential of a chemical released into an evaluative environment to cause human non-cancer effects
Respiratory effects	$PM_{2.5}$ eq	Exposure to elevated particulate matter < 2.5μm

[a] TRACI additionally characterizes fossil fuel, land use, and water use categories, however these categories are not assessed in SimaPro as they are not standardized metrics

[b] midpoint level criteria was taken verbatim from the EPAs communication of TRACI methods (Bare, Norris, Pennington, & Mckone, 2003) to avoid miscommunication of specified midpoints

[c] global warming potentials are based on a 100-year time horizon

Table S2.2. Primary soil parameters in DSSAT and their assigned values based field measurements (measured) when available and default parameters from DSSAT's deep silty loam soil profile (default) otherwise. Values are reported for the uppermost soil layer. *Total nitrogen varied across harvests based on residual N levels from the previous harvest.

Variable	Unit	Value	Source
lower limit	$cm^3\ cm^{-3}$	0.228	default
drained upper limit	$cm^3\ cm^{-3}$	0.385	default
saturate upper limit	$cm^3\ cm^{-3}$	0.532	measured
root growth factor	(0 - 1)	1	default
bulk density	$g\ cm^{-3}$	1.4	measured
organic carbon	%	2.34	measured
clay particles	%	42	measured
silt particles	%	41	measured
coarse fraction	(0 - 1)	0	default
total nitrogen	%	0.13*	measured
pH in water		8.1	measured

Weather Data

We acquired weather data for our site from the California Irrigation Management System (CIMIS) Meloland station, located 4.4 miles east of DREC. As data from the Meloland weather station was only available from 12 December 1989 to present, records from nearby stations were used to build the 30 year weather data set. The Calpatria station, located approximately 30 miles northeast of DREC, has recorded weather data since 17 July 1983 and the El Centro station, located 11 miles east of DREC, recorded data from 8 November 1982 to 27 May 1987 (see supporting information, Figure S2.2). Overlapping periods of record between El Centro and Calpatria and Calpatria and Meloland were used to standardize the data using following equation:

$P_S = (P_O - i) * (1/s)$

Where P_S = the standardized value of a given weather parameter, P_O = the original value of a given weather parameter (units varied by parameter), i = y intercept, and s = slope.

Once El Centro data was standardized to Calpatria, Calpatria data was standardized to Meloland data following the same method. Finally, El Centro data was standardized to Meloland data using the inverse slope and intercept data derived from the regression of Calpatria data against Meloland data

Table S2.3. Regression statistics for standard linear regressions of overlapping periods of weather data Meloland and El Centro and Meloland and Calpatria. Here, ^{O} and ^{S} signify the original and standardized regression statistics, respectively.

Parameter	r^2	*p-value*	*slope* ^{O}	*slope* ^{S}	*intercept* ^{O}	*intercept* ^{S}
			El Centro data regressed against Calpatria data			
Evapotranspiration (mm)	0.80	< 0.001	0.95	1.00	0.28	0.00
Precipitation (mm)	0.34	< 0.001	0.59	0.62	0.11	0.11
Solar radiation (w m^{-2}*)*	0.96	< 0.001	0.95	1.00	4.89	0.00
Maximum T_{air} *(°C)*	0.98	< 0.001	1.00	1.00	0.09	0.00
Minimum T_{air} *(°C)*	0.96	< 0.001	0.96	1.00	0.07	0.00
Relative humidity (%)	0.81	< 0.001	0.90	1.00	7.27	0.00
Dew point (°C)	0.84	< 0.001	0.90	1.00	1.57	-0.68
Wind run (km)	0.83	< 0.001	0.97	1.00	-3.95	0.00
			Calpatria data regressed against Meloland Data			
Evapotranspiration (mm)	0.93	< 0.001	0.94	1.00	0.18	0.00
Precipitation (mm)	0.21	< 0.001	0.46	0.35	0.13	0.10
Solar radiation (w m^{-2}*)*	0.91	< 0.001	0.97	1.00	11.61	0.00
Maximum T_{air} *(°C)*	0.99	< 0.001	0.99	1.00	0.09	0.00
Minimum T_{air} *(°C)*	0.96	< 0.001	1.00	1.00	-1.94	0.00
Relative humidity (%)	0.68	< 0.001	0.85	1.00	11.59	0.00
Dew point (°C)	0.89	< 0.001	0.93	1.00	1.23	0.00
Wind run (km)	0.72	< 0.001	0.63	1.00	57.49	0.00

Cultivar Calibration

Extensive cultivar adjustments were necessary to simulate forage sorghum as only grain sorghum cultivars are currently available in the DSSAT database. We first raised the heat tolerance (T_{max}) to 47 °C, as our crop remained physiologically active at this temperature (Oikawa et al. 2015b). We then conducted a sensitivity analysis of all sorghum cultivars in the DSSAT database to determine a candidate cultivar for modification to a forage sorghum. Out of 51 cultivars, only 3 matured at a rate similar to our crop and, among those, only 1 (cultivar MN1500) produced substantial vegetative biomass. We then adjusted MN1500 using modified parameters generated to simulate sweet sorghum (Lopez et al. 2017) as a starting point for modeling forage sorghum. These modifications included an amended program file provided by Lopez et. al, which increased shoot allocation as well as modified crop coefficients for reduced allocation to the panicle and roots (i.e. G2 from 6.0 to 0.4 and RTPC from 0.25 to 0.16, respectively in DSSAT).

To calibrate our forage sorghum model, we modeled cumulative net primary productivity (NPP) throughout the season, which directly correlates to total biomass accumulation, from net ecosystem exchange data (NEE; Figure S2.2.1). We first estimated heterotrophic respiration (R_{hetero}) based on net ecosystem exchange when the field was fallow and irrigated. We then calculated NPP by summing NEE and R_{hetero}. Using sensitivity analyses and cross-parameter manipulations we adjusted the parameters of Lopez-modified MN1500 by checking model outputs of plant growth and growth stages against cumulative NPP and observed phenological events, respectively. The resulting changes reduced delay of reproductive maturation on long days (i.e. days where photoperiod exceeds critical day length) and increased leaf production (i.e. PHINT from 49 to 80 and G1 from 1 to 25, respectively in DSSAT).

Our final modification was to increase radiation use efficiency (RUE) from 3.6 to 4.1 (Figure S2.2.1). Although this value exceeds sorghum RUEs in the literature (White et al. 2015; Narayanan et al. 2013), this modifications provided the necessary amplification in productivity without adversely impacting phenology. Yield values achieved following this modification aligned well with our observed yields for all harvests (Table 2.1).

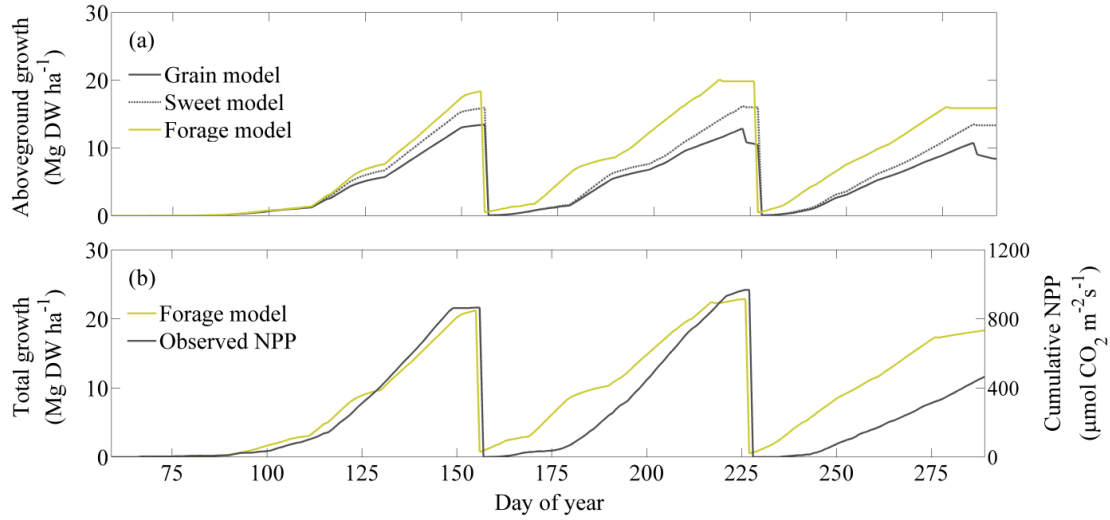

Figure S2.1 Major phases of model modification to simulate forage sorghum. The impact of sorghum model adjustment and calibration on simulated vegetative (i.e. aboveground) growth (kg dry weight ha^{-1}) is reflected in panel (a). Panel (b) shows the agreement between cumulative daily NPP (solid black) collected from our field site and the modeled total growth (i.e. above and belowground; solid dark green).

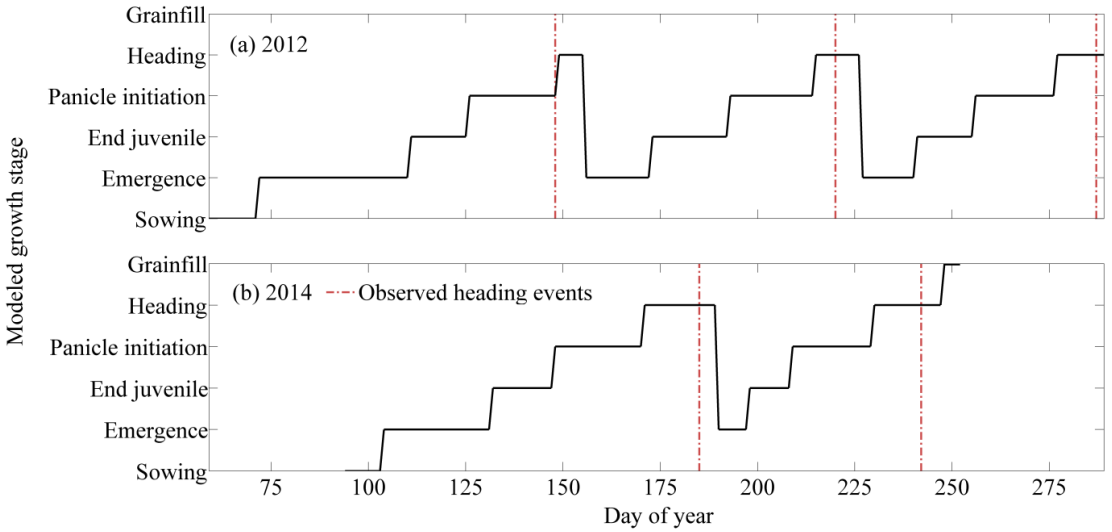

Figure S2.2. Modeled phenological transitions across three growth cycles over two years (black lines) and field observations of heading events (i.e. where heading occurs in $\geq$ 25% of the stand, as assessed visually; red lines). Observations match modeled transitions to heading within a window of 10 days.

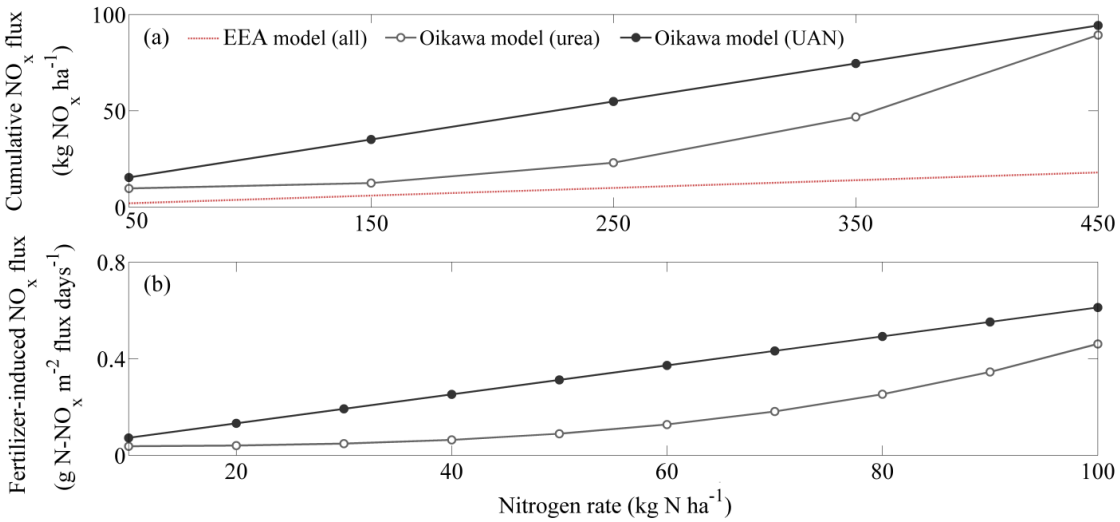

Figure S2.3. Empirical models used to determine annual NO_x fluxes induced by fertilization events. The EEA model is a tier one NO_x model using a single emission factor. The Oikawa model for urea is based on field measurements of NO_x flux following application of broadcast urea fertilizer. These fluxes lasted approximately 20 days before returning to base flux levels. The Oikawa model for UAN is based on field measurements of NO_x flux following application of UAN in irrigation water. These fluxes lasted approximately 25 days before returning to base flux levels. Base NO_x flux (pre- and post-fertilizer) for Oikawa NO_x models was determined to be 0.0012 (g N m^{-2} day^{-1}) (Oikawa et al. 2015a).

WTW emissions assuming low efficiency conversion

Low efficiency scenarios (290 l ethanol Mg DW^{-1}) assumed ammonia fiber explosion pre-treatment based on corn stover conversion using AFEX technology (Kim and Dale 2004) simultaneous saccharification and co-fermentation conversion processes, and Rankine cycle energy recovery processes (Spatari, Bagley, and MacLean 2010) with 1.21 kWh electricity produced l $ethanol^{-1}$.

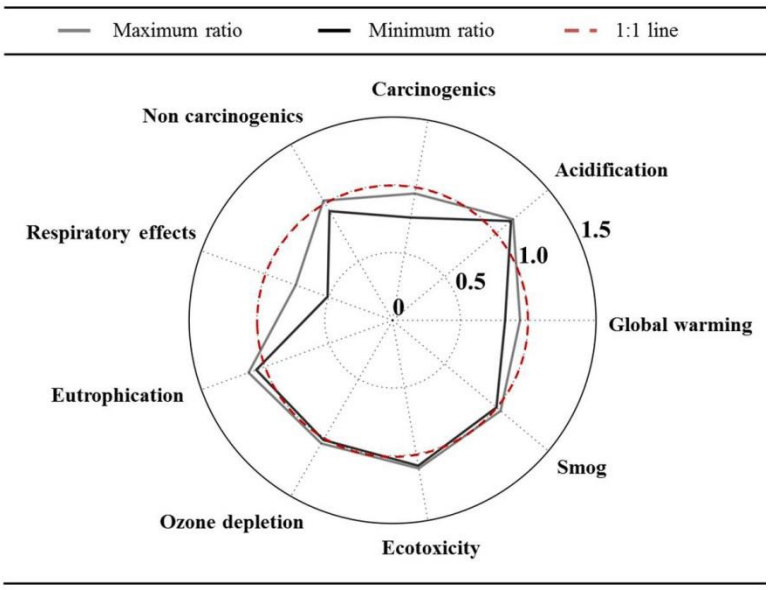

Figure S2.4. Ratio of WTW emissions under low-efficiency conversion relative to those under high-efficiency conversion. Minimum and maximum ratios reflect minimum and maximum differences in WTW emissions across modeled N management scenarios, respectively. Respiratory effects were the most notably affected, declining under low-efficiency conversion by as much as 50%. Emissions to global warming and carcinogenics also declined in low-efficiency conversion scenarios. Emissions to acidification, eutrophication, and ecotoxicity were slightly lower in high-efficiency conversion scenarios, while emissions to non carcinogenics, smog, and ozone depletion were relatively unaffected.

Table S2.4. WTW emissions from injected nitrogen scenarios for impact categories which varied by >10% across N sources.

N scenario		**Acidification**	**Eutrophication**	**Carcinogenics**
source	*rate kg ha^{-1}*	*mmol H^+ eq MJ^{-1}*	*mg N eq MJ^{-1}*	*mg benzen eq MJ^{-1}*
Urea	*50*	18.68	60.67	28.52
	150	20.66	52.56	23.84
	250	21.65	50.30	22.40
	350	22.48	49.64	21.82
	450	23.85	50.58	21.87
AnAm	*50*	13.34	53.72	27.16
	150	12.44	42.14	21.91
	250	12.19	38.30	20.18
	350	12.11	36.50	19.39
	450	12.23	35.86	19.15
UAN	*50*	14.13	55.00	29.38
	150	13.66	44.05	25.33
	250	13.59	40.49	24.12
	350	13.64	38.90	23.69
	450	13.94	38.54	23.97

Table S2.5. Well-to-wheel GHGs for conventional and alternative fuel sources, where CE denotes E_{85} fuel from cellulosic ethanol. Emissions from sorghum-derived CE are reported based on the range of carbon intensities observed across all N management scenarios simulated. All CE emissions shown here include electricity co-products allocated via system expansion (i.e. displacement) (CARB 2009; Adler et al. 2012). CE from dry milled corn additionally includes a protein co-product credit allocated via system expansion.

Fuel source	**GHG ($g\ CO_2\ eq\ MJ^{-1}$)**
Gasoline (US)	91 [a]
	84 [b]
Gasoline (CA reformulated)	95 [a]
Natural gas	75 [a]
CE from sorghum biomass	29 – 44 [b]
CE from dry milled corn	55 [a]
CE from corn stover	30 [c]
CE from sugarcane	20 [a]
CE from switchgrass	32 [c]
CE from wheat straw	30 [c]

[a] (CARB, 2009)
[b] This study
[c] (Adler, Dalgleish, & Ellner 2012)

2.8 References for Supporting Information

Adler, Paul R., Del Grosso, Stephen J., Inman, Daniel, *et al*. 2012. "Mitigation Opportunities for Life-Cycle Greenhouse Gas Emissions during Feedstock Production across Heterogeneous Landscapes." In *Managing Agricultural Greenhouse Gases*, 203–19. Elsevier.

Bare, Jane C, Norris, Gregory A, Pennington, David W, Mckone, Thomas. 2003. "The Tool for the Reduction and Assessment of Chemical and Other Environmental Impacts." *Journal of Industrial Ecology* 6 (3–4): 48–78.

CARB. 2009. "Proposed Regulation for Implementing Low Carbon Fuel Standards (Staff Report: Initial Statement of Reasons)." Vol. 1. California Air and Resource Board, Sacramento, CA.

Kim, Seungdo & Dale, Bruce E.. 2004. "Global Potential Bioethanol Production from Wasted Crops and Crop Residues." *Biomass and Bioenergy* 26 (4): 361–75.

Lopez, Jose R., Erickson, John E., Asseng, Senthold, and Lopez-Bobeda, Edmundo. 2017. "Modification of the CERES Grain Sorghum Model to Simulate Optimum Sweet Sorghum Rooting Depth for Rainfed Production on Coarse Textured Soils in a Sub-Tropical Environment." *Agricultural Water Management* 181: 47–55.

Narayanan, S., Aiken, R.M., Prasad, P.V.V., Xin, Z., and Yu, J. 2013. "Water and Radiation Use Efficiencies in Sorghum." *Crop Ecology & Physiology* 105 (3): 649–56.

Oikawa, P.Y., Ge, C., Wang, J., *et al*. 2015. "Unusually High Soil Nitrogen Oxide Emissions Influence Air Quality in a High-Temperature Agricultural Region." *Nature Communications* 6 (November). Nature Publishing Group: 8753.

Oikawa, P.Y., G.D. Jenerette, and D.A. Grantz. 2015. "Offsetting High Water Demands with High Productivity: Sorghum as a Biofuel Crop in a High Irradiance Arid Ecosystem." *GCB Bioenergy* 7 (5): 974–83.

Spatari, Sabrina, Bagley, David M., MacLean, Heather L. 2010. "Life Cycle Evaluation of Emerging Lignocellulosic Ethanol Conversion Technologies." *Bioresource Technology* 101 (2): 654–67.

White, J. W., Alagarswamy, G., Ottman, M. J., Porter, C.H., Singh, U., Hoogenboom, G. 2015. "An Overview of CERES–Sorghum as Implemented in the Cropping System Model Version 4.5." *Agronomy Journal* 107 (6): 1987.

Chapter 3

Evaluating the GHG mitigation-potential of alternate wetting and drying in rice through life cycle assessment

Cara Fertitta-Roberts, Patricia Y. Oikawa, G. Darrel Jenerette

---

3.1 Abstract

Alternate wetting and drying (AWD), has gained increasing attention as a promising strategy for mitigating greenhouse gas emissions (GHG) in flooded rice systems. AWD involves periodic drainage of rice paddies in order to inhibit methane (CH_4) emissions. To date, studies evaluating this practice have been limited in their scope and resolution. Our study uses the Peatland Ecosystem Photosynthesis Respiration and Methane Transport model (PEPRMT) to simulate high resolution CH_4 fluxes and life cycle assessment modeling to evaluate the mitigation potential of AWD in California rice production from a globally relevant perspective. Rice production was modeled under continuous flooding and under five AWD schedules ranging in the severity and frequency of dry-downs. Our simulations only resulted in reduced grain yields when dry-downs were frequent and/or severe. For these scenarios, adverse yield impacts negated some of the benefits of AWD. CH_4 flux mitigation under AWD simulated using PEPRMT was approximately half that reported from chamber measurements, highlighting the importance of high resolution field data to better characterize GHGs from rice systems.

Reduced yields and conservative CH_4 mitigation in our model lessened the overall mitigation potential of AWD. When the entire rice life cycle was considered, mitigation of overall global warming potential (GWP) was further reduced by the presence of additional GHG sources, which comprised roughly half of life cycle GWP. Our simulations resulted in $\leq$ 11% reductions in GWP kg^{-1} across all AWD scenarios and saw an increase in GWP when yields were severely impacted. Together, our results highlight the importance of reducing uncertainties in methane emissions and considering a life cycle perspective expressed on a yield basis in characterizing the mitigation potential of AWD. Using a high resolution CH_4 model and life cycle assessment, we found the advantages of AWD to be more limited than previously reported.

3.2 Introduction

Rice is conventionally grown in flooded fields to control the spread of weeds and encourage crop establishment. This seasonal flooding alters soil biogeochemical fluxes, resulting in greenhouse gas emissions (GHGs) in rice systems approximately four times those of other major cereal cropping systems (Linquist et al. 2012a). This difference in GHG-intensity is largely attributed to methane (CH_4) fluxes induced by anaerobic soil conditions (Wassmann et al. 1998; Linquist et al. 2012). Accordingly, one way to mitigate GHG emissions from rice is to introduce aerobic conditions by periodically draining the field throughout the growing season. This practice is known as alternate wetting and drying (AWD). Using periodic chamber measurements of CH_4 flux, some studies have suggested AWD may reduce seasonal CH_4 emissions by as much as 90%

relative to continuous flooding (CF) (Linquist et al. 2015; LaHue et al. 2016). However, field trials of AWD reporting CH_4 emissions have been limited and rely on extrapolation of manual flux measurements to estimate seasonal CH_4 efflux. Further, AWD has yet to be evaluated from a life cycle perspective in comparison with CF rice. Life cycle assessment (LCA) better contextualizes global warming potential (GWP) by considering all GHG sources incurred during rice production. If other sources of GHGs are significant, mitigation of CH_4 emissions will result in lesser mitigation of overall GWP. LCA further contextualizes GWP mitigation potential by expressing emissions in terms of a desired functional unit, such as yield. A major barrier in implementing AWD is concern over the impact to grain yield. If yields are compromised under AWD, its mitigation potential may be similarly compromised.

AWD has been shown to reduce grain yields by 1.8 – 8.7 % on average, however, effects of AWD on yield vary substantially across studies (Carrijo et al. 2017). Much of this variability has been attributed to differences in the severity, frequency, and timing of dry-downs. Yields may be reduced under AWD by acute water stress, reduced nitrogen use efficiency as a consequence of increased volatile losses, and increased competitive pressure following dry-down periods (Roel et al. 1999; Linquist et al. 2015; LaHue et al. 2016; Carrijo et al. 2017). Previous work has shown that grain yields tend to decline when soil volumetric water content (VWC) is less than saturating (Bouman & Tuong 2001). However, others have shown yields to be unaffected at as low as 60% saturating VWC (Bouman 2007; Kislev & Peterson 1982; Pandey et al. 2014). Timing of dry-downs can also be particularly important in reducing nitrogen losses and in avoiding weed

establishment during dry periods (Brodt et al. 2014; Carrijo et al. 2017). Allowing sufficient time for nutrient absorption prior to initiating a dry-down can reduce nutrient loss and subsequent yield reductions (Linquist et al. 2015). Similarly, allowing the rice crop to establish until canopy closure prior to introducing dry-down periods can prevent the establishment of weeds and subsequent competition for nutrients (LaHue et al. 2016). Although more frequent and severe AWD schedules are more likely to induce greater stress and compound yield reductions, they are also more likely have greater CH_4-mitigation potential.

CH_4 production is stimulated by anaerobic conditions associated with decomposition of organic matter (Conrad 2002). Draining the field periodically during the growing season creates aerobic conditions, inhibiting CH_4 production. Accordingly, more frequent and severe dry-downs should increase CH_4 mitigation. The response of CH_4 to soil oxygenation is opposite that of nitrous oxide (N_2O), another potent greenhouse gas (Hou et al. 2000). N_2O production is stimulated during both drying and re-wetting periods (Bouwman 1998). This efflux of N_2O emissions could compromise the GHG mitigation benefits of AWD, particularly as the GWP of N_2O is roughly 68 – 89% higher than that of CH_4. However, as N_2O emissions from rice tend to be several orders of magnitude lower than corresponding CH_4 emissions, increasing N_2O fluxes in AWD rice are generally reported to be more-or-less negligible relative to corresponding reductions in CH_4 fluxes (Yan et al. 2009; B. A. Linquist et al. 2012; Brodt et al. 2014; LaHue et al. 2016; Linquist et al. 2016). Still, higher N_2O flux means higher losses of soil nitrogen, which may contribute to adverse yield impacts.

It is important to consider these yield impacts when evaluating the GHG mitigation potential of AWD, as declines in grain yield must ultimately be compensated for with an increase in rice production elsewhere. LCA is a particularly useful tool for evaluating tradeoffs between productivity and GHG emissions derived from multiple sources. This quantitative modeling methodology is used to inventory emissions occurring throughout the entire life cycle of a product (Cherubini et al. 2009; Guinée et al. 2011), making it more comprehensive than field measurements alone. In accordance with International Organization for Standardization (ISO) guidelines, a life cycle is defined by through a clear scope and system boundaries (ISO 2006a; ISO 2006b). The scope defines the extent of processes within the life cycle considered, for example cradle-to-farm gate, cradle-to-mill, or cradle-to-table. System boundaries define the extent to which associated material, energy, and waste flows are considered (SAIC 2006). A life cycle inventory (LCI) is then complied, which details all material, energy, and waste flows of GHGs within the defined scope and system boundaries. This GHG inventory is characterized into a GWP based on the warming potential of each individual GHG relative to CO_2, and expressed in terms of CO_2 equivalents (CO_2e).

GHG emissions in rice systems are typically extrapolated from manual chamber measurements of gas flux (Pittelkow et al. 2014; Linquist et al. 2015; LaHue et al. 2016). While modeling seasonal fluxes from chamber data is common practice, sampling scheme and choice of extrapolation method can strongly bias seasonal emissions modeled from chamber measurements (Venterea 1991; Sass et al. 2002). Previous work in peatlands has shown that CH_4 flux can lag behind transitions in water table height by as

much as 20 days (Moore & Dalva 1993; Kettunen et al. 1999; Sturtevant et al. 2016). Changes in the water table can also lead to large CH_4 emission events or pulses which are difficult to capture with discontinuous chamber measurements (Knox et al. 2016). As most field studies assessing GHGs from rice systems sample at daily intervals only in the days prior to and following wetting or drying events (Bossio 1999; Fitzgerald et al. 2000; Redeker et al. 2000; McMillan et al. 2007; Adviento-Borbe et al. 2013; Pittelkow et al. 2013; Pittelkow et al. 2014; Simmonds, Anders, et al. 2015; Linquist et al. 2015; LaHue et al. 2016), delayed spikes in CH_4 flux may be under-sampled or missed entirely (Knox et al. 2016; Sturtevant et al. 2016). Alternatively, IPCC models have been used to estimate GHG flux in rice systems. However, these coarse models, based on generic emission factors, have been shown to substantially overestimate emissions in CA rice systems and underestimate emissions elsewhere (Wang et al. 2010; Thanawong et al. 2014; Brodt et al. 2014). Further, the IPCC model only distinguishes between 1 and > 1 mid-season dry down and does not account for dry-down severity, making it relatively insensitive to specific AWD schedules (Lasco et al. 2006).

The recently developed Peatland Ecosystem Photosynthesis Respiration and Methane Transport model (PEPRMT) was parameterized for northern California peatlands and seasonal wetlands, making it easily adaptable to CA rice systems. PEPRMT has great potential for modeling methane flux under AWD as it is sensitive not only to factors such as light, temperature, and substrate availability, but also to water table height (Oikawa et al. 2017). PEPRMT simulates changes in carbon pools, at half-hourly intervals, providing high temporal resolution. CH_4 production and oxidation are

then calculated at daily time steps throughout the season using equations adapted from the DAMM model (Davidson et al. 2012; Oikawa et al. 2014; Oikawa et al. 2017). These factors make PEPRMT a more refined and sensitive model for predicting CH_4 flux in rice paddies than infrequent chamber measurement up-scaling or the existing IPCC model.

Here, we use PEPRMT to assess the GWP of California rice production under CF and AWD irrigation from a life cycle perspective. Although California is responsible for < 2% of global rice production (CRC 2009), grain yields in the state are twice as high as the global average (Brodt et al. 2014). California also imposes some of the strictest environmental regulations and offers incentives for GHG-mitigation measures in the form of carbon credits (CARB 2014), making it an apt study system for evaluating the GHG-mitigation potential of AWD. We modeled a typical northern California rice production system in Butte County to simulate a range of AWD scenarios. Crop model output was coupled with PEPRMT and LCA models to evaluate GHG intensity. We asked how AWD, practiced at varying frequencies and severities, would influence the life cycle GWP of a typical CA rice production system. We hypothesize the mitigation potential of AWD would be constrained by two factors when evaluated at the life cycle perspective: the contributions of non-methane GHG sources in the rice life cycle and adverse yield impacts resultant form increased nutrient and water stress, particularly when dry-downs are more frequent and severe.

3.3 Materials and Methods

Using a coupled modeling approach, we investigated the impacts of AWD on the GWP of a typical California rice production system (Figure 3.1). Field data and phenological models available through UCANR's Agronomy Research & Information Center for Rice were used to parameterize a rice model in DSSAT (Decision Support System for Agrotechnology Transfer v.4.5, Georgia USA). We modeled grain yields for a medium grain rice cultivar (M-205) grown in Butte County under six irrigation management scenarios run over 30 years. Inputs and outputs of the crop model were coupled with downstream emission models to build life cycle inventories in SimaPro v.8 (Pré Consultants 2013), which were characterized using TRACI 2.0 (Bare et al. 2003). CH_4 emissions were modeled in PEPRMT (Oikawa et al. 2017) and using an IPCC tier one model (Lasco et al. 2006) for comparison. Other downstream GHGs and indirect emissions (e.g. NO_x, SO_x, VOCs) were modeled using IPCC (De Klein et al. 2006), EEA (Hutchings et al. 2016), EPA (EPA 2007; EPA 2009), and SAEFL (SAEFL 2000) models.

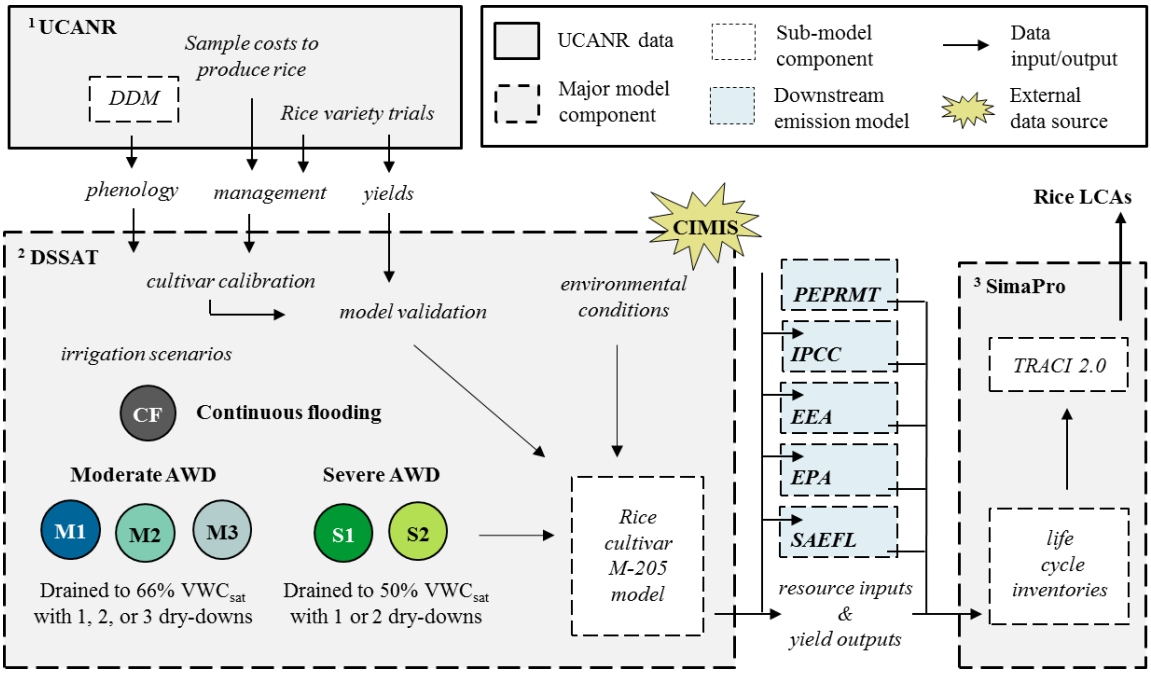

Figure 3.1. Overview of methodological processes used to evaluate life cycle impacts of CF and AWD rice production strategies.

Rice model parameterization

We parameterized a CERES rice model in DSSAT to simulate production of rice cultivar M-205 in Butte County, which is among the top rice producing counties in California in terms of both harvested area and grain yields (CRC 2009). DSSAT is a process-based crop modeling system that couples weather, soil, and crop growth modules to simulate crop production under a variety of environmental conditions and management strategies (Jones et al. 2003). M-205 is a high-yielding medium grain cultivar, that has become increasingly popular in mild inland counties like Butte (Jodari et al. 2001; CASS 2009, Brodt et al 2014). UCANR data was used to parameterize and validate our model of M-205. In addition to reporting more than a decade of yield data collected through

their Rice Variety Trials, UCANR has developed a Degree Day Model (DDM), which predicts phenological transitions based on daily thermal time and cardinal temperatures of the selected cultivar, as well as inputs of planting location and date (available at: http://rice.ucanr.edu/). We modeled M-205 management in Butte County assuming water-seeding at a rate of 161 kg ha^{-1} with an 82% establishment rate (Jodari et al. 2001; Espino et al. 2015), continuous flooding at 12.7 cm depth, and 200 kg N ha^{-1} (Greer et al. 2012; Espino et al. 2015).

Although Butte County was our focal area, we simulated rice production in all major M-205 producing regions available in the DDM in order to maximize our data inputs for parameterization of the M-205 cultivar in DSSAT. Weather data for these counties were acquired from the California Irrigation Management Information System (CIMIS). We generated a soil profile for a mildly acidic, silty clay soil (pH 6.0, 50% clay, 35% silt, and 15% sand), as is typical of inland northern California rice paddies (Wells 1972; Bossio 1999; Fitzgerald et al. 2000; Reed 2002; Burkett & Conlin 2006; Pittelkow et al. 2013; Pittelkow et al. 2014; Simmonds, Li, et al. 2015). Soil organic carbon (1.63%), nitrogen content (0.13%), bulk density (0.94 g cm^{-3}), extractable phosphorus (11.3 mg kg^{-1}), and exchangeable potassium (0.08 mmol kg^{-1}) were based on previously published soil profiles for rice production in Butte and Colusa Counties (Bossio 1999; Fitzgerald et al. 2000; Bird et al. 2001; Pittelkow et al. 2013; Pittelkow et al. 2014). We assumed rice straw residues from the previous season were incorporated at 12 cm depth and that these residues were comprised of 0.65% N and 0.43% phosphorus (Devevre & Horwath 2000; Bird et al. 2001; Dobermann & Fairhurst 2002).

To parameterize our M-205 model, we selected a cultivar with the closest phenological dynamics to those predicted by the DDM for M-205 through sensitivity analysis. To refine phenological parameters for M-205 in our model, we simulated phenological transitions in each county across 12 planting dates, spanning from 20 April to 14 June, in 5 day increments in both the DDM and our DSSAT crop model. Crop model simulations were run over 30 years, from 1985 – 2014. We then ran cross-parameter sensitivity analyses to determine the parameters best suited to simulate M-205 phenology. Fitted parameters resulted in modeled phenological transitions which occurred within an average of 5 days of those projected by the DDM across planting dates, weather years, and counties (Table S3.1).

We validated our model using yield data published in 2002 – 2014 UCANR Rice Variety Trials (http://rice.ucanr.edu/Reports-Publications/Agronomy_Papers/). These trials reported average dry weight yields for M-205 from rice paddies throughout Butte County. Accordingly, we maintained the assumption of typical management practices used in our phenology calibration. Under this assumption, fit between modeled and reported yields were in Butte County were good given our goal of more generalized results that were not over-parameterized ($r^2 = 0.56$; $p < 0.01$; Figure 3.3).

Rice model scenario analyses

We simulated rice production in Butte County over 30 years across one continuously flooded scenario and five AWD scenarios (Figure 3.1). Management practices were maintained from our initial production model, expect in the case of AWD irrigation schedules. AWD irrigation scenarios varied in the severity (M = moderate, S = severe) and frequency (1, 2, or 3) of mid-season dry-downs. Moderate AWD schedules were characterized by shorter dry-downs which drained soil VWC to 66% of saturated VWC, corresponding to the mid-point between field capacity and the permanent wilting point. Generally dry-downs within 60% of saturated soil VWC are considered "safe AWD", in that yields tend to be minimally impacted (Bouman 2007; Kislev & Peterson 1982; Pandey et al. 2014). Severe dry-downs drained soil VWC to 50% of saturated VWC, just shy of the permanent wilting point. When feasible, the initial flood in AWD schedules was maintained until canopy closure to encourage establishment (Figure S3.1) (LaHue et al. 2016). To minimize N losses, we avoided dry-downs until at least two weeks after a fertilization event (Linquist et al. 2015).

Irrigation management scenarios were simulated over 30 historical weather years (1985 – 2014) to account for environmental variability. As seasonal (multi-year) DSSAT models require irrigation schedules to be maintained on consistent dates across years, we imposed filtering criteria during data processing to exclude years in which climatic conditions interrupted our imposed AWD cycles. Our filtering criteria required soil VWC at the end of each dry-down cycle to be within 10% of the target VWC value (Figure

S3.1). Additionally, all irrigation schedules included a pre-harvest dry down at approximately 4 weeks prior to harvesting. Soil VWC was required to dry to at least the permanent wilting point prior to harvest. Data from non-compliant years were excluded. Following filtering, each treatment retained $\geq$ 15 years of data.

Life cycle assessment: scope and system boundaries

LCAs of CA rice production under various irrigation management scenarios were constructed in SimaPro in compliance with ISO 14040 and 14044 standards (ISO 2006a; ISO 2006b). Emissions were assessed at a cradle-to-mill to scope, which considered all inputs to production, transport, drying, and milling of the rice product and associated waste products and co-products. This included emissions from residue incorporation and off-season flooding. We used second order system boundaries throughout our analyses, considering all relevant material, energy, and waste flows. Embodied energy sources associated with facilities and machinery were only accounted for in the case of resource inputs originating from the Ecoinvent database (Wernet et al. 2016) within SimaPro v.8. Emissions were assessed on the basis of 1 kg dried, milled rice. We assumed 90% of rice grain was milled to white rice and 10% to brown rice (Brodt et al. 2014).

Life cycle inventories: upstream flows

Chemical inventories of resource inputs to our rice production models were selected from SimaPro databases. We used U.S. regional unit process data when possible and European unit process data when U.S. data was unavailable. Resource inputs to rice crop production included rice seed, fertilizers, pesticides, and fuel combusted during

farm-operations. Agrochemical applications were based on regimes recommended for CA rice production (Table S3.2) (Linquist et al. 2012b; Brodt et al. 2014; Espino et al. 2015; UCANR 2016). If pesticide and insecticide quantities were not specified in the literature, we assumed application rates corresponded to those recommended by product manufacturers. When LCIs for specific agrochemical compounds were not available in SimaPro databases, we selected proxies for these chemical compounds or their active ingredient(s) (Table S3.2) (Brodt et al. 2014). Fuel inputs of diesel and kerosene were estimated based on assumed field operations and associated fuel consumption rates found in the literature (Table S3.3) (Downs & Hansen 1998; Hanna 2005; Deliberto & Salassi 2010; Brodt et al. 2014).

Following rice crop production, we assumed rice grain was transported to a processing facility to be dried and milled. Milling generates co-products of rice hulls and bran. We assumed hulls were transported to a bioenergy facility, where they were converted to electricity, and bran was transported to a feedlot and used for cattle feed. Inputs of energy for transportation, drying, and milling were adapted from Brodt et. al (2014) (Table S3.3). Co-products from rice milling were accounted for in our rice LCIs via systems expansion (i.e. displacement) in accordance with ISO 14044 standards (ISO 2006b). Rates of hull and bran production during milling and GHG emissions subsequently displaced from the hull-derived electricity and bran substituted for cattle feed were also adapted from Brodt et. al (2014).

Life cycle inventories: downstream methane

Annual methane emissions were estimated using the PEPRMT model, a process-based biogeochemical model that predicts CO_2 and CH_4 exchange in restored wetlands (Oikawa et al. 2017). We parameterized PEPRMT using 3 years of CO_2 and CH_4 eddy covariance data at a rice field in the Sacramento-San Joaquin River Delta, CA, reserving 2 years of data for model validation (Figure 3.2). We then compared the validated the model to soil chamber CH_4 flux data from Butte County collected in 2008 – 2009 in a CF rice system (Bossio 1999; Fitzgerald et al. 2000; Pittelkow et al. 2013; Pittelkow et al. 2014; Simmonds et al. 2015). In accordance with conventional rice farming in the region, the PEPRMT model assumed the field was flooded from May 10 to Aug 20 at 12.7 cm above the soil surface. We assumed rice straw incorporation at 12 cm depth following harvest and off-season flooding from 20 October through 20 January to encourage rice straw decomposition (Bird et al. 2001; Brodt et al. 2014). Leaf area index (LAI) modeled in DSSAT was used as an input to the PEPRMT model. Meteorological model inputs (air temperature and radiation) were acquired from CIMIS in Durham. The model followed similar emission dynamics as the chamber data, however, consistently estimated CH_4 fluxes lower than those measured with chambers (slope = 1.92, intercept = 0.23, r2 = 0.59, $p < 0.001$). We then used the parameterized and validated PEPRMT model to run AWD simulations for Butte county. For moderate and severe AWD scenarios, we assumed water table height reached 15 cm and 50 cm, respectively, during dry-downs. Using CIMIS meteorological data, we ran the model for the 9 years between 1985 – 2015 during which all irrigation scenarios fit the filtering criteria. Again, LAI from DSSAT

was used to run PEPRMT. Mean values for annual CH_4 flux across years were used for LCAs, as well values one standard deviation above and below the mean.

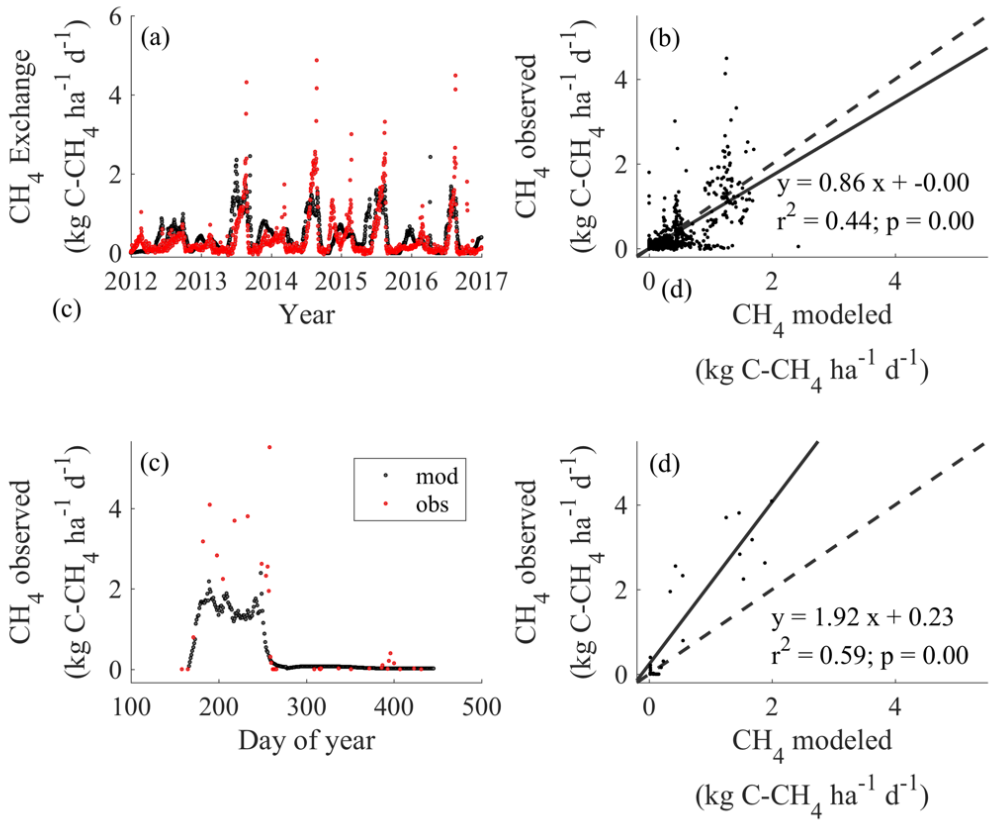

Figure 3.2. PEPRMT model performance of (panels a & b) CH_4 ecosystem exchange measurements collected at a rice paddy in the Sacramento-San Joaquin River Delta, CA, USA and (panels c & d) soil chamber CH_4 flux measurements collected at a rice paddy in Butte County, CA, USA. The model was parameterized using 3 years of data (2012 – 2014) collected in the Delta and validated using 2 years of data from the Delta (2015 – 2016). Panel a shows daily observed and modeled CH_4 ecosystem exchange rates for all 5 years. Panel b shows model-data agreement based on validation years only (slope = 0.86, $r^2 = 0.44$ $p < 0.001$). Cumulative CH_4 fluxes predicted with PEPRMT during model validation years was similar to observed CH_4 exchange (observed cumulative CH_4 = 24.96 g C-CH_4 m^{-2}; modeled = 29.02 g C-CH_4 m^{-2}). Panel c shows daily observed and modeled CH_4 exchange rates are for 1 growing season in a continuously flooded field in Butte County. Panel d shows model-data agreement for the entire field season (slope = 1.92, $r^2 = 0.59$ $p < 0.001$).

Life cycle inventories: other downstream flows

We modeled downstream emissions of N_2O using an IPCC tier 1 model (De Klein et al. 2006). This model accounts for both direct and indirect emissions of N_2O based on flood conditions, applied N, residue management, and changes in soil organic matter (SOM) content. We modeled N_2O fluxes under AWD by scaling seasonal emissions predicted with the flooded rice emission factor and the non-flooded crop emission factor by the percentage of days the field was flooded and the percentage of days the field was dry, respectively. We used the standard tier one emission factors for flooded and non-flooded systems, as well as their lower uncertainty limits, in order to capture uncertainty around N_2O. Air pollutants from fertilizer applications classified as indirect GHGs (e.g. NO_x, SO_x, VOCs) were modeled using emission factors published by the European Environment Agency (EEA) (Hutchings et al. 2016).

GHG emissions from use of diesel and kerosene were estimated using IPCC tier 1 combustion models (Waldron et al. 2006). Published emission factors were used to estimate indirect GHGs produced by diesel combustion (SAEFL 2000; Winther et al. 2016). These emissions were not modeled for kerosene as roughly 99% of kerosene is combusted as CO_2 and H_2O (Waldron et al. 2006).

Life cycle impact assessment: characterization

We characterized GWP in rice LCIs using the Tool for the Reduction and Assessment of Chemical and other environmental Impacts (TRACI 2 v. 3.03; Environmental Protection Agency, Washington DC, USA). TRACI models GWP on a

100-year time horizon based on the complied GHG inventories (Bare et al. 2003). A 100-year time horizon assumes CH_4 and N_2O are roughly 25 and 298 times more potent than CO_2, respectively. Characterization then allows expression of the overall warming potential on the basis of CO_2 equivalents (CO_2e) so results may be easily compared regardless of the variety and distribution of GHG sources in the life cycle.

3.4 Results

Crop model validation

Modeled yields were with 10% of measured yields and generally followed the same patterns as measured yields across years except in 2007 and 2008, when modeled yields rose slightly while measured yields declined, and in 2012 when modeled yields decreased while measured yields increased. We tested for the source of discrepancies in these particular years, but no significant relationships were found between any of the weather parameter inputs to DSSAT and modeled yield or in the difference between measured and modeled yield.

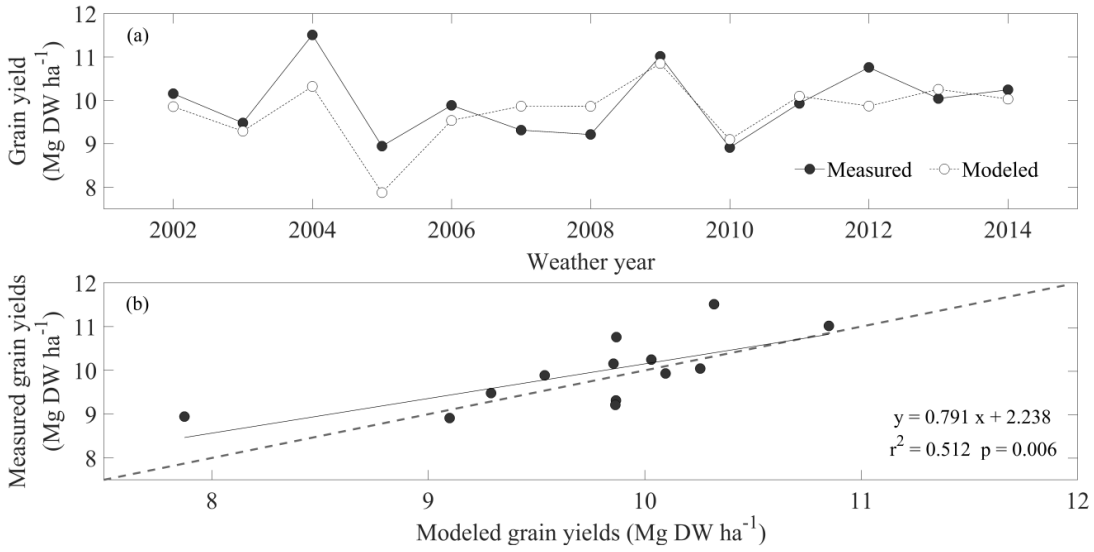

Figure 3.3. Fit between modeled and measured yields across 13 weather years (2002 – 2014). Panel (a) shows measured (filled markers) and modeled (open markers) yields by year. Most years, modeled yields followed the same patterns as measured yields. Panel (b) shows average measured yields for Butte county regressed against modeled yields.

Grain yield under AWD

Simulated yields were only significantly impacted in our most frequent and severe AWD scenarios. One-way ANOVA with multiple comparisons showed no significant difference between the average grain yields of CF, M1, M2, S1, and S2 scenarios across weather years (Figure 3.4a). Only our M3 scenario, which simulated three moderate mid-season dry-downs, resulted in significantly lower average grain yields than simulated CF rice. However, yields varied significantly within treatments across years, which minimized significant differences across treatments. As we were more interested in the latter, we calculated annual adverse yield impacts by subtracting AWD yields from CF yields (Figure 3.4b). One-way ANOVA of adverse yield impacts across years revealed

significant yield reductions in both M3 and S2 scenarios, where simulated yields were 23 ± 10% and 10 ± 7% lower than CF yields, respectively.

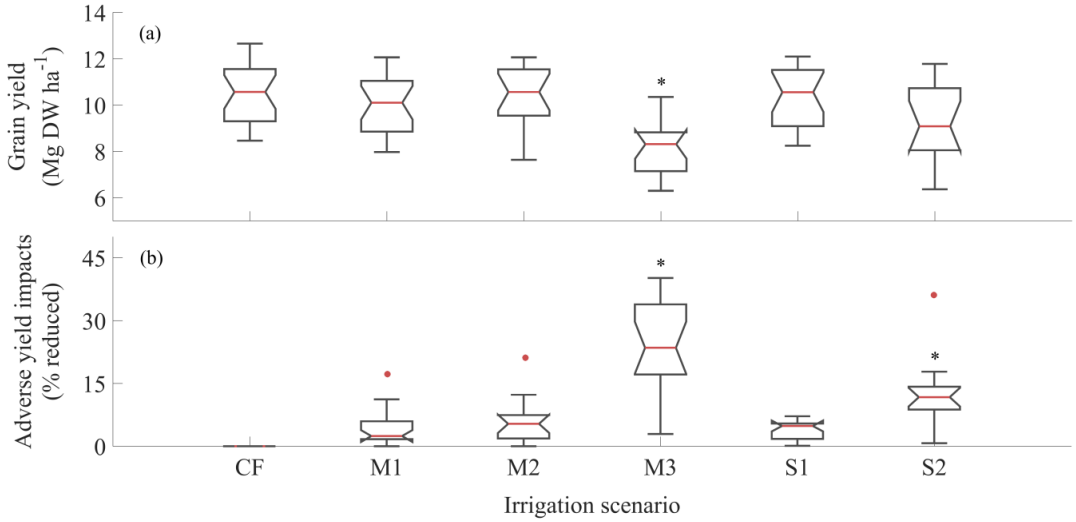

Figure 3.4. Average yields and adverse yield impacts across simulated years. Panel (a) shows average yields and standard deviations across weather years for each treatment. Here, asterisks denote where average yields across yields are significantly different from CF yields. Panel (b) shows average adverse yield impacts and standard deviations across weather years, determined as: [(CF yield – AWD yield) / CF yields] * 100. Here, asterisks denote where adverse yield impacts in AWD scenarios are significantly different from 0 given a 95% confidence interval. In both panels, red bands depict the true mean, boxes display the 25'th and 75'th percentile around the mean, and red dots indicate outliers.

Field emissions of CH_4

Methane emissions simulated in PEPRMT showed a lag in CH_4 flux following initial flooding and re-flooding events. Both the number and duration of dry-downs influenced the magnitude of CH_4 spikes following drainage events. Drainage-induced

dips in CH_4 emission occurred within the dry-down window in severe AWD scenarios but persisted beyond the duration of the dry-down for moderate AWD scenarios. Overall, dry-downs reduced CH_4 emissions, but the response was not always immediate and varied in magnitude depending on the timing, severity, and frequency of dry-downs.

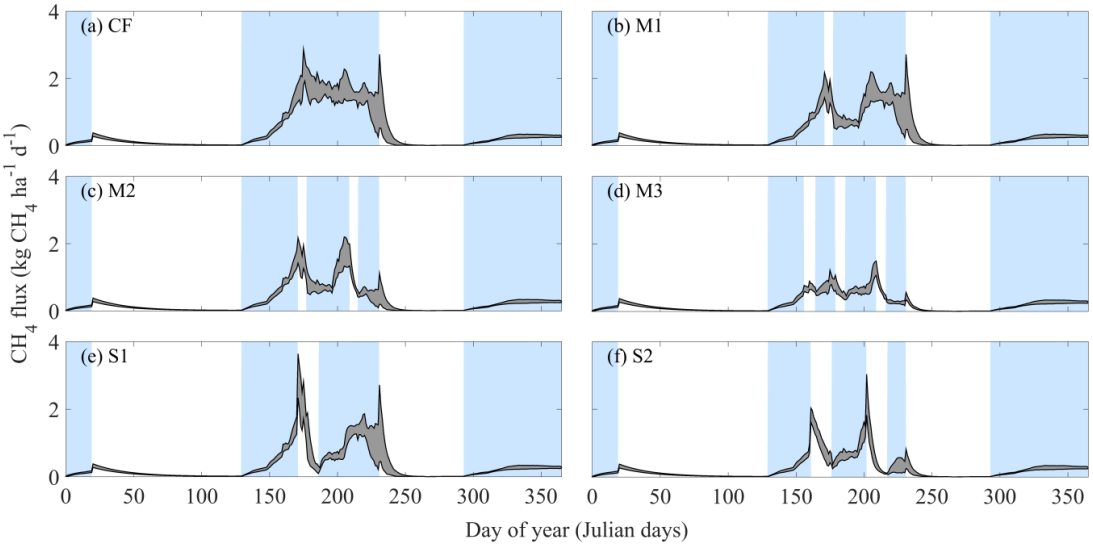

Figure 3.5. Daily CH_4 flux simulated with PEPRMT across irrigation scenarios. The light blue shading indicates days when the field was flooded, while the white area indicates days when the field was drained. The grey band shows mean daily CH_4 flux bounded by one standard deviation above and below the mean.

Annual CH_4 emissions modeled in PEPRMT were generally in good agreement with those previously reported for CA rice when managed with continuous flooding (Table 3.1). However, CH_4 fluxes simulated in PEPRMT tended to be much higher for AWD managed rice than those reported from chamber studies in the United Sates. Annual CH_4 emissions modeled in PEPRMT ranged from 88 – 150 kg CH_4 ha^{-1} across irrigation scenarios (Table 3.1). Relative to CF rice, CH_4 emissions simulated in

PEPRMT declined by 17, 30, and 46% in M1, M2, and M3 scenarios, respectively. More severe dry-downs increased mitigation of CH_4 emissions at a given dry-down frequency, with S1 and S2 scenarios resulting in 22% and 41% lower annual fluxes than our CF scenario. Seasonal CH_4 emissions were estimated to be roughly four to five times higher across treatments using the IPCC tier one model (Table 3.1).

Table 3.1. Field emissions of CH_4 from CF and AWD rice

	Seasonal CH_4 Emissions (kg CH_4-C ha^{-1})						
Source	***CF***	***M1***	***M2***	***M3***	***S1***	***S2***	**Study Location**
Present study (PEPRMNT)	150	125	105	81	117	88	California, US
Present study (IPCC Tier 1)	739	443	384	384	443	384	California, US
LaHue et al (2016)	175		75[a]				California, US
Linquist et al (2015)	105			7[a]		8[a]	Arkansas, US
Brodt et al (2014)	262						California, US
Pittelkow et al (2013)	152						California, US
Hokazono & Hayashi (2012)			190[a]				Japan
Linquist et al (2012)	133						Global average
McMillan et al (2007)	252						California, US
Fitzgerald et al (2000)	203						California, US

[a] AWD was classified as moderate when dry downs were within the "safe AWD" threshold and as severe when dried beyond this threshold. Actual AWD scheduling varied slightly form the treatments in the present study.

GWP across irrigation scenarios

Cradle-to-mill GWP, expressed on an area basis, was 7 – 22% lower in AWD scenarios than in our CF scenario. Emissions declined with increasing frequency (7.2% at M1, 11.7% at M2, and 21.5% at M3) and severity (8.3% at S1 and 16.1% at S2) of AWD (Table 3.2). On a yield basis, the mitigation benefits of AWD were less straight forward (Figure 3.6). While most scenarios showed a decline in GWP kg^{-1}, our M3 scenario

increased yield-scaled GWP by 4.2% relative to CF scenarios. The GHG-mitigation potential of other AWD strategies varied from 3 – 9%, with one moderate dry-down (M1) having to lowest mitigating affects and two moderate dry-downs (M2) having the highest.

Table 3.2. Land area and yield-scaled GWP in the rice life cycle across scenarios

	GWP [a] *(Mg CO_2e ha^{-1})*	**GWP** [a] *(kg CO_2e kg^{-1})*
CF	7.74 *(7.0 – 8.5)*	1.01 *(0.9 – 1.1)*
M1	7.18 *(6.5 – 7.9)*	0.98 *(0.9 – 1.1)*
M2	6.84 *(6.3 – 7.4)*	0.92 *(0.8 – 1.0)*
M3	6.08 *(5.6 – 6.4)*	1.05 *(0.8 – 1.1)*
S1	7.10 *(6.4 – 7.8)*	0.95 *(0.9 – 1.0)*
S2	6.50 *(5.0 – 7.0)*	0.95 *(0.8 – 1.0)*

[a] *mean (min – max across sources of uncertainty)*
[b] *mean ± standard deviation*

When LCAs were modeled assuming yields one standard deviation above and below the mean, GWP was reduced by 10 – 12% and increased by 12 – 16%, respectively, across scenarios (Figure 3.6a). Yield uncertainty had modest impacts on the mitigation potential of M1, M2, and S1 scenarios, where both adverse yield impacts and uncertainty around yields were low. However, higher yield uncertainty around our M3 and S2 scenarios had more notable impacts. In the case of our M3 scenario, GWP ranged from 2.1 to 6.9% higher than CF rice when modeled with upper and lower uncertainty limits for grain yield, respectively. GHG mitigation potential in our S2 scenario ranged from 2.4 to 8.7%, respectively.

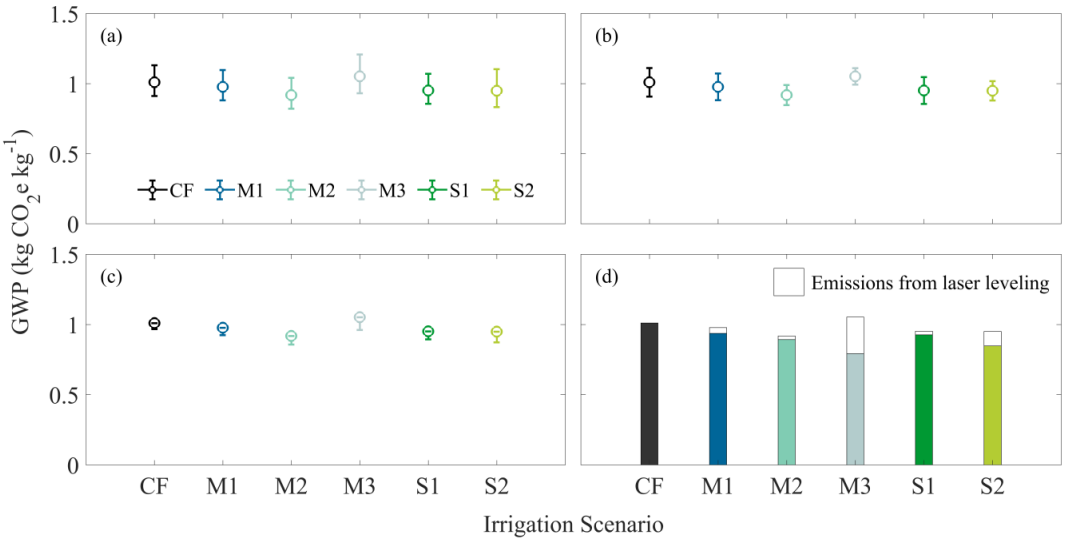

Figure 3.6. Yield-scaled GWP for CF and AWD rice with uncertainty around four LCI inputs. Panel (a) shows variance in GWP assuming mean grain yields and one standard deviation above and below the mean for each treatment. Similarly, panel (b) shows GWP assuming mean annual CH_4 flux and one standard deviation above and below the mean. Panel (c) shows LCAs assuming default tier 1 emission factors for N_2O and lower uncertainty limits for these emission factors. Panel (d) shows GWP assuming no laser leveled (solid bar) and with laser leveling (white bar).

Uncertainty around CH_4 emission simulated with PEPRMT had a lesser effect on overall GWP but a greater effect on the mitigation potential of individual AWD scenarios. Assuming one standard deviation above and below mean CH_4 emission modeled in PEPRMT, GWP varied by 6 – 10% across irrigation scenarios (Figure 3.6b). As the frequency and severity of AWD scenarios increased, uncertainty around annual CH_4 emission declined and, as a result, mitigation potential grew more variable. In the most extreme case, the GWP of our M3 scenario ranged from 0.1% to 10% higher than CF rice when assuming the upper and lower uncertainty limits for CH_4 emissions,

respectively. In our M2 and S2 scenarios, mitigation potential of AWD relative to CF varied between 7 – 11% and 3 – 8%. Despite higher uncertainty around CH_4 emissions, the mitigation potential of M1 and S1 scenarios was impacted by < 0.4%.

In the case of N_2O, only the lower uncertainty limits for the IPCC's N_2O emission factors were considered, as N_2O modeled with the default emission factor greatly exceeded previously published measurements of N_2O in rice systems (Table S3.4). Assuming these reduced emission factors, GWP declined by 4% in CF rice and as much as 9% in AWD scenarios (Figure 3.6c). Increasing frequency and severity of AWD resulted in greater reductions in GWP. As a result, the mitigation potential of AWD scenarios rose by roughly 1 – 5%. In our M3 scenario, this translated to a GWP 1% lower than that of CF rice, compared to a GWP 4% higher assuming the IPCC's default N_2O emission factor.

Among fuel-consumptive processes, laser leveling posed the greatest demands on fuel use. For continuously flooded rice and AWD scenarios with similar modeled yields (M1, M2, S1), GHG emissions attributed to fuel combustion during leveling contributed to < 5% of overall GWP (Figure 3.6d). However, in M3 and S2 scenarios, GHG emissions from laser leveling comprised 25 and 11% of GWP, respectively. Assuming no leveling, GWP in our M3 scenario was only 2% higher than in CF rice and the mitigation potential of our S2 scenario rose from 6 to nearly 9%. The mitigation potential of M1, M2, and S1 scenarios also rose when no laser leveling was assumed, but by < 1%.

Contributions to rice GWP

Methane emissions constituted 88 – 95% of GWP from all field emissions in our continuously flooded rice model and 74 – 93% of GWP from field emissions in AWD scenarios, where field emission constitute volatile losses of N_2O and CH_4 resultant from soil biogeochemical fluxes during crop production. These field emissions constituted only 36 – 51 % of total life cycle GWP, reducing the contribution of CH_4 to 27 – 49% of total rice GWP. Roughly a quarter of life cycle GWP was derived from fuel combustion of diesel and kerosene during rice production and transport (Table S3.5). Upstream GHGs from fertilizers and pesticides constituted 14 – 21% and 2 – 4% of GWP, respectively. Downstream GHGs from fertilizer were included in field emissions, and constitute the vast majority of N_2O emissions. The remaining 10 – 15% of GWP was derived from drying and milling .

3.5 Discussion

Overall, we found AWD to be a moderately effective practice for reducing the GWP of California rice. Mitigation of CH_4 emissions in AWD scenarios modeled in PEPRMT was somewhat modest, and these benefits were further muted through inclusion of all GHGs in the rice life cycle. Field emissions of CH_4 and N_2O comprised less than half of life cycle GWP kg grain^{-1}, effectively halving the benefits of AWD reported based on field emissions alone. Simulated yields were not significantly reduced under AWD when dry-downs were moderate or infrequent, but were adversely impacted when dry-downs where frequent and severe. In these cases, adverse yield impacts negated some or

all of the CH_4 mitigation benefits of AWD when GWP was evaluated on a yield-scaled basis. Together, these factors led to modest benefits from AWD, suggesting the GHG mitigation potential of this irrigation strategy may be less than previously reported when assessed from a life cycle perspective.

Life cycle GWP of CF and AWD rice

Despite the contributions of global rice production to the GHG-footprint of agriculture, few LCAs of rice have been conducted (Blengini & Busto 2009; Keatinge et al. 2012; Hokazono & Hayashi 2012; Thanawong et al. 2014; Brodt et al. 2014). Of these limited assessments, only one was conducted for California rice, which evaluated cradle-to-mill emissions for medium grain rice under CF (Brodt et al. 2014). Using average field emissions of CH_4 and N_2O aggregated from 8 studies across 6 sites, this study reported a GWP of 1.47 kg CO_2 eq kg milled rice^{-1}. Our study found the GWP of CF rice to be lower (~1.01 kg CO_2 eq kg milled rice^{-1} at comparable N fertilizer rates), largely due to differences in seasonal CH_4 emissions (Table 3.1). Other published LCAs of rice are based on production systems with substantially lower yields and varying management practices, which limits direct comparison of emissions reported on a land area basis (ha^{-1}) (Blengini & Busto 2009; Keatinge et al. 2012; Hokazono & Hayashi 2012; Thanawong et al. 2014).

Although no LCA considering both CF and AWD rice have been undertaken, several studies have characterized the mitigation potential of AWD based on field emissions of CH_4 and N_2O. Expressed on a land area basis, we saw a more modest

decline in GWP under AWD than chamber studies have reported. When GWP was scaled by grain yield, the mitigation potential of AWD was further reduced. We found AWD to mitigate no more than 9% of GWP kg^{-1} on average, 11% when uncertainty around yield, CH_4, N_2O, and fuel were considered. In our M3 scenario, where simulated yields were most adversely impacted, GWP tended to increase relative to CF rice. Three factors contributed to the modest response of GWP to alternate wetting and drying in our study: adverse yield impacts simulated for some AWD scenarios, the relatively modest response of annual CH_4 emissions to AWD simulated in PEPRMT, and the cradle-to-mill scope of our analysis.

Yield impacts across scenarios

AWD did not significantly impact grain yields in our M1, M2, or S1 simulations, however, our more frequent and severe schedules resulted in notable yield reductions. Relative yield stability in moderate and/or infrequent AWD schedules and moderate yield reduction simulated in our S2 scenarios are in relatively good agreement with previously reported values (Linquist et al. 2015; Carrijo et al. 2017). However, our M3 scenario suffered a much higher yield penalty than those typically reported from field studies under "safe" AWD, where soil VWC remains $\geq$ 60% above below saturation (Linquist et al. 2015; Carrijo et al. 2017). These adverse yield impacts are particularly important as they substantially influence yield-scaled GWP. From a global perspective, assessing GWP on a yield basis is more appropriate, as declining yields ultimately must be compensated for by planting more land area to meet production demands. Although CH_4

emissions declined by nearly half in our M3 scenario, yield-scaled GWP increased relative to CF rice. Notably, M3 yields simulated in our model showed the highest variability across weather years and the highest variability in year-by-year adverse yield impacts relative to CF simulations, suggesting high yield uncertainty for this scenario. However, even when uncertainty around yield was considered, GWP was higher for our M3 scenario than for CF rice. These results emphasize the importance of adverse yield impacts in determining of the migratory benefits of AWD from a global perspective.

Simulated field emissions of CH_4 and N_2O

CH_4 emissions from CF rice modeled with PEPRMT were within the observed range for continuously flooded CA rice (Table 3.1), but sparse data exist to characterize CH_4 emissions typical of AWD rice. When compared with studies reporting CH_4 flux for CF and AWD treatments, our results showed relatively modest declines in CH_4 flux for AWD rice. A study of AWD in Arkansas reported a 48% decline in CH_4 emissions ha^{-1} under moderate AWD and 93% decline under severe AWD (Linquist et al. 2015), reductions more than double those observed for corresponding scenarios in our study. In California rice, moderate AWD with two dry-downs reduced CH_4 ha^{-1} by 60% relative to CF (LaHue et al. 2016), exactly twice the reduction observed in our M2 scenario. Hokazono & Hayashi reported CH_4 emissions under one moderate dry-down higher than those modeled in our study, but the lack of a CF reference scenario makes it difficult to corroborate agreement between this study and our own. CH_4 emissions determined using the IPCC tier 1 model were roughly 2 – 3 times higher those derived from PEPRMT, but did tend to simulate greater emission reductions under AWD. However, this model has

been previously shown to overestimate emissions in CA rice systems by two-fold (Brodt et al. 2014). Further, the IPCC model assumes emissions decline by 40% with one mid-season dry down and 48% with > 1 mid-season dry-down without sensitivity to dry-down severity (Lasco et al. 2006). Overall, our study suggests much lower CH_4 mitigation potential than previous studies and the current IPCC model.

Differences in CH_4 mitigation under AWD arise from large uncertainties in seasonal CH_4 flux modeling. Field studies of AWD have used weekly chamber measurements of CH_4 flux to extrapolate annual fluxes. Though most studies increase their sampling frequency before and after significant management events, such as fertilization and drainage, biogeochemical fluxes can be large and transient, like pulses, as well as lag in their response to these events, making this sampling scheme insufficient for capturing seasonal flux dynamics (Knox et al. 2016; Sturtevant et al. 2016). Seasonal fluxes are typically extrapolated using linear interpolation between sampling periods, which can fail to adequately capture these pulse dynamics (Pittelkow et al. 2014; Adviento-Borbe et al. 2015; Linquist et al. 2015; LaHue et al. 2016). Further, both sampling locations and sample size for flux measurements are limited in most studies. These chamber measurements effectively provide only a snapshot of activity, which varies in both space and time. As CH_4 pulses evolve rapidly, these measurements are equally likely to capture the beginning or end of a CH_4 pulse as they are to capture the peak of the pulse (Knox et al. 2016). Accordingly, this method may under- or overestimate annual fluxes relative to eddy covariance data, even when fit between chamber and eddy covariance measurements is good (Schrier-Uijl et al. 2010).

Beyond pulse emissions of CH_4 following dry-downs, results from the PEPRMT model suggest lags between soil water status and biochemical responses of CH_4 emissions. Lagged responses to dry downs are likely caused by changing redox states in the soil. Immediately following a dry down, oxygen re-enters the soil profile allowing methanogens to be out-competed. It may take several days for redox conditions to change from anaerobic to aerobic, especially if the dry-down is moderate and short-lived. The presence of these pulses and lags in CH_4 flux response suggest high temporal resolution data is required to capture complex flux dynamics. Unfortunately, there is not sufficient eddy covariance data to validate the model at high temporal resolution for Butte county rice and our modeling comparison with chamber data indicate that the chambers measured significantly higher fluxes than estimated using PEPRMT. It is common for chamber data to overestimate CH_4 and CO_2 fluxes. However, parameterization of PEPRMT in a rice paddy in the Sacramento Delta showed good fit to eddy covariance data for CH_4 flux ($r^2 = 0.44$). The significant contrast between CH_4 mitigation modeled in PEPRMT versus that modeled from chamber measurements highlight the need for high resolution CH_4 flux data to better characterize the mitigation potential of AWD.

N_2O played a much smaller role in determining GWP than CH_4, constituting roughly 5 – 15% of GWP across scenarios. Nonetheless, these emissions were more significant in our assessment than in previous studies of AWD. We calculated N_2O fluxes using an IPCC tier 1 model, which assumes 1% of all N applied to the soil is lost as N_2O when the soil is dry and 0.3% is lost when the soil is flooded (De Klein et al. 2006). N_2O emissions modeled in our study exceeded previously reported values by nearly an order

of magnitude (Bossio 1999; Fitzgerald et al. 2000; Redeker et al. 2000; McMillan et al. 2007; Adviento-Borbe et al. 2013; Pittelkow et al. 2013; Pittelkow et al. 2014; Simmonds et al. 2015). Overestimation of N_2O emissions in the present study may underestimate the advantages of AWD, as N_2O emissions increase with increasing frequency and severity of AWD. When we assumed the lower uncertainty limit of default IPCC emission factors, modeled N_2O emissions were more similar to previously reported values. This assumption increased mitigation benefits for AWD.

Scope of analysis: a life cycle perspective

Together, field emissions of CH_4 and N_2O constituted less than a half of yield-scaled GWP in our study. Previous LCAs of rice report higher contributions from field emissions, ranging from 62 – 68% of GWP (Blengini & Busto 2009; Brodt et al. 2014; Thanawong et al. 2014). Lower contributions of field emissions in our study may be attributable to slightly lower CH_4 emissions, but are more likely due to differences in emissions derived from alternative sources in the life cycle. Non-field emissions generated 0.33 – 0.51 CO_2 eq kg milled grain^{-1} in our study, compared to 0.45 CO_2 eq kg milled grain^{-1} in Brodt et al (2014). However, fuel was a larger source of GHGs in our study, with fuel consumed during laser leveling accounting for more than half of total fuel use (Figure S3.5).

Omitting fuel consumed during laser leveling increased the mitigation benefits of AWD, particularly for our more frequent and severe schedules. Although fuel inputs were consistent across irrigation scenarios, M3 and S1 scenarios showed the greatest adverse

yield impacts. Therefore, when GWP was assessed on a yield-basis, more fuel was required to achieve 1 kg grain for these scenarios. In our uncertainty analysis, reduced fuel use had an impact roughly equivalent to that of reduced N_2O emissions on life cycle GWP, suggesting these lesser acknowledged GHG sources can play an important role in determining mitigation benefits of AWD rice. While AWD has been estimated to reduce field emissions of CH_4 by anywhere from 40 to upwards of 90%, field emissions constituted only 1/3 – ½ of total GWP in our study. Thus, when AWD is considered from a life cycle perspective, its mitigation potential is less than half that reported from field emissions alone. This context is particularly important from a global perspective, where milled rice, rather than fresh rice, is the desired commodity on which markets are based.

Synthesis

The American Carbon Registry recently made AWD eligible for carbon credits (CARB 2014), but our results suggest that the benefits of AWD have not been adequately assessed. Using high resolution gas flux modeling in a life cycle assessment framework, our study revealed more modest mitigation benefits from AWD than have been previously reported based on manual chamber measurements of emissions. Life cycle assessment is an important tool for evaluating the GWP of rice from a comprehensive and globally relevant perspective. Adverse yield impacts, conservative differences in CH_4 emissions across irrigation strategies modeled in PEPRMT, and GHG contributions from alternative sources in the rice life cycle drove these modest differences in GWP. Further improvements to CH_4 emission estimation in rice systems is needed, but our results

suggest the mitigation potential of alternate wetting and drying has been overestimated. Both high resolution gas flux data and a life cycle perspective are required to ensure effective mitigation of GWP in rice systems.

3.6 References:

Adviento-Borbe, M.A. et al., 2015. Methane and Nitrous Oxide Emissions from Flooded Rice Systems following the End-of-Season Drain. *Journal of environmental quality*, 44(4), pp.1071–9.

Adviento-Borbe, M.A. et al., 2013. Optimal Fertilizer Nitrogen Rates and Yield-Scaled Global Warming Potential in Drill Seeded Rice. *Journal of Environment Quality*, 42(6), p.1623.

Bare, J.C. et al., 2003. The Tool for the Reduction and Assessment of Chemical and Other Environmental Impacts. *Journal of Industrial Ecology*, 6(3–4), pp.48–78.

Bird, J.A. et al., 2001. Immobilization of Fertilizer Nitrogen in Rice: Effects of Straw Management Practices. *Soil Science Society of America Journal*, 65, pp.1143–1152.

Blengini, G.A. & Busto, M., 2009. The life cycle of rice: LCA of alternative agri-food chain management systems in Vercelli (Italy). *Journal of Environmental Management*, 90(3), pp.1512–1522.

Bossio, D., 1999. Methane pool and flux dynamics in a rice field following straw incorporation. *Soil Biology and Biochemistry*, 31(9), pp.1313–1322.

Bouman, B.A.., 2007. *Water management in irrigated rice: coping with water scarcity*.

Bouman, B.A.. & Tuong, T.., 2001. Field water management to save water and increase its productivity in irrigated lowland rice. *Agricultural Water Management*, 49(1), pp.11–30.

Bouwman, A.F., 1998. Environmental science: Nitrogen oxides and tropical agriculture. *Nature*, 392(6679), pp.866–867.

Brodt, S. et al., 2014. Life cycle greenhouse gas emissions in California rice production. *Field Crops Research*, 169, pp.89–98.

Burkett, D.W. & Conlin, A.E., 2006. *Soil Survey of Butte Area, California, Parts of Butte and Plumas Coumnties*.

CARB, 2014. Proposed Compliance Offset Protocol Rice Cultivation Projects. *California Air and Resources Board*. Available at: https://www.arb.ca.gov/cc/capandtrade/protocols/riceprotocol.htm [Accessed April 14, 2017].

Carrijo, D.R., Lundy, M.E. & Linquist, B.A., 2017. Rice yields and water use under alternate wetting and drying irrigation: A meta-analysis. *Field Crops Research*, 203, pp.173–180.

CASS, 2009. *California Field Crop Review*, Washington D.C.

Cherubini, F. et al., 2009. Energy- and greenhouse gas-based LCA of biofuel and bioenergy systems: Key issues, ranges and recommendations. *Resources, Conservation and Recycling*, 53(8), pp.434–447.

Conrad, R., 2002. Control of microbial methane production in wetland rice fields. *Nutrient Cycling in Agroecosystems*, 64(1/2), pp.59–69.

CRC, 2009. *California Rice Statistics and related National and International Data*, Sacramento, CA.

Davidson, E.A. et al., 2012. The Dual Arrhenius and Michaelis-Menten kinetics model for decomposition of soil organic matter at hourly to seasonal time scales. *Global Change Biology*, 18(1), pp.371–384.

Deliberto, M.A. & Salassi, M.E., 2010. *Estimated Costs of Precision Grading Sugarcane Fields, 2010*, Baton Rouge, LA.

Devevre, O.C. & Horwath, W.R., 2000. Decomposition of rice straw and microbial carbon use e • ciency under di€ erent soil temperatures and moistures. *Soil Biology & Biogeochemistry*, 32, pp.1773–1785.

Dobermann, A. & Fairhurst, T.H., 2002. Rice Straw Management. *Better Crops International*, 16, pp.7–11.

Downs, H.W. & Hansen, R.W., 1998. Estimating Farm Fuel Requirements. *Fact Sheet*, (5.006). Available at: www.ext.colostate.edu [Accessed December 30, 2016].

EPA, 2009. *Air Emissions Factors Quantification*, Washington D.C., US.

Espino, L.A. et al., 2015. *2015 Sample Costs to Produce Rice*, Sacramento, CA.

Fitzgerald, G.J., Scow, K.M. & Hill, J.E., 2000. Fallow season straw and water management effects on methane emissions in California rice. *Global Biogeochemical Cycles*, 14(3), pp.767–776.

Greer, C.A. et al., 2012. *2012 Sample Costs to Produce Rice*, Sacramento, California.

Guinée, J.B. et al., 2011. Life Cycle Assessment: Past, Present, and Future. *Environmental Science & Technology*, 45(1), pp.90–96.

Hanna, M., 2005. Fuel Required for Field Operations. *Iowa State University Extension & Outreach: Ag Decision Maker*.

Hokazono, S. & Hayashi, K., 2012. Variability in environmental impacts during conversion from conventional to organic farming: a comparison among three rice production systems in Japan. *Journal of Cleaner Production*, 28, pp.101–112.

Hou, A.X. et al., 2000. Methane and Nitrous Oxide Emissions from a Rice Field in Relation to Soil Redox and Microbiological Processes. *Soil Science Society of America Journal*, 64(6), p.2180.

Hutchings, N. et al., 2016. Crop production and agricultural soils. In *EMEP/EEA air pollutant emission inventory guidebook*. Geneva, Swtizerland.

ISO, 2006a. *14040: Environmental management–life cycle assessment–principles and framework*, International Organization of Standardization, Geneva, Swtizerland.

ISO, 2006b. *14044: Environmental management–life cycle assessment–requirements and guidelines*, International Organization of Standardization, Geneva, Swtizerland.

Jodari, F. et al., 2001. M-205 Rice: Description and Management Guidelines. *Agronomy Fact Sheet Series*. Available at: http://rice.ucanr.edu/files/196761.pdf.

Jones, J.. et al., 2003. The DSSAT cropping system model. *European Journal of Agronomy*, 18(3–4), pp.235–265.

Keatinge, J.D.H. et al., 2012. Vegetable gardens and their impact on the attainment of the Millennium Development Goals. *Biological Agriculture & Horticulture*, 28(2), pp.71–85.

Kettunen, A. et al., 1999. Methane production and oxidation potentials in relation to water table fluctuations in two boreal mires. *Soil Biology and Biochemistry*, 31(12), pp.1741–1749.

Kislev, Y. & Peterson, W., 1982. Prices, Technology, and Farm Size. *Journal of Political Economy*, 90(3), pp.578–95.

De Klein, C. et al., 2006. N2O Emissions from Managed Soils and CO2 Emissions from Lime and Urea Application. In *2006 IPCC Guidelines for National Greenhouse Gas Inventories*. Geneva, Swtizerland.

Knox, S.H. et al., 2016. Biophysical controls on interannual variability in ecosystem-scale CO2 and CH4 exchange in a California rice paddy. *Journal of Geophysical Research: Biogeosciences*, 121(3), pp.978–1001.

LaHue, G.T. et al., 2016. Alternate wetting and drying in high yielding direct-seeded rice systems accomplishes multiple environmental and agronomic objectives. *Agriculture, Ecosystems & Environment*, 229, pp.30–39.

Lasco, R.D. et al., 2006. Cropland. In *2006 IPCC Guidelines for National Greenhouse Gas Inventories*. Geneva, Swtizerland.

Linquist, B. et al., 2012. An agronomic assessment of greenhouse gas emissions from major cereal crops. *Global Change Biology*, 18(1), pp.194–209.

Linquist, B.A. et al., 2016. *California Rice Varieties: Description and Performance Summary of the 2015 and Multiyear Statewide Rice Variety Tests in California*, Davis, California.

Linquist, B.A. et al., 2012. Fertilizer management practices and greenhouse gas emissions from rice systems: A quantitative review and analysis. *Field Crops Research*, 135, pp.10–21.

Linquist, B.A. et al., 2015. Reducing greenhouse gas emissions, water use, and grain arsenic levels in rice systems. *Global Change Biology*, 21(1), pp.407–417.

McMillan, A.M.S., Goulden, M.L. & Tyler, S.C., 2007. Stoichiometry of CH4 and CO2 flux in a California rice paddy. *Journal of Geophysical Research*, 112.

Moore, T.R. & Dalva, M., 1993. The influence of temperature and water table position on carbon dioxide and methane emissions from laboratory columns of peatland soils. *Journal of Soil Science*, 44(4), pp.651–664.

Oikawa, P.Y. et al., 2017. Evaluation of a hierarchy of models reveals importance of substrate limitation for predicting carbon dioxide and methane exchange in restored wetlands. *Journal of Geophysical Research: Biogeosciences*, 122(1), pp.145–167.

Oikawa, P.Y. et al., 2014. Unifying soil respiration pulses, inhibition, and temperature hysteresis through dynamics of labile soil carbon and O2. *Journal of Geophysical Research: Biogeosciences*, 119(4), pp.521–536.

Pandey, A. et al., 2014. Organic matter and water management strategies to reduce methane and nitrous oxide emissions from rice paddies in Vietnam. *Agriculture, Ecosystems & Environment*, 196, pp.137–146.

Pittelkow, C.M. et al., 2014. Nitrogen Management and Methane Emissions in Direct-Seeded Rice Systems. *Agronomy Journal*, 106(3), p.968.

Pittelkow, C.M. et al., 2013. Yield-scaled global warming potential of annual nitrous oxide and methane emissions from continuously flooded rice in response to nitrogen input. *Agriculture, Ecosystems & Environment*, 177, pp.10–20.

Pré Consultants, 2013. SimaPro 8.

Redeker, K.R. et al., 2000. Emissions of methyl halides and methane from rice paddies. *Science (New York, N.Y.)*, 290(5493), pp.966–9.

Reed, W., 2002. *Soil Survey of Colusa County, California*.

Roel, A., Heilman, J.L. & McCauley, G.N., 1999. Water use and plant response in two rice irrigation methods. *Agricultural Water Management*, 39(1), pp.35–46.

SAEFL, 2000. *Handbuch Offroad-Datenbank*, Bern, Switzerland.

SAIC, 2006. *Life Cycle Assessment: Principles and Practice*,

Sass, R.L. et al., 2002. Spatial and temporal variability in methane emissions from rice paddies: Implications for assessing regional methane budgets. *Nutrient Cycling in Agroecosystems*, 64(1/2), pp.3–7.

Schrier-Uijl, A.P. et al., 2010. Comparison of chamber and eddy covariance-based CO2 and CH4 emission estimates in a heterogeneous grass ecosystem on peat. *Agricultural and Forest Meteorology*, 150(6), pp.825–831.

Simmonds, M.B., Li, C., et al., 2015. Modeling methane and nitrous oxide emissions from direct-seeded rice systems. *Journal of Geophysical Research: Biogeosciences*, 120(10), pp.2011–2035.

Simmonds, M.B., Anders, M., et al., 2015. Seasonal Methane and Nitrous Oxide Emissions of Several Rice Cultivars in Direct-Seeded Systems. *Journal of Environment Quality*, 44(1), p.103.

Sturtevant, C. et al., 2016. Identifying scale-emergent, nonlinear, asynchronous processes of wetland methane exchange. *Journal of Geophysical Research: Biogeosciences*, 121(1), pp.188–204.

Thanawong, K., Perret, S.R. & Basset-Mens, C., 2014. Eco-efficiency of paddy rice production in Northeastern Thailand: a comparison of rain-fed and irrigated cropping systems. *Journal of Cleaner Production*, 73, pp.204–217.

UCANR, UC IPM Rice Invertebrate Pest Resources. *UCANR Agronomy Research & Information Center for Rice*. Available at: http://rice.ucanr.edu/Guidelines/Insects/ [Accessed December 3, 2016].

US EPA, OCSPP, O., 2007. Tier I Rice Model - Version 1.0 - Guidance for Estimating Pesticide Concentrations in Rice Paddies.

Venterea, R.T., 1991. Theoretical Comparison of Advanced Methods for Calculating Nitrous Oxide Fluxes using Non-steady State Chambers. *Soil Science Society of America Journal Soil Sci. Soc. Am. J*, 77, pp.709–720.

Waldron, C.D. et al., 2006. Mobile Combustion. In *IPCC Guidelines for National Greenhouse Gas Inventories*.

Wang, M. et al., 2010. Life cycle assessment of a rice production system in Taihu region, China. *International Journal of Sustainable Development & World Ecology*, 17(2), pp.157–161.

Wassmann, R. et al., 1998. Methane production capacities of different rice soils derived from inherent and exogenous substrates. *Plant and Soil*, 203(2), pp.227–237.

Wells, F.A., 1972. *Soil Survey of Yolo County, California*, Woodland, CA.

Wernet, G. et al., 2016. The ecoinvent database version 3 (part I): overview and methodology. *The International Journal of Life Cycle Assessment*, 21(9), pp.1218–1230.

Winther, M. et al., 2016. Combustion: Non road mobile machinery. In *EMEP/EEA air pollutant emission inventory guidebook*. Geneva, Swtizerland.

Yan, X. et al., 2009. Global estimations of the inventory and mitigation potential of methane emissions from rice cultivation conducted using the 2006 Intergovernmental Panel on Climate Change Guidelines. *Global Biogeochemical Cycles*, 23(2).

3.7 Supporting Information

Table S3.1. Mean RMSE across counties, of DSSAT and Degree Day model predictions of phenological transitions across 12 planting dates and 30 weather years under optimized phenological parameters expressed in days after planting (DAP).

Phenological transition (DAP)	**Planting date**												
	20-Apr	*25-Apr*	*30-Apr*	*05-May*	*10-May*	*15-May*	*20-May*	*25-May*	*30-May*	*04-Jun*	*09-Jun*	*14-Jun*	***Avg***
Juvenile to panicle	12.3	9.2	7.6	4.6	3.2	0.7	1.5	1.9	2.1	2.8	2.1	3.9	4.3
Panicle to heading	7.7	6.1	1.2	2.0	1.1	2.4	4.0	4.1	3.8	5.1	4.6	5.6	4.0
Heading to maturity	9.7	8.1	4.8	4.0	3.4	3.5	4.0	4.0	4.0	4.7	4.9	5.6	5.1
All transitions	10.9	8.7	6.4	4.7	3.2	2.2	2.5	2.8	2.8	3.0	2.9	3.7	**4.5**

Table S3.2. RMSE and percent difference of reported and modeled yields, averaged across years.

Data source	**Grain yield (Mg DW ha^{-1})**			
	Butte	**Colusa**	**Yuba**	**All counties**
	Mean *(sd)*			
Reported yields [a]	10.50 *(0.88)*	10.92 *(0.91)*	10.05 *(0.99)*	10.49 *(0.92)*
Modeled yields	10.78 *(0.74)*	10.91 *(0.58)*	10.89 *(0.66)*	10.84 *(0.68)*
% Difference	2.63%	-0.08%	8.07%	3.26%

[a] *Averaged across all reporting locations in each county*

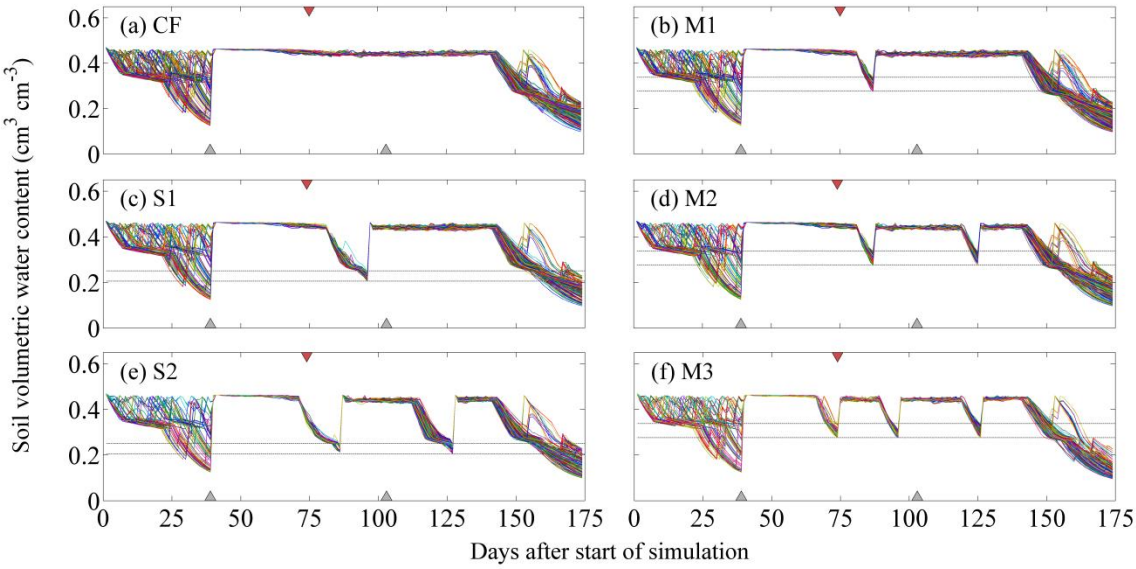

Figure S3.1. Soil VWC filtering criteria for irrigation schedules. Data are shown for all compliant years and both counties. Dotted black lines show the upper and lower limits of the applied filtering criteria for mid-season dry downs. Limits were 0.28 – 0.34 and 0.21 – 0.25 cm^3 cm^{-3} for mild (M) and severe (S) AWD schedules, respectively. Fertilizer events are denoted by grey triangles. Floods were maintained $\geq$ 14 days post-fertilization. Red triangles denote the average date of canopy closure across fertilizer treatments. When possible, flooding was maintained until canopy closure.

Table S3.2. Assumed agrochemical inputs to rice production

Agrochemical	Active ingredient	SimaPro LCI input	Base Qnt (kg ha^{-1})	Add Qnt [a] (kg ha^{-1})	Details & sources
Fertilizers					
Aqua ammonia	82% N	ammonia, liquid	40 – 145 kg N ha^{-1}		1 pre-plant application to 100% of ha, injected at 10 cm depth prior to the initial flood (Espino et al., 2015)
MAP	16% N & 20% P	mono-ammonium phosphate	35 kg N ha^{-1}		1 application to 100% of ha, broadcast prior to the initial flood (Brodt et al., 2014)
Potash	N/A	potassium chloride	56 kg K_2O ha^{-1}		1 application to 100% of ha, broadcast prior to the initial flood (Brodt et al., 2014)
Zinc sulfate	N/A	zinc mono-sulfate	16.82 kg $ZnSO_4$ ha^{-1}		1 application to 50% of ha, broadcast prior to the initial flood (Espino et al., 2015)
Ammonium sulfate	N/A	ammonium sulfate	0 – 50 kg N ha^{-1}		0 – 1 application to 100% of ha, broadcast aerially mid-season (Espino et al., 2015)
Pesticides & Insecticides					
Bolero	84% theobencarb	[thio]carbamate compounds	83	83	1 – 2 applications to 100% of ha (Espino et al., 2015)
Warrior	11.4% lambda-cyhalothrin	pyretroid compounds	0.12		1 application to 15% of ha and one to 5% of ha (Espino et al., 2015; UCANR, 2016)
Copper sulfate	99% CuS pentahydrate	copper oxide	0.45		1 application to 20% of ha, assumes 1.01 kg CuS, adjusted for each compound by molecular weight (Espino et al., 2015)
		sulfuric acid	0.55		
Regiment	80% bispyribac sodium	benzoic compounds	0.07	0.04	1 – 2 applications to 100% of ha and 1 application to 80% of ha (Espino et al., 2015)
Tank mix	70% propanil	propanil [b]	5.08		1 application to 100% of ha, assumes 13.45 l ha^{-1} tank mix (Espino et al., 2015)
	25.2% theobencarb	[thio]carbamate compounds	117		

[a] For fertilizers, a range of application rates is provided instead of base and additional quantities, as fertilizer inputs of aqua ammonia and ammonium sulfate varied across scenarios based on cumulative N rate simulated. For pesticides, additional quantities refer to supplemental pesticide applications required for AWD scenarios in which the first dry-down occurs prior to canopy closure.

[b] The propanil LCI was modeled based on stoichiometric relationships of compounds required for propanil synthesis. This inventory does not account for enzymes required for synthesis, by-products generated during synthesis, storage materials, or transport to a regional storehouse.

Table S3.3. Assumed field and rice processing operations and associated their energy inputs

Operation	Energy input (L, therm, or kWh ha^{-1})		Details & sources
Rice production			
transport	diesel	1.72	agrochemicals & rented equip to field (Brodt et al., 2014)
chisel	diesel	20.58	chisel plough, twice (Hanna, 2005)
disc	diesel	18.2	4WD tractor (Brodt et al., 2014)
disc	diesel	12.16	tandem disc, twice (Hanna, 2005)
level	diesel	288.85	precision grading (Deliberto & Salassi, 2010)
rolled	diesel	3.27	rolling cultivator (Downs & Hansen, 1998)
fertilizer app	diesel	5.14	injected, 100% of ha (Hanna, 2005)
fertilize app	diesel	1.40	broadcast, 100% of ha (Hanna, 2005)
planting	kerosene	4.95	water seeding (Brodt et al., 2014)
herbicide app	kerosene	1.12 [a]	aerial, grass herbicide to 100% of ha (Brodt et al., 2014)
pesticide app	kerosene	0.19	aerial, pesticide to 15% of ha (Brodt et al., 2014)
pesticide app	kerosene	0.90	aerial 20%, pesticide to 20% (Brodt et al., 2014)
herbicide app	kerosene	1.03 [a]	aerial, grass & broadleaf to 100% (Brodt et al., 2014)
herbicide app	kerosene	1.12	aerial, clean-up to 100% (Brodt et al., 2014)
herbicide app	kerosene	1.03	aerial, grass & broadleaf to 80% (Brodt et al., 2014)
fertilize app	kerosene	2.01	aerial, 50% of ha (Brodt et al., 2014)
pesticide app	kerosene	0.06	aerial, pesticide to 5% of ha (Brodt et al., 2014)
pesticide app	kerosene	0.82	aerial, pesticide to 80% of ha (Brodt et al., 2014)
harvest	diesel	9.35	small grain combine (Downs & Hansen, 1998)
mow levees	diesel	51.4	flail mow (Brodt et al., 2014)
chop stubble	diesel	13.7	utility tractor (Brodt et al., 2014)
disc	diesel	18.2	4WD tractor (Brodt et al., 2014)
Rice transport and processing			
transport	diesel	8.23	grain to drying facility (Brodt et al., 2014)
drying	natural gas	38.96	heating (Brodt et al., 2014)
drying	electricity	539.30	heating & mechanical operation (Brodt et al., 2014)
milling	electricity	315.80	90% white, 10% brown (Brodt et al., 2014)
transport	diesel	2.86	co-product transport

[a] Reflects the minimum energy inputs for these operations. In rice management scenarios requiring additional herbicide inputs, these inputs were doubled.

Table S3.4. Field emissions of N_2O from CF and AWD rice

	Seasonal N_2O Emissions (kg N_2O ha^{-1})						
Source	***CF***	***M1***	***M2***	***M3***	***S1***	***S2***	**Study Location**
Present study (IPCC Tier 1)	1.65	1.90	2.15	2.40	2.03	2.40	California, US
LaHue et al (2016)	0.10		0.14[a]				California, US
Linquist et al (2015)	0.01			0.23[a]		0.51[a]	Arkansas, US
Brodt et al (2014)	0.31						California, US
Pittelkow et al (2013)	0.65						California, US
Hokazono & Hayashi (2012)			0.95[a]				Japan
Linquist et al (2012)	0.44						Global average

[a] AWD was classified as moderate when dry downs were within the "safe AWD" threshold and as severe when dried beyond this threshold. Actual AWD scheduling varied slightly form the treatments in the present study.

Table S3.5. Percent of cradle-to-mill GWP kg dried $grain^{-1}$ from non-field emissions

	Fuel	**Fertilizer**	**Pest**	**Milling & Drying**
CF	21	14	2	12
M1	23	16	3	11
M2	24	18	3	13
M3	27	21	4	10
S1	23	17	3	13
S2	25	20	3	15

3.8 References for Supporting Information

Brodt, S., Kendall, A., Mohammadi, Y., Arslan, A., Yuan, J., Lee, I., & Linquist, B. (2014). Life cycle greenhouse gas emissions in California rice production. *Field Crops Research*, *169*, 89–98.

Deliberto, M. A., & Salassi, M. E. (2010). *Estimated Costs of Precision Grading Sugarcane Fields, 2010* (Vol. 2010). Baton Rouge, LA.

Downs, H. W., & Hansen, R. W. (1998). Estimating Farm Fuel Requirements. *Fact Sheet*, (5.006). Retrieved from www.ext.colostate.edu

Espino, L. A., Mutters, R. G., Buttner, P., Klonsky, K., Stewart, D., & Tumber, K. P. (2015). *2015 Sample Costs to Produce Rice*. Sacramento, CA.

Hanna, M. (2005). Fuel Required for Field Operations. Retrieved from https://www.extension.iastate.edu/agdm/crops/html/a3-27.html

UCANR. (2016). UC IPM Rice Invertebrate Pest Resources. Retrieved December 3, 2016, from http://rice.ucanr.edu/Guidelines/Insects/